

WRDC-TR-90-9003

2

WRDC-TR-90-9003
Volume II

**UNIFORM THEORY OF DIFFRACTION
(UTD) SCATTERING FROM STRUCTURES,
INCLUDING HIGHER ORDER TERMS**



**Volume II: Edge Wave Edge and Vertex
Diffraction**

ElectroScience Laboratory
The Ohio State University
1320 Kinnear Road
Columbus, OH 43212

November 1990
Final Report for Period April 1986 - December 1989

Approved for Public Release; Distribution is Unlimited

DTIC
ELECTE
DEC 20 1990
S B D

Signature Technology Directorate
Wright Research and Development Center
Air Force Systems Command
Wright Patterson Air Force Base, OH 45433-6523

AD-A230 339

NOTICE

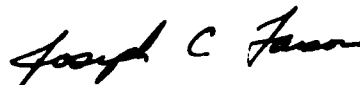
When Government drawings, specifications, or other data are used for any purpose other than in connection with a definitely Government-related procurement, the United States Government incurs no responsibility or any obligation whatsoever. The fact that the government may have formulated or in any way supplied the said drawings, specifications, or other data, is not to be regarded by implication, or otherwise in any manner construed, as licensing the holder, or any other person or corporation; or as conveying any rights or permission to manufacture, use, or sell any patented invention that may in any way be related thereto.

This report is releasable to the National Technical Information Service (NTIS). At NTIS, it will be available to the general public, including foreign nations.

This technical report has been reviewed and is approved for publication.

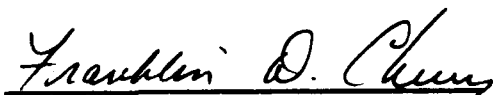


J. EARL JONES, Project Engineer
Defensive Avionics Division
Signature Technology Directorate



JOSEPH. C. FAISON, Chief
Defensive Avionics Division
Signature Technology Directorate

FOR THE COMMANDER



FRANKLIN D. CHERRY, Director
Signature Technology Directorate

If your address has changed, if you wish to be removed from our mailing list, or if the addressee is no longer employed by your organization please notify WRDC/SNA, WPAFB, OH 45433-6523 to help us maintain a current mailing list.

Copies of this report should not be returned unless return is required by security considerations, contractual obligations, or notice on a specific document.

UNCLASSIFIED

SECURITY CLASSIFICATION OF THIS PAGE

REPORT DOCUMENTATION PAGE				Form Approved OMB No. 0704-0188	
1a. REPORT SECURITY CLASSIFICATION UNCLASSIFIED			1b. RESTRICTIVE MARKINGS NONE		
2a. SECURITY CLASSIFICATION AUTHORITY N/A			3. DISTRIBUTION/AVAILABILITY OF REPORT Approved for Public Release; Distribution is Unlimited		
2b. DECLASSIFICATION/DOWNGRADING SCHEDULE N/A					
4. PERFORMING ORGANIZATION REPORT NUMBER(S) 718295-9			5. MONITORING ORGANIZATION REPORT NUMBER(S) WRDC-TR- 90-9003, Vol. II		
6a. NAME OF PERFORMING ORGANIZATION Ohio State University ElectroScience Laboratory		6b. OFFICE SYMBOL (if applicable)	7a. NAME OF MONITORING ORGANIZATION Wright Research and Development Center Signature Technology Directorate (WRDC/SNA)		
6c. ADDRESS (City, State, and ZIP Code) 1320 Kinnear Road Columbus, OH 43212			7b. ADDRESS (City, State, and ZIP Code) Wright-Patterson AFB, OH 45433-6523		
8a. NAME OF FUNDING/SPONSORING ORGANIZATION		8b. OFFICE SYMBOL (if applicable)	9. PROCUREMENT INSTRUMENT IDENTIFICATION NUMBER F33615-86-K-1023		
8c. ADDRESS (City, State, and ZIP Code)			10. SOURCE OF FUNDING NUMBERS		
			PROGRAM ELEMENT NO. 61101F	PROJECT NO. ILIR	TASK NO. A6
11. TITLE (Include Security Classification) UNIFORM THEORY OF DIFFRACTION (UTD) SCATTERING FROM STRUCTURES, INCLUDING HIGHER ORDER TERMS ; VOLUME II: Edge Wave Edge and Vertex Diffraction					
12. PERSONAL AUTHOR(S) Ivrissimtzis, Leonidas P.; and Marhefka, Ronald J.					
13a. TYPE OF REPORT Final		13b. TIME COVERED FROM APR 86 TO DEC 89	14. DATE OF REPORT (Year, Month, Day) November 1990		15. PAGE COUNT 104
16. SUPPLEMENTARY NOTATION This report volume is Volume II of six volumes. This report was submitted as a M. Sc. thesis by L. Ivrissimtzis in 1988.					
17. COSATI CODES			18. SUBJECT TERMS (Continue on reverse if necessary and identify by block number) Uniform Theory of Diffraction (UTD), Geometric Theory of Diffraction (GTD), Ray Theory, Electromagnetic Scattering, Radar Cross Section (RCS)		
FIELD	GROUP	SUB-GROUP			
19. ABSTRACT (Continue on reverse if necessary and identify by block number) The diffraction of an edge wave by the vertex and the edges of a semi-infinite wedge (a trihedron) is studied. The edge wave is produced by an infinitesimal electric dipole source located in close vicinity of one of the edges of the trihedron and suffi- ciently far from the vertex. The radiation integral of the currents that would flow over an infinite wedge, which is then truncated, is evaluated asymptotically, yielding an end- point effect. The final result is improved by introducing a fringe current component in- duced by the terminating edges, and exhibits fairly good agreement with moment method computations and measured data. The field diffracted by a corner and propagating along the edge of a flat plate structure can be obtained via reciprocity. The edge wave corner diffraction coefficient thus derived may be utilized for the calculation of corner-to-corner and corner-to-edge diffraction mechanisms. <i>Keywords</i>					
20. DISTRIBUTION/AVAILABILITY OF ABSTRACT <input checked="" type="checkbox"/> UNCLASSIFIED/UNLIMITED <input type="checkbox"/> SAME AS RPT. <input type="checkbox"/> DTIC USERS			21. ABSTRACT SECURITY CLASSIFICATION Unclassified		
22a. NAME OF RESPONSIBLE INDIVIDUAL J. Earl Jones			22b. TELEPHONE (Include Area Code) (513)- 255-9335		22c. OFFICE SYMBOL WRDC/SNA

This volume of the Final Technical Report for Contract No. F33615-86-K-1023 was originally submitted as a Master of Science Thesis to The Ohio State University Department of Electrical Engineering by Leonidas P. Ivrisimtzis in 1988.



Accession For	
NTIS GRA&I	<input checked="" type="checkbox"/>
DTIC TAB	<input type="checkbox"/>
Unannounced	<input type="checkbox"/>
Justification	
By	
Distribution/	
Availability Codes	
Dist	Avail and/or Special
A-1	

TABLE OF CONTENTS

LIST OF FIGURES	iv
I. Introduction	1
II. Edge Waves	4
2.1 Introduction.	4
2.2 The canonical solution to the half plane problem. Some limiting cases.	5
2.3 The limiting behavior of the dyadic Green's function for a dipole radiating in the close vicinity of the infinite edge of a wedge. . .	9
2.4 The half plane case.	11
2.5 Discussion and numerical results.	13
III. A Physical Optics Approximation of the Edge Wave Vertex Diffracted Field	18
3.1 Introduction.	18
3.2 Formulation of the Physical Optics solution.	19
3.3 The Physical Optics vertex diffracted wave.	24
3.4 Numerical results and discussion.	27
IV. An Equivalent Current Approach	34
4.1 Introduction.	34

IV.	An Equivalent Current Approach	34
4.1	Introduction.	34
4.2	The equivalent edge currents concept.	35
4.2.1	Generalized equivalent currents. The half plane case. . .	38
4.3	Michaeli's edge currents in an oblique edge fixed frame.	42
4.4	Vertex diffraction of an edge wave excited by a dipole.	45
4.4.1	Edge wave vertex diffracted field.	48
4.4.2	Edge wave edge diffracted field.	61
4.4.3	A transition function for the guiding edge diffracted field. . .	64
4.5	Discussion and numerical results.	65
V.	Conclusions	78
A.	A Uniform Asymptotic Approximation of the Integral $I_p(k) =$ $\int_0^\infty G(t) t^{-p-1} dt$ for $\Re(p) < 0$	80
B.	Edge Wave Transition Functions	86
	REFERENCES	93

LIST OF FIGURES

1	An infinitesimal electric dipole source radiating in the close vicinity of one of the edges of a semi-infinite wedge.	2
2	Half plane illuminated by an arbitrarily polarized plane wave. . . .	6
3	An infinitesimal electric dipole source radiating in the close vicinity of the edge of an infinite perfectly conducting wedge.	8
4	Far field region $\hat{\beta}$ -directed wave of the infinitesimal dipole source of Fig. 3 at an azimuthal angle $\phi = 45^\circ$ for: A) $\rho' = 0.025\lambda_0$, $\phi' = 135^\circ$, B) $\rho' = 0.05\lambda_0$, $\phi' = 75^\circ$, C) $\rho' = 0.075\lambda_0$, $\phi' = 180^\circ$	15
5	Far field region $\hat{\phi}$ -directed wave of the infinitesimal dipole source of Fig. 3 at an azimuthal angle $\phi = 45^\circ$ for: A) $\rho' = 0.025\lambda_0$, $\phi' = 135^\circ$, B) $\rho' = 0.05\lambda_0$, $\phi' = 75^\circ$, C) $\rho' = 0.075\lambda_0$, $\phi' = 180^\circ$	15
6	Far field region $\hat{\beta}$ -directed wave of the infinitesimal dipole source of Fig. 3 at an azimuthal angle $\phi = 105^\circ$ for: A) $\rho' = 0.025\lambda_0$, $\phi' = 135^\circ$, B) $\rho' = 0.05\lambda_0$, $\phi' = 75^\circ$, C) $\rho' = 0.075\lambda_0$, $\phi' = 180^\circ$	16
7	Far field region $\hat{\phi}$ -directed wave of the infinitesimal dipole source of Fig. 3 at an azimuthal angle $\phi = 105^\circ$ for: A) $\rho' = 0.025\lambda_0$, $\phi' = 135^\circ$, B) $\rho' = 0.05\lambda_0$, $\phi' = 75^\circ$, C) $\rho' = 0.075\lambda_0$, $\phi' = 180^\circ$	16
8	Far field region $\hat{\beta}$ -directed wave of the infinitesimal dipole source of Fig. 3 at an azimuthal angle $\phi = 165^\circ$ for: A) $\rho' = 0.025\lambda_0$, $\phi' = 135^\circ$, B) $\rho' = 0.05\lambda_0$, $\phi' = 75^\circ$, C) $\rho' = 0.075\lambda_0$, $\phi' = 180^\circ$	17

9	Far field region $\hat{\phi}$ -directed wave of the infinitesimal dipole source of Fig. 3 at an azimuthal angle $\phi = 165^0$ for: A) $\rho' = 0.025\lambda_0$, $\phi' = 135^0$, B) $\rho' = 0.05\lambda_0$, $\phi' = 75^0$, C) $\rho' = 0.075\lambda_0$, $\phi' = 180^0$	17
10	Geometry for the edge wave edge and vertex diffraction problem. .	19
11	Geometry for the asymptotic evaluation of the radiation integral of the surface edge wave currents.	20
12	The square plate used in the numerical application of the Physical Optics solution.	28
13	Far field region $\hat{\beta}$ -directed wave radiated by the dipole of Fig. 12 at an azimuthal angle $\phi = 30^0$	30
14	Far field region $\hat{\beta}$ -directed wave radiated by the dipole of Fig. 12 at an azimuthal angle $\phi = 45^0$	30
15	Far field region $\hat{\beta}$ -directed wave radiated by the dipole of Fig. 12 at an azimuthal angle $\phi = 90^0$	31
16	Far field region $\hat{\beta}$ -directed wave radiated by the dipole of Fig. 12 at an azimuthal angle $\phi = 120^0$	31
17	Far field region $\hat{\beta}$ -directed wave radiated by the dipole of Fig. 12 at an azimuthal angle $\phi = 150^0$	32
18	Far field region $\hat{\beta}$ -directed wave radiated by the dipole of Fig. 12 at an azimuthal angle $\phi = 180^0$	32
19	Far field region $\hat{\phi}$ -directed wave radiated by the dipole of Fig. 12 at an azimuthal angle $\phi = 120^0$	33
20	Far field region $\hat{\phi}$ -directed wave radiated by the dipole of Fig. 12 at an azimuthal angle $\phi = 150^0$	33

21	Oblique edge fixed coordinate system for the definition of Michaeli's equivalent currents.	43
22	Angular sector geometry for the comparison of the generalized and Michaeli's equivalent edge currents.	56
23	Far field $\hat{\beta}$ -directed component at an elevation angle $\beta = 30^\circ$ for the angular sector geometry of Fig. 22.	58
24	Far field $\hat{\phi}$ -directed component at an elevation angle $\beta = 30^\circ$ for the angular sector geometry of Fig. 22.	58
25	Far field $\hat{\beta}$ -directed component at an elevation angle $\beta = 90^\circ$ for the angular sector geometry of Fig. 22.	59
26	Far field $\hat{\phi}$ -directed component at an elevation angle $\beta = 90^\circ$ for the angular sector geometry of Fig. 22.	59
27	Far field $\hat{\beta}$ -directed component at an elevation angle $\beta = 150^\circ$ for the angular sector geometry of Fig. 22.	60
28	Far field $\hat{\phi}$ -directed component at an elevation angle $\beta = 150^\circ$ for the angular sector geometry of Fig. 22.	60
29	Far field $\hat{\beta}$ -directed field at an azimuthal angle $\phi = 60^\circ$ for the square plate of Fig. 12.	69
30	Far field $\hat{\beta}$ -directed field at an azimuthal angle $\phi = 90^\circ$ for the square plate of Fig. 12.	70
31	Far field $\hat{\beta}$ -directed field at an azimuthal angle $\phi = 120^\circ$ for the square plate of Fig. 12.	71
32	Far field $\hat{\beta}$ -directed field at an azimuthal angle $\phi = 135^\circ$ for the square plate of Fig. 12.	72
33	Far field $\hat{\beta}$ -directed field at an azimuthal angle $\phi = 150^\circ$ for the square plate of Fig. 12.	73

34	Far field $\hat{\beta}$ -directed field at an azimuthal angle $\phi = 180^0$ for the square plate of Fig. 12.	73
35	Geometry of the monopole-rectangular plate configuration used for comparison with measured data.	74
36	Far field $\hat{\beta}$ -directed field at an azimuthal angle $\phi = 180^0$ for the rectangular plate of Fig. 35. <u>Solid line</u> : Calculated field, <u>Dashed line</u> : Measured field, <u>Dotted line</u> : Moment method solution.	75
37	Far field $\hat{\beta}$ -directed field at an azimuthal angle $\phi = 150^0$ for the rectangular plate of Fig. 35. <u>Solid line</u> : Calculated field, <u>Dashed line</u> : Measured field, <u>Dotted line</u> : Moment method solution.	76
38	Amplitude of the edge wave transition function.	90
39	Phase of the edge wave transition function.	91

CHAPTER I

Introduction

The diffraction of scalar (acoustical) waves by the tip of an elliptical perfectly conducting cone was studied by Krauss and Levine [1]. Satterwhite and Kouyoumjian [2] examined the vector electromagnetic problem and presented a Green's dyadic for a source radiating in the presence of an angular sector. However, their solution, expressed in terms of non-closed form Lamé functions, is cumbersome for numerical calculations. Furthermore, so far it has not appeared possible to asymptotically identify a "corner diffraction coefficient" from this eigenfunction representation.

Recently, Burnside and Pathak [3] proposed a corner diffraction coefficient which successfully predicted the corner effect of numerous plate structures. Their solution is based on the asymptotic evaluation of the radiation integral involving the equivalent currents that would exist in the absence of the corner. A corner diffraction term is then established by heuristically, but at present empirically, modifying the final result. Sikta [4] modified the spread factor of the diffracted field in [3] and applied a limiting process to derive the wave diffracted by the corner and propagating along one of the edges of a plane right angular sector. By introducing an empirically established "reflection coefficient" he utilized his edge wave corner diffraction coefficient in the calculation of the double and triple diffraction by two adjacent corners of a flat plate structure.

The equivalent current approach is adopted herein to study the vertex diffraction of an electromagnetic wave guided along one of the edges of a semi-infinite wedge. The geometry of the problem is illustrated in Fig. 1. The dipole source is radiating in the close vicinity of the edge and excites a paraxial field guided by one of the edges of the trihedron - hence the term "edge wave". Explicit expressions of this field are derived in Chapter II based on the limiting behavior of the Green's dyadic for an infinite wedge [7] and small distances of the dipole from the edge, and the canonical solution (Fresnel integral representation) to the half plane problem for plane wave grazing incidence. A simple edge diffraction coefficient can then be established valid for small distances of the source from the edge and for paraxial field calculations.

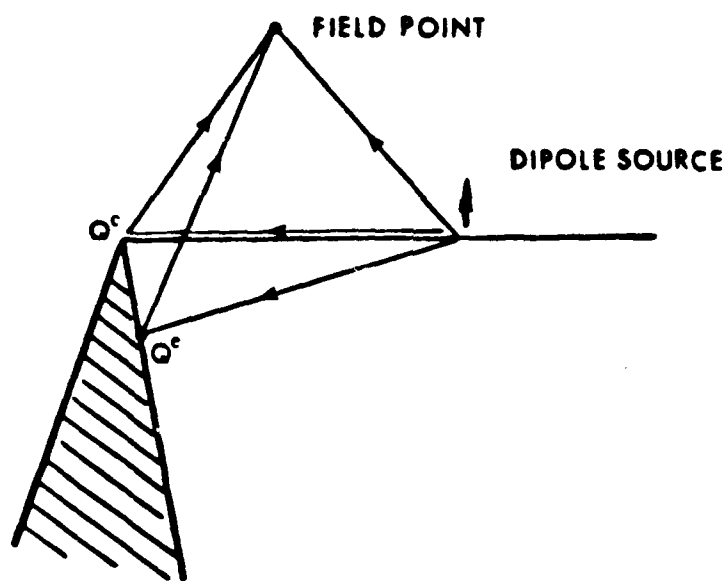


Figure 1: An infinitesimal electric dipole source radiating in the close vicinity of one of the edges of a semi-infinite wedge.

In Chapter III a Physical Optics approximation of the vertex diffracted field is presented, based on the currents that would be induced by the edge guided wave for an infinite wedge which is then truncated. The asymptotic evaluation

of the surface currents radiation integral appropriately encounters the edge wave singularity consistent with Meixner's edge condition [5].

The concept of equivalent currents is generally examined in Chapter IV. The end point contribution to the radiation integral of these currents "excited" by the impinging edge wave is interpreted as a vertex diffraction term. Two types of equivalent currents for arbitrary aspects of observation is shown to yield comparable results. Edge wave vertex and edge wave edge diffraction coefficients can then be established by an empirical modification of the asymptotic field expressions. The validity of the approach is confirmed via comparison with moment method results and pattern measurements for a small dipole radiating in the close vicinity of one of the edges of a polygonal plate.

Every structure considered in the present work is assumed perfectly conducting. Furthermore, an $\exp(j\omega_0 t)$ time dependence has been adopted and suppressed in the following analysis.

CHAPTER II

Edge Waves

2.1 Introduction.

The term "edge waves" in the present work defines waves propagating along the edge of a (possibly curved) wedge. The edge wave is actually a form of a maxwellian field guided by the edge, and exhibiting the proper singularity in accordance with Meixner's edge condition.

As shown later in this chapter, such a paraxial singular field can be excited either by a plane wave at grazing incidence, or by a dipole radiating in the close vicinity of the edge. The vertex of a terminated edge illuminated by a plane or spherical wave can also excite an edge wave. Independently of the excitation, but sufficiently far from its source, the edge wave behaves and can be treated as a ray optical field. However, application of ray optical techniques (UTD) is not straightforward, mainly due to the singular behavior of the paraxial fields. An asymptotic high frequency approximation which encounters this peculiarity is attempted in Chapters III and IV.

Two types of excitation of an edge wave are examined in this chapter: a plane wave grazing the edge of a half plane and an elementary dipole radiating in the near vicinity of the edge of an infinite wedge. The limiting behavior of the fields predicted by the canonical solution for the half plane problem and the leading term of the power series expansion of the Green's dyadic with respect to the numerical

distance $k_0\rho'$ of the point source from the edge (where $k_0 = 2\pi/\lambda$ denotes the free space wavenumber) are examined. The two cases are related via reciprocity so that a simple edge diffraction dyadic coefficient can be readily established and applied in the approximation of the patterns of complex sources radiating in the close vicinity of the edge or in paraxial field calculations.

2.2 The canonical solution to the half plane problem. Some limiting cases.

A perfectly conducting half plane is illuminated by an arbitrarily polarized plane wave, as depicted in Fig. 2. For convenience, the origin of our reference frame has been chosen to coincide with the origin Q^e of the Keller cone of diffracted rays, defined by the angle β' of incidence and the observation point $R(\rho, \phi, z)$. Since the only dependence of the total field on the z coordinate is incorporated into the factor $\exp(-jk_0z \cos \beta')$, the problem is essentially quasi two dimensional. It can be easily shown that the $\hat{\rho}$ and $\hat{\phi}$ -directed field components can be expressed in terms of the E_z and H_z components via the equations

$$\vec{E}_t = -jk_z \frac{\nabla_t E_z}{k_0^2 - k_z^2} + j\omega_0\mu_0 \frac{\vec{z} \times \nabla_t H_z}{k_0^2 - k_z^2} \quad (2.1a)$$

$$\vec{H}_t = -jk_z \frac{\nabla_t H_z}{k_0^2 - k_z^2} - j\omega_0\epsilon_0 \frac{\vec{z} \times \nabla_t E_z}{k_0^2 - k_z^2} \quad (2.1b)$$

where $k_z = k_0 \cos \beta'$, $\omega_0 = k_0/\sqrt{\mu_0\epsilon_0}$ and μ_0, ϵ_0 are the permeability and the permittivity of the free space. The operator ∇_t is defined by

$$\nabla_t \triangleq \hat{\rho} \frac{\partial}{\partial \rho} + \hat{\phi} \frac{1}{\rho} \frac{\partial}{\partial \phi} \quad (2.2)$$

Sommerfeld's canonical solution to the half plane problem can be expressed in a compact form in terms of the modified Fresnel Integral. In particular, we have

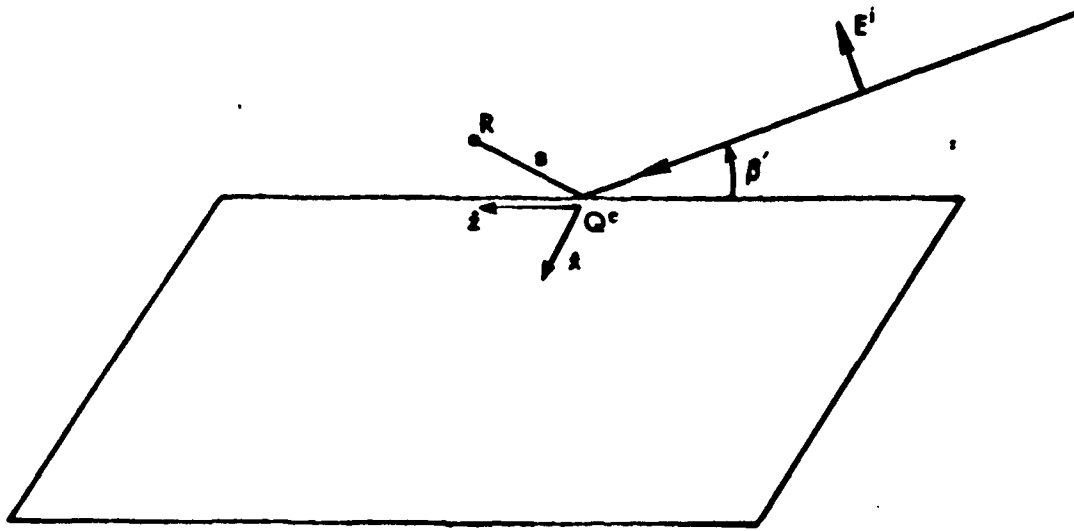


Figure 2: Half plane illuminated by an arbitrarily polarized plane wave.

$$\begin{Bmatrix} E_z \\ H_z \end{Bmatrix} = \begin{Bmatrix} E_z^i(Q^c) \\ H_z^i(Q^c) \end{Bmatrix} \{u^i(\rho, \phi; \phi'; \beta') \mp u^r(\rho, \phi; \phi'; \beta')\} \exp(-jk_0 s) \quad (2.3)$$

where we substituted

$$u^{i,r}(\rho, \phi; \phi'; \beta') = K_-(-\sqrt{2k_0\rho \sin \beta'} \cos \frac{\phi \mp \phi'}{2}) \quad (2.4)$$

and s can be expressed in terms of the coordinates (ρ, ϕ, z) of the observation point R as

$$s = \rho \sin \beta' + z \cos \beta' \quad (2.5)$$

The function $K_-(x)$ is the modified Fresnel Integral defined by [6]

$$K_-(x) = \frac{1}{\sqrt{\pi}} F_-(x) \exp\{j(x^2 + \pi/4)\} \quad (2.6)$$

$$F_-(x) = \int_x^\infty \exp(-jt^2) dt \quad (2.7)$$

Incorporating eqs. (2.3)-(2.7) into eqs. (2.1a)-(2.1b) and performing the differentiations one can readily obtain a complete representation of the transverse (to the z direction) components of the electric and magnetic fields. Namely, one finds that

$$\begin{aligned}
 E_\rho(\rho, \phi, z) = & \left\{ E_{\beta'}^i(Q^e) \cos \beta' [u^i \cos(\phi - \phi') - u^r \cos(\phi + \phi')] \right. \\
 & + E_{\phi'}^i(Q^e) [u^i \sin(\phi - \phi') + u^r \sin(\phi + \phi')] \\
 & + \frac{2 \exp(-j\pi/4)}{\sqrt{2\pi k_0 \rho \sin \beta'}} \sin \frac{\phi}{2} \\
 & \left. \cdot [E_{\beta'}^i(Q^e) \cos \beta' \sin \frac{\phi'}{2} + E_{\phi'}^i(Q^e) \cos \frac{\phi'}{2}] \right\} \exp(-jk_0 z)
 \end{aligned} \tag{2.8a}$$

$$\begin{aligned}
 E_\phi(\rho, \phi, z) = & \left\{ -E_{\beta'}^i(Q^e) \cos \beta' [u^i \sin(\phi - \phi') - u^r \sin(\phi + \phi')] \right. \\
 & + E_{\phi'}^i(Q^e) [u^i \cos(\phi - \phi') + u^r \cos(\phi + \phi')] \\
 & + \frac{2 \exp(-j\pi/4)}{\sqrt{2\pi k_0 \rho \sin \beta'}} \cos \frac{\phi}{2} \\
 & \left. \cdot [E_{\beta'}^i(Q^e) \cos \beta' \sin \frac{\phi'}{2} + E_{\phi'}^i(Q^e) \cos \frac{\phi'}{2}] \right\} \exp(-jk_0 z)
 \end{aligned} \tag{2.8b}$$

while the transverse magnetic field \vec{H}_t can be obtained by using duality.

Of particular interest in our work is the limiting behavior of the above expressions for small values of the parameter

$$\epsilon(\rho; \beta') = k_0 \rho \sin \beta' \tag{2.9}$$

Eqs. (2.8a)-(2.8b) can then be represented by a power series expansion of the form

$$\vec{E}(\rho, \phi, z) = \frac{\vec{C}_{-1/2}(\phi, z)}{\sqrt{\epsilon}} + \sum_{l=0}^{\infty} \vec{C}_l(\phi, z) \epsilon^l \tag{2.10}$$

As $\epsilon(\rho; \beta') \rightarrow 0$ one may write

$$E_z(\rho, \phi, z) = O(\epsilon^0) \quad (2.11)$$

$$\begin{aligned} \bar{E}_t(\rho, \phi, z) = & \sqrt{\frac{2}{\pi k_0 \rho \sin \beta'}} \exp(-j\pi/4) (\hat{\rho} \sin \frac{\phi}{2} + \hat{\phi} \cos \frac{\phi}{2}) \\ & \cdot \left[E_{\beta'}^i(Q^e) \cos \beta' \sin \frac{\phi'}{2} + E_{\phi'}^i(Q^e) \cos \frac{\phi'}{2} \right] \exp(-jk_0 s) \\ & + \bar{O}(\epsilon^0) \end{aligned} \quad (2.12)$$

where $\bar{O}(\epsilon^l)$ denotes the remainder in the power series expansion and its order with respect to ϵ .

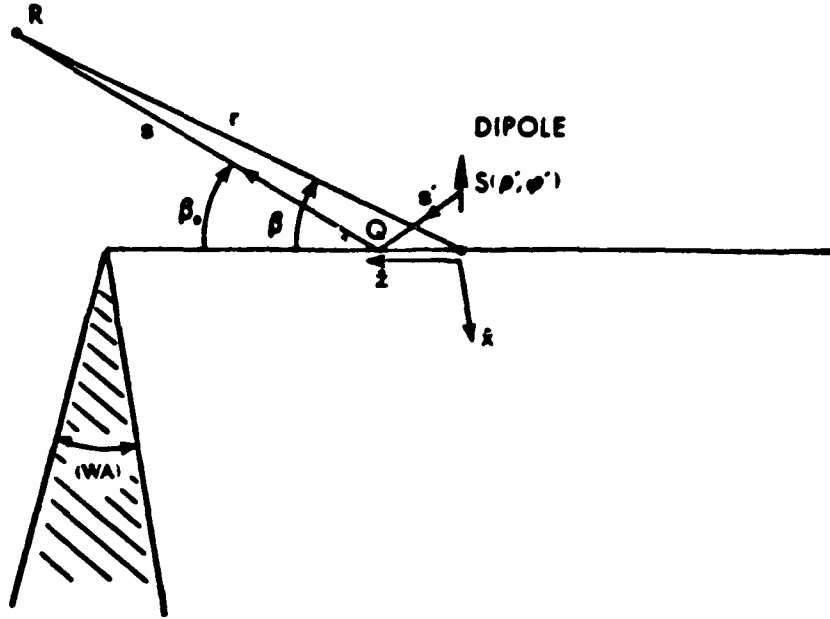


Figure 3: An infinitesimal electric dipole source radiating in the close vicinity of the edge of an infinite perfectly conducting wedge.

At grazing incidence the leading term in the power series expansion of $\bar{E}_t(\rho, \phi, z)$ represents a wave guided along the edge of the half plane (an edge wave) given by

$$\bar{E}^{ew}(\rho, \phi, z) = \sqrt{\frac{2}{\pi k_0 \rho}} \exp(-j\pi/4) (\hat{\rho} \sin \frac{\phi}{2} + \hat{\phi} \cos \frac{\phi}{2})$$

$$S(\beta', \phi') \exp(-jk_0 z) \quad (2.13)$$

where

$$S(\beta', \phi') = \frac{[E_{\beta'}^i(Q^e) \sin(\phi'/2) + E_{\phi'}^i(Q^e) \cos(\phi'/2)]}{\sqrt{\sin \beta'}} \quad (2.14)$$

is a source related factor. The wave described by eqs. (2.13), (2.14) satisfies the wave equation, the Meixner's edge condition and dominates the field in the paraxial region.

2.3 The limiting behavior of the dyadic Green's function for a dipole radiating in the close vicinity of the infinite edge of a wedge.

Let us consider the more general reciprocal problem of a point source $\vec{j}^e = \vec{p}^e \delta(\vec{r} - \vec{r}')$ radiating in the presence of a perfectly conducting infinite wedge as depicted in Fig. 3. The field produced by this dipole-wedge configuration can be formally written as

$$\vec{E}(\vec{r}) = j\omega_0\mu_0 \vec{\Gamma}(\vec{r}, \vec{r}') \cdot \vec{p}^e \quad (2.15)$$

where $\vec{\Gamma}(\vec{r}, \vec{r}')$ is the Green's dyadic for the wedge. An eigenfunction series representation of $\vec{\Gamma}(\vec{r}, \vec{r}')$ is given in [7].

For convenience the source point is located at $S(\rho', \phi', 0)$, ($r' = \rho'$, $\beta' = \pi/2$). Furthermore, let $k_0 r \gg 1$, so that the spherical Hankel functions of the second kind involved in the series representation assume their asymptotic form. The limiting form of the Green's dyadic for small values of the parameter $\epsilon = k_0 \rho' \sin \beta$ is of interest here. After some tedious manipulation it can be shown that

$$\begin{aligned} \vec{\Gamma}(\vec{r}, \vec{r}') = & C(\nu) (k_0 \rho' \sin \beta')^{\nu-1} (\hat{\beta} \cos \beta \sin \nu \phi + \hat{\phi} \cos \nu \phi) \\ & (\hat{\rho}' \sin \nu \phi' + \hat{\phi}' \cos \nu \phi') \frac{\exp(-jk_0 r)}{r} + \bar{O}(\epsilon^0) \end{aligned} \quad (2.16)$$

with the constant factor $C(\nu)$ defined by

$$C(\nu) = \frac{\nu \Gamma(2\nu + 2) \exp\{j(\nu + 1)\pi/2\}}{\sqrt{\pi} 2^{3\nu+1} \Gamma(\nu) \Gamma(\nu + 1) \Gamma(\nu + 3/2)} \quad (2.17)$$

and

$$\nu = \frac{1}{n} ; \quad n = \frac{2\pi - (WA)}{\pi} \quad (2.18)$$

where (WA) denotes the wedge angle. Hence, the total field for a general wedge is written as

$$\begin{aligned} \bar{E}(\vec{r}) = & j\omega_0\mu_0 C(\nu) (k_0\rho' \sin\beta)^{\nu-1} (\hat{\beta} \cos\beta \sin\nu\phi + \hat{\phi} \cos\nu\phi) \\ & \cdot (p_{\rho'}^e \sin\nu\phi' + p_{\phi'}^e \cos\nu\phi') \frac{\exp(-jk_0r)}{r} + \bar{O}(\epsilon^0) \end{aligned} \quad (2.19)$$

which, in the case of the half plane, reduces to the following expression:

$$\begin{aligned} \bar{E}(\vec{r}) = & -\frac{\sqrt{k_0} Z_0 \exp(j\pi/4)}{2\pi\sqrt{2\pi}} A^e(\rho', \phi') \\ & \cdot \frac{\hat{\beta} \cos\beta \sin(\phi/2) + \hat{\phi} \cos(\phi/2)}{\sqrt{\sin\beta}} \frac{\exp(-jk_0r)}{r} + \bar{O}(\epsilon^0) \end{aligned} \quad (2.20)$$

where

$$A^e(\rho', \phi') = \frac{p_{\rho'}^e \sin(\phi'/2) + p_{\phi'}^e \cos(\phi'/2)}{\sqrt{\rho'}} \quad (2.21)$$

is a constant source factor. The remainder $\bar{O}(\epsilon^0)$ in eq. (2.19) can be expressed in a closed form only for the case of the half plane. Specifically, it can be obtained via reciprocity from eqs. (2.8a)-(2.8b) after subtracting the edge wave term. In the case of a general wedge angle the remainder is essentially a power series of the small parameter ϵ , the coefficients of which can be derived from the eigenfunction series representation of the Green's dyadic.

The lower order term in the RHS of eq. (2.19) dominates in the paraxial region (edge wave) and reveals the strong coupling between the dipole source and the edge. It is a spherical ray optical wave that satisfies Maxwell's equations.

Clearly, the behavior of the electric field intensity of the edge wave is independent of the orientation of the source.

2.4 The half plane case.

As pointed out in the previous section an exact closed form representation of the Fraunhofer region field produced by the dipole \vec{p}^e radiating in the presence of an infinite half plane can be obtained by applying the reciprocity theorem to eqs. (2.8a)-(2.8b). For small distances of the dipole from the edge one can retain only the two leading terms in the power series expansion of the modified Fresnel integrals involved in the canonical solution. It turns out that the total radiated field can be described by the superposition of three terms:

i) The incident field produced by the dipole in the absence of the half plane multiplied by a factor of $1/2$,

ii) The field produced by the image of the dipole source with respect to an infinite plane multiplied by a factor of $1/2$,

iii) An edge associated field, which may be treated as an edge diffracted wave (emanating from Q^e) in a UTD sense.

It should be noted that the components i), ii) illuminate the whole space and not only the regions bounded by the Geometrical Optics incident and reflected shadow boundaries. Under this consideration the total field is uniform everywhere and satisfies the appropriate boundary conditions on the conducting half plane. In a matrix notation one can write for the radiated field

$$\begin{pmatrix} E_\beta(\vec{r}) \\ E_\phi(\vec{r}) \end{pmatrix} = \begin{pmatrix} E_\beta^{ew}(\vec{r}) \\ E_\phi^{ew}(\vec{r}) \end{pmatrix} + \frac{jk_0 Z_0}{8\pi} \frac{\exp(-jk_0 r)}{r} \begin{pmatrix} \exp\{jk_0 \rho' \sin \beta \cos(\phi - \phi')\} \\ \exp\{jk_0 \rho' \sin \beta \cos(\phi - \phi')\} \end{pmatrix}$$

$$\begin{aligned}
& \cdot \left\{ \begin{array}{ccc} -\cos \beta \cos(\phi - \phi') & -\cos \beta \sin(\phi - \phi') & \sin \beta \\ \sin(\phi - \phi') & -\cos(\phi - \phi') & 0 \end{array} \right\} \\
& + \exp\{jk_0 \rho' \sin \beta \cos(\phi + \phi')\} \\
& \cdot \left\{ \begin{array}{ccc} \cos \beta \cos(\phi + \phi') & -\cos \beta \sin(\phi + \phi') & -\sin \beta \\ -\sin(\phi + \phi') & -\cos(\phi + \phi') & 0 \end{array} \right\} \\
& \cdot \left\{ \begin{array}{c} p_{\rho'}^e \\ p_{\phi'}^e \\ p_{z'}^e \end{array} \right\} \quad (2.22)
\end{aligned}$$

in which $E^{\bar{e}u}(\bar{r})$ denotes the edge associated term. The latter can be readily obtained from eqs. (2.13), (2.14) or eqs. (2.20), (2.21). By empirically generalizing those results the diffracted field can be expressed in a more familiar notation by the following equation:

$$\begin{aligned}
\left\{ \begin{array}{c} E_{\beta_0}^{\bar{e}u} \\ E_{\phi}^{\bar{e}u} \end{array} \right\} &= \frac{2 \exp(-j\pi/4)}{\sqrt{2\pi k_0 \sin \beta_0}} \\
& \cdot \left\{ \begin{array}{cc} \sin \frac{\phi'}{2} \sin \frac{\phi}{2} & \cos \beta_0 \cos \frac{\phi'}{2} \sin \frac{\phi}{2} \\ \sec \beta_0 \sin \frac{\phi'}{2} \cos \frac{\phi}{2} & \cos \frac{\phi'}{2} \cos \frac{\phi}{2} \end{array} \right\} \left\{ \begin{array}{c} E_{\beta_0}^{\text{ir}}(Q^e) \\ E_{\phi}^{\text{ir}}(Q^e) \end{array} \right\} \\
& \cdot \sqrt{\frac{s'}{s(s+s')}} \exp(-jk_0 s) \quad (2.23)
\end{aligned}$$

The various parameters involved in the above expression are shown in Fig. 3. Also, $E_{\beta_0, \phi}^{\text{ir}}(Q^e)$ are the ray optical components of the total field incident at the point Q^e and produced by the dipole source, namely

$$\left\{ \begin{array}{c} E_{\beta_0}^{\text{ir}} \\ E_{\phi}^{\text{ir}} \end{array} \right\} = -jk_0 Z_0 \frac{\exp(-jk_0 s')}{4\pi s'} \left\{ \begin{array}{c} \cos \beta_0' p_{\rho'}^e \\ p_{\phi'}^e \end{array} \right\} \quad (2.24)$$

with $\beta'_0 = \beta_0$ denoting the diffraction angle. It should be mentioned that eq. (2.23) reduces to the correct limiting expression of the field in the paraxial region of the edge ($\beta_0 \rightarrow 0$), exhibiting the appropriate edge singularity.

2.5 Discussion and numerical results.

The accuracy of the "edge wave" solution given by eqs. (2.23)-(2.24) in predicting the field for small distances of a point dipole source from the edge of a half plane is illustrated in Figs. 4-9, in comparison with the exact Sommerfeld (Fresnel integral) representation, for several azimuthal angles ϕ of the observation point which, for simplicity, is removed at infinity. The infinitesimal source has a dipole moment radially directed and it is located at the points $(\rho', \phi') = (0.025\lambda_0, 135^\circ), (0.05\lambda_0, 75^\circ), (0.075\lambda_0, 180^\circ)$, in terms of the associated system of cylindrical coordinates centered at the projection of the point source onto the edge of the half plane. The amplitude pattern of the $\hat{\beta}$ - and $\hat{\phi}$ -directed field components is then plotted against the elevation angle of the observation point. Comparison with the exact representation of the total field shows that a distance $\rho' < 0.05\lambda_0$ is adequate for the total field to be accurately described (within 1.0 dB of magnitude) by eqs. (2.23)-(2.24). As a matter of fact, the accuracy is improved for smaller distances of the dipole or the field point (i.e., when grazing incidence is approached) from the edge of the half plane. In the latter case the total field exhibits a singular behavior which is consistent with the edge condition.

Clearly, the analysis of the waves associated with the edge of an infinite wedge fails in the case of finite or semi-infinite edges. First, the edge wave term should be suitably modified so that the singularity in the extension of the edge is eliminated. Second, the corner effects should be incorporated in the total solution. Asymp-

totically, the end point effect is additively introduced into the total solution and corresponds to a corner diffracted ray. On the other hand, the edge wave singularity is compensated multiplicatively with the introduction of the proper transition dyadic. Within this context, for a dipole radiating in the close vicinity of a terminated edge and sufficiently far from the corner (in the angular sector case), the total field can be written as

$$\vec{E}^t = \vec{E}^0 + E\vec{e}_w \cdot \vec{T} + \vec{E}^d \quad (2.25)$$

where \vec{E}^0 is half the field produced by the dipole and its image with respect to the plane of the plate in free space, \vec{E}^d is the sum of the corner and, possibly, the terminating edge diffracted field and \vec{T} is a transition dyadic to be determined. An empirical definition of this transition dyadic is given in Chapter IV.

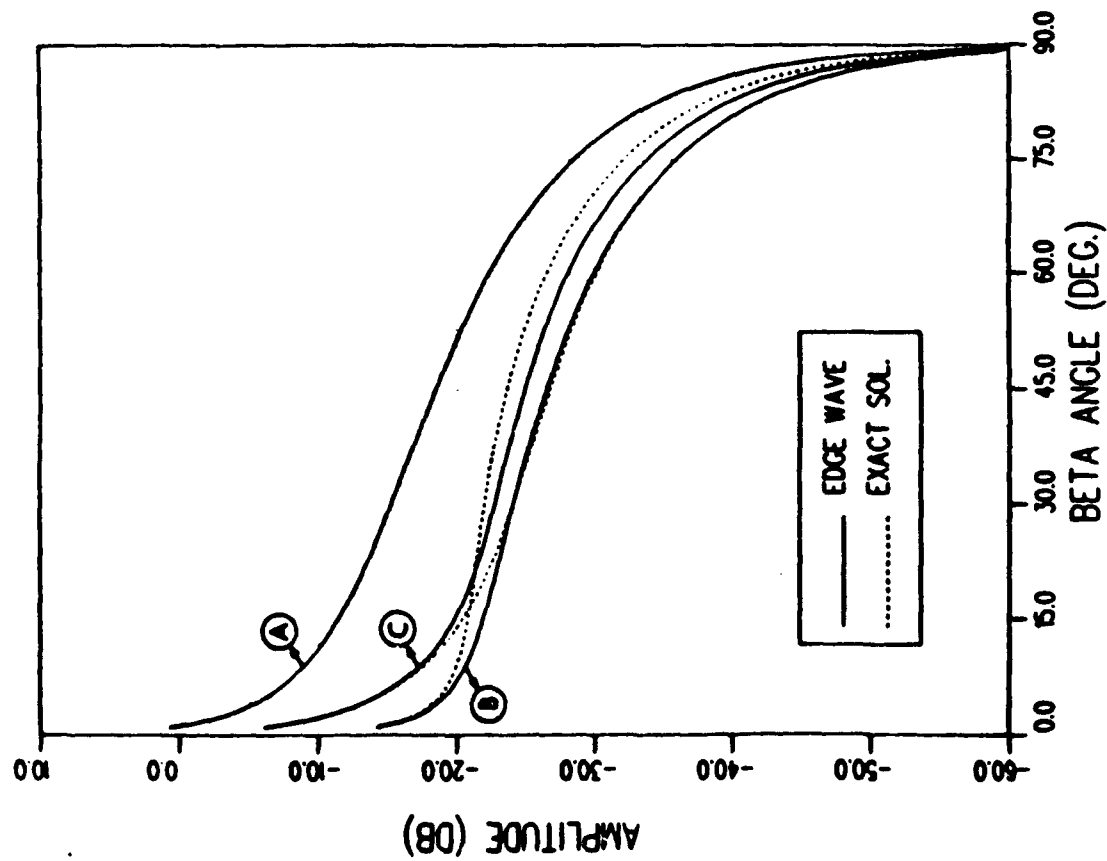


Figure 4: Far field region β -directed wave of the infinitesimal dipole source of Fig. 3 at an azimuthal angle $\phi = 45^\circ$ for:
A) $\rho' = 0.025\lambda_0$, $\phi' = 135^\circ$, B) $\rho' = 0.05\lambda_0$, $\phi' = 75^\circ$,
C) $\rho' = 0.075\lambda_0$, $\phi' = 1^\circ$.

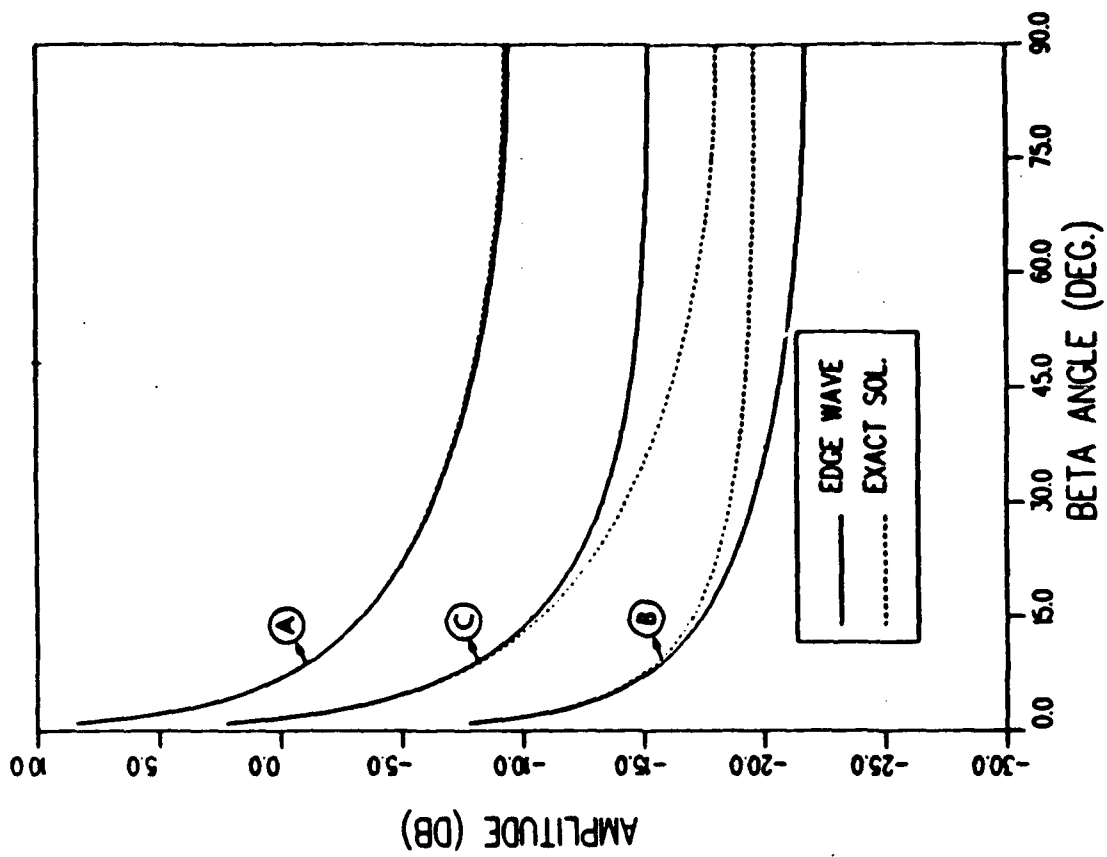


Figure 5: Far field region β -directed wave of the infinitesimal dipole source of Fig. 3 at an azimuthal angle $\phi = 45^\circ$ for:
A) $\rho' = 0.025\lambda_0$, $\phi' = 135^\circ$, B) $\rho' = 0.05\lambda_0$, $\phi' = 75^\circ$,
C) $\rho' = 0.075\lambda_0$, $\phi' = 180^\circ$.

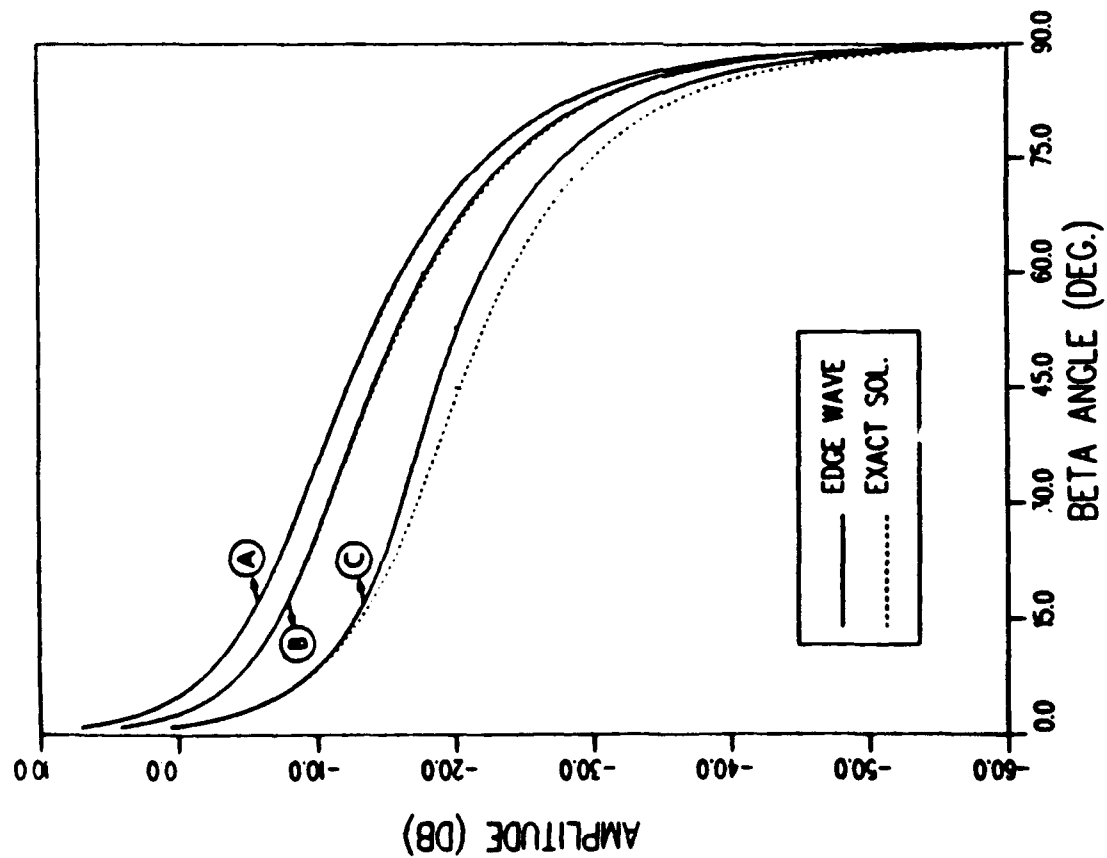


Figure 6: Far field region β -directed wave of the infinitesimal dipole source of Fig. 3 at an azimuthal angle $\phi = 105^\circ$ for:
 A) $\rho' = 0.025\lambda_0$, $\phi' = 135^\circ$, B) $\rho' = 0.05\lambda_0$, $\phi' = 75^\circ$,
 C) $\rho' = 0.075\lambda_0$, $\phi' = 180^\circ$.

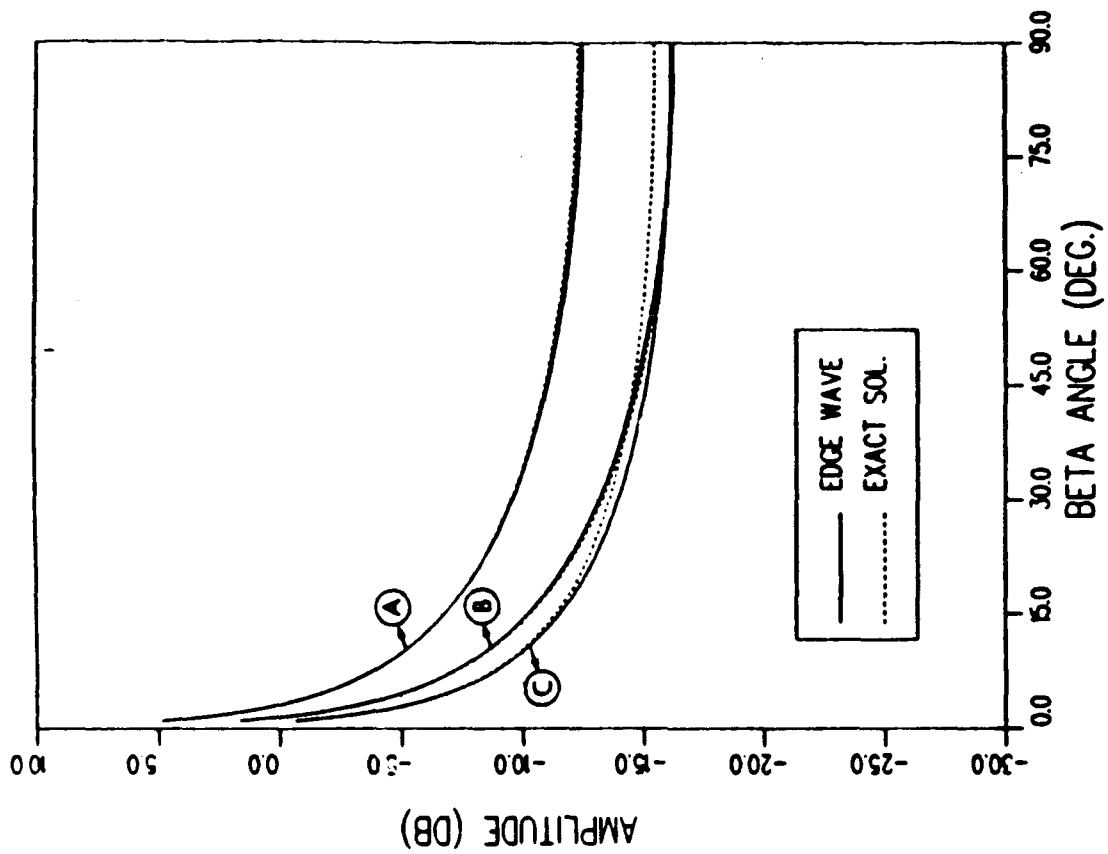


Figure 7: Far field region β -directed wave of the infinitesimal dipole source of Fig. 3 at an azimuthal angle $\phi = 105^\circ$ for:
 A) $\rho' = 0.025\lambda_0$, $\phi' = 135^\circ$, B) $\rho' = 0.05\lambda_0$, $\phi' = 75^\circ$,
 C) $\rho' = 0.075\lambda_0$, $\phi' = 180^\circ$.

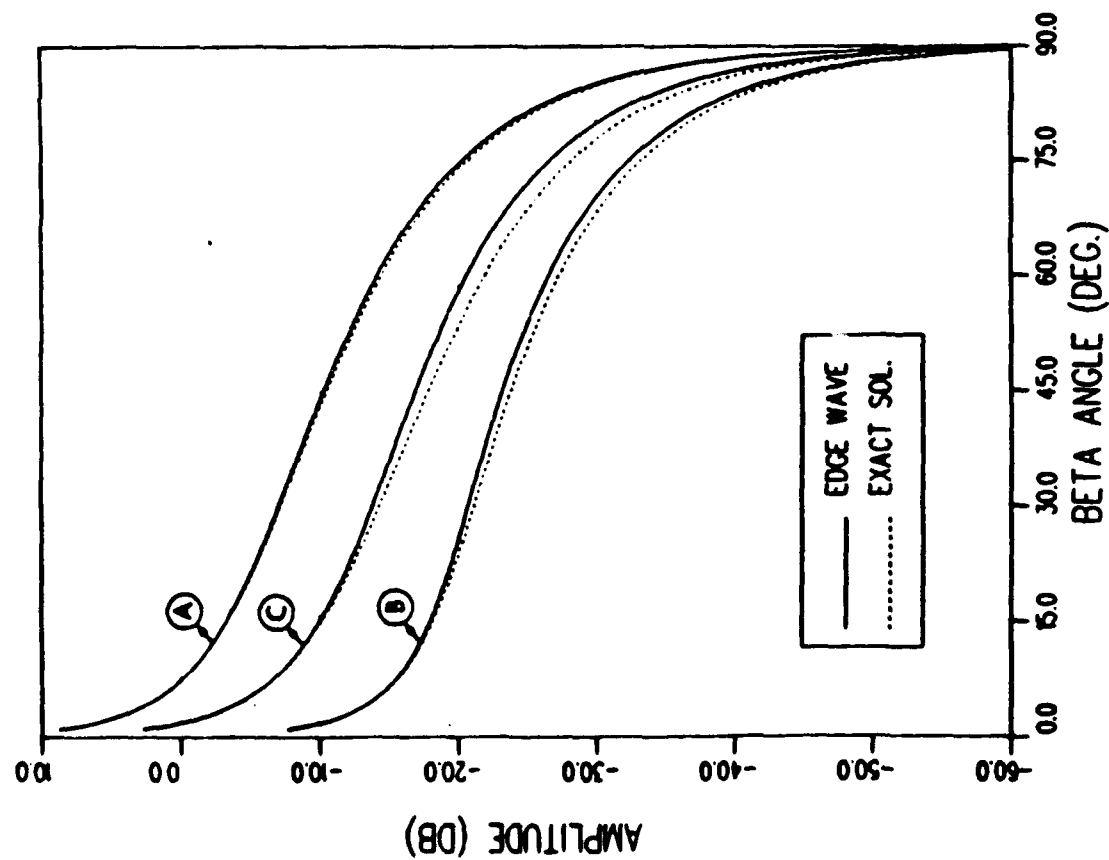


Figure 8: Far field region β -directed wave of the infinitesimal dipole source of Fig. 3 at an azimuthal angle $\phi = 165^\circ$ for:
 A) $\rho' = 0.025\lambda_0$, $\phi' = 135^\circ$, B) $\rho' = 0.05\lambda_0$, $\phi' = 75^\circ$,
 C) $\rho' = 0.075\lambda_0$, $\phi' = 180^\circ$.

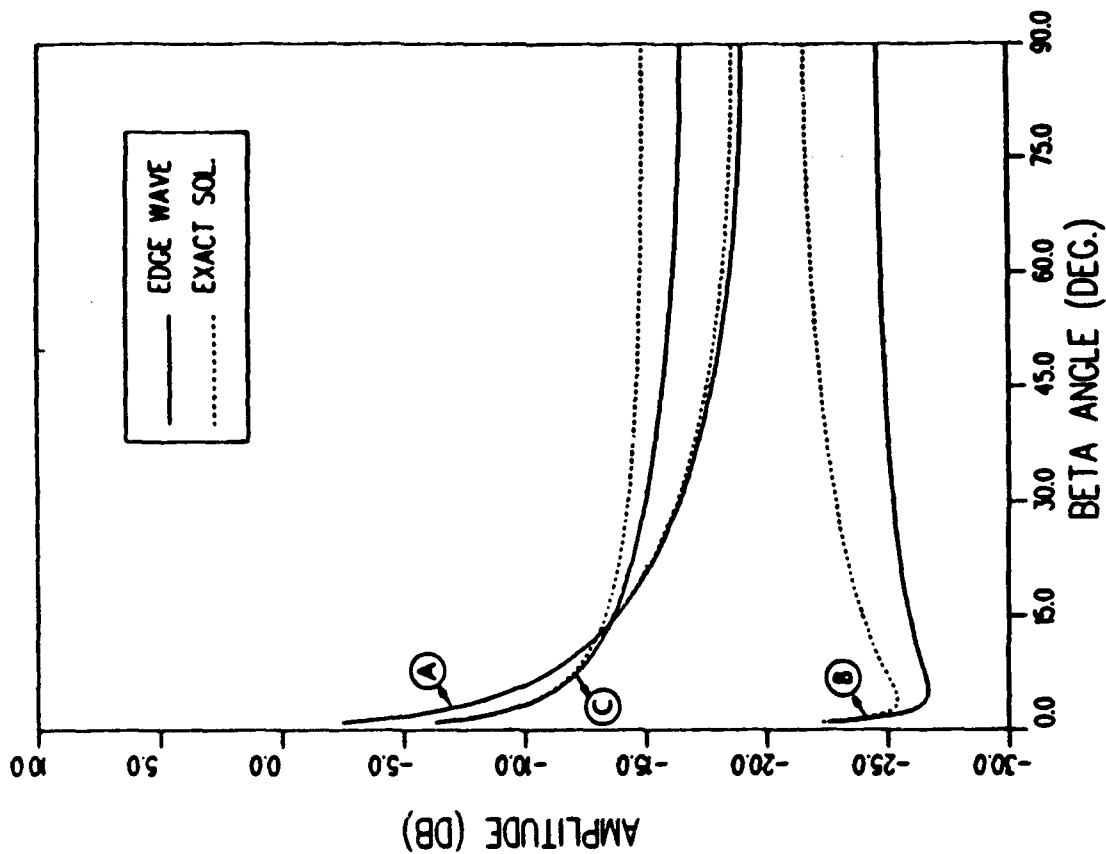


Figure 9: Far field region ϕ -directed wave of the infinitesimal dipole source of Fig. 3 at an azimuthal angle $\phi = 165^\circ$ for:
 A) $\rho' = 0.025\lambda_0$, $\phi' = 135^\circ$, B) $\rho' = 0.05\lambda_0$, $\phi' = 75^\circ$,
 C) $\rho' = 0.075\lambda_0$, $\phi' = 180^\circ$.

CHAPTER III

A Physical Optics Approximation of the Edge Wave Vertex Diffracted Field

3.1 Introduction.

One of the simplest approaches to high frequency scattering problems is the Physical Optics approximation. This method assumes the surface of a perfectly conducting scatterer is locally plane and approximates the total field at the points of the surface illuminated by the incident wave with the superposition of the incident and reflected field. The field is considered zero at the shadowed part of the surface. The scattered wave is then evaluated via the radiation integral of the induced surface currents. Normally, Physical Optics fails to adequately approximate the scattered field in observation directions sufficiently away from the specular and backscatter directions.

The study of the edge wave corner diffraction mechanism with the Physical Optics approach, however, is conceptually different. The excitation dipole is located in the close vicinity of the edge of a finite wedge and sufficiently far from its vertex as shown in Fig. 10. The induced surface currents are approximated by the currents that would flow over the surface of an infinite wedge. The end point contribution to the radiation integral is then interpreted as a corner diffracted wave.

This approach is expected generally to yield an acceptable approximation of

the diffracted field whenever the edge wave current flow lines are not significantly distorted in the vicinity of the vertex. Moment method results in general justify this assumption.

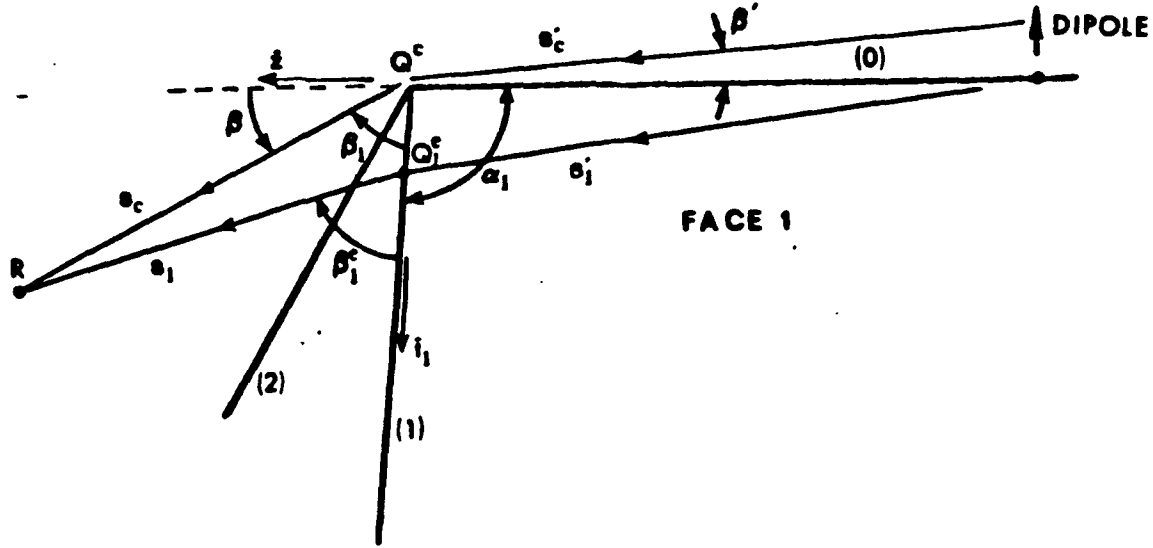


Figure 10: Geometry for the edge wave edge and vertex diffraction problem.

3.2 Formulation of the Physical Optics solution.

For convenience, let us restrict our attention to face 1 ("0" face) of the wedge. The result for face 2 ("N" face) can be readily obtained by means of a simple transformation. The field associated with the currents $\vec{j}_1(\vec{r}')$ flowing over the face 1 surface can be evaluated via the radiation integral

$$\vec{E}_1(\vec{s}_c) = jk_0 Z_0 \int \int_{S_1} \hat{R} \times \hat{R} \times \vec{j}_1(\vec{r}') \frac{\exp(-jk_0 R)}{4\pi R} ds' \quad (3.1)$$

where \vec{s}_c is the vector from Q^c pointing to the observation point, $\hat{R} = (\vec{s}_c - \vec{r}')/R$ and $R = \|\vec{s}_c - \vec{r}'\|$ (Fig. 11). The integration takes place over the truncated face

of the wedge. It is presumed that $\vec{j}_1(\vec{r}') can be adequately approximated by the actual induced currents as if the wedge was infinite, namely$

$$\vec{j}_1(\vec{r}') \approx \hat{n}_1 \times \vec{H}^{cw}(\vec{r}')|_{S_1} \quad (3.2)$$

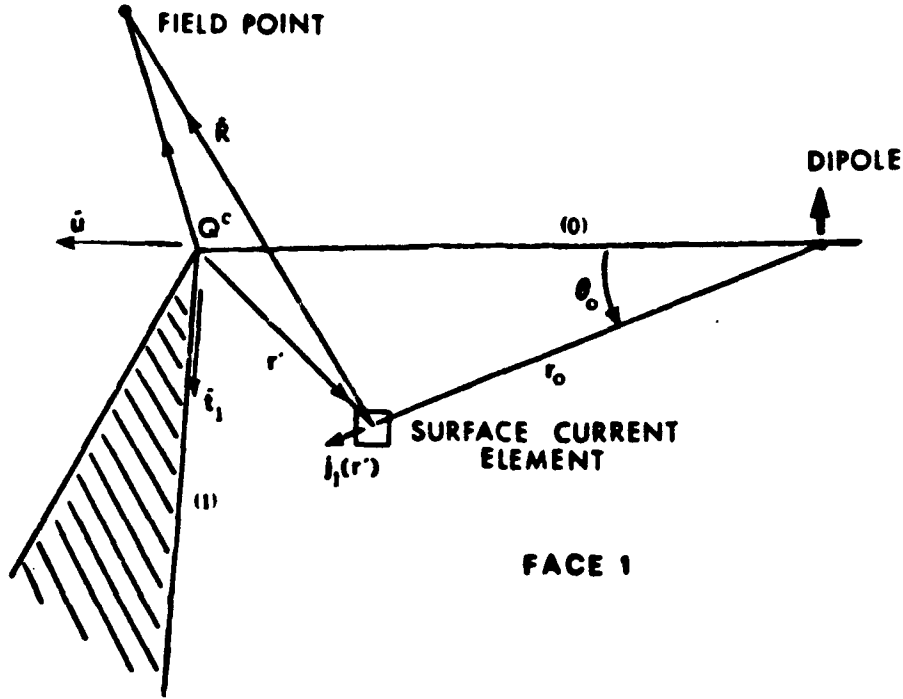


Figure 11: Geometry for the asymptotic evaluation of the radiation integral of the surface edge wave currents.

where $\vec{H}^{cw}(\vec{r}')$ is the magnetic field produced by the dipole radiating in the close vicinity of the edge of an infinite wedge. The end point (vertex) contribution to the surface radiation integral of eq. (3.1) is of interest here. For convenience, let us introduce the oblique system of coordinates associated with the terminating edge (edge (1) in Fig. 10), defined by the unit vectors

$$\hat{u} = \hat{z} \quad ; \quad \hat{t}_1 = \hat{x} \sin \alpha_1 - \hat{z} \cos \alpha_1$$

so that:

$$x = t_1 \sin \alpha_1 \quad ; \quad z = u - t_1 \cos \alpha_1$$

In the above equations α_1 denotes the angle formed by the guiding edge and the terminating edge (edge (1)) of face 1 of the wedge. The Jacobian determinant of the above transformation is then found to be equal to

$$\left| \frac{\partial(z, x)}{\partial(u, t_1)} \right| = \sin \alpha_1$$

and eq. (3.1) results into the following expression:

$$\begin{aligned} \vec{E}_1(\vec{s}_c) \approx & \vec{E}_1^{ew}(\vec{s}_c) \cdot \vec{T}(\vec{s}_c) - jk_0 Z_0 \sin \alpha_1 \\ & \int_0^\infty \int_0^\infty \hat{R} \times \hat{R} \times \vec{j}_1(u, t_1) \frac{\exp(-ik_0 R)}{4\pi R} du dt_1 \end{aligned} \quad (3.3)$$

The first term in the RHS of eq. (3.3) expresses the guiding edge (edge (0) of Fig. 10) associated wave (edge wave) multiplicatively corrected by the transition dyadic $\vec{T}(\vec{s}_c)$, due to the semi-infinite rather than infinite nature of the structure, whereas the second term incorporates the edge (1) effect as well as the vertex contribution. Thereafter, our attention is restricted to the second term only.

The double integral in eq. (3.3) can be reduced to a line integral along the terminating edge, by considering the end point contribution with respect to the variable u . A non-uniform asymptotic approximation readily follows after integration by parts. Next, a uniform representation is derived by heuristically introducing the suitable transition function to the final result.

For large distances of the dipole from the terminating edge, using the results of section 2.3, one observes that

$$\begin{aligned} \vec{j}_1(u, t_1) \approx & jk_0^\nu C(\nu) A_\nu^e(\rho', \phi') \sin^{\nu-1} \theta_0 \\ & \frac{\exp(-jk_0 r_0)}{r_0} (\hat{x} \sin \theta_0 + \hat{z} \cos \theta_0) \end{aligned} \quad (3.4)$$

in which

$$r_0 = \sqrt{t_1^2 \sin^2 \alpha_1 + (u - t_1 \cos \alpha_1 + s_c')^2},$$

$$\sin \theta_0 = t_1 \sin \alpha_1 / r_0, \quad \cos \theta_0 = (u - t_1 \cos \alpha_1 + s'_c) / r_0,$$

$$A_\nu^e(\rho', \phi') = \rho'^{\nu-1} (p_{\rho'}^e \sin \nu \phi' + p_{\phi'}^e \cos \nu \phi'),$$

s'_c is the distance of the dipole source from the vertex, and the constant $C(\nu)$ is defined by eq. (2.17). It is reminded that $\nu = 1/n$, where $(2 - n)\pi$ is the wedge angle. Also, $(\rho', \phi', -s'_c)$ determines approximately the location of the dipole with respect to the corresponding cylindrical system of coordinates. Thus, eq. (3.3) may be written explicitly

$$\begin{aligned} \bar{E}_1(\bar{s}_c) \approx & \bar{E}_1^{ew}(\bar{s}_c) \cdot \bar{T}(\bar{s}_c) + k_0^{\nu+1} Z_0 \sin \alpha_1 C(\nu) A_\nu^e(\rho', \phi') \\ & \cdot \int_0^\infty \int_0^\infty \hat{R} \times \hat{R} \times (\hat{x} \sin \theta_0 + \hat{z} \cos \theta_0) \sin^{\nu-1} \theta_0 \\ & \cdot \frac{\exp \{-jk_0(R + r_0)\}}{4\pi R r_0} du dt_1 \end{aligned} \quad (3.5)$$

whence, integrating by parts with respect to the variable u , one obtains the (non-uniform) asymptotic approximation:

$$\begin{aligned} \bar{E}_1(\bar{r}) \approx & \bar{E}_1^{ew}(\bar{s}_c) \cdot \bar{T}(\bar{r}) - j k_0^\nu Z_0 \sin^\nu \alpha_1 \\ & \cdot \int_0^\infty \hat{R} \times \hat{R} \times [\hat{x} t_1 \sin \alpha_1 + \hat{z} (s'_c - t_1 \cos \alpha_1)] t_1^{\nu-1} \\ & \cdot \frac{\exp \{-jk_0(R + r_0)|_{u=0}\}}{4\pi R r_0^{\nu+1} \frac{\partial}{\partial u}(R + r_0)|_{u=0}} dt_1 \end{aligned} \quad (3.6)$$

It is well known that Physical Optics does not predict the correct edge diffracted field away from the geometrical optics shadow boundary. Therefore, it would be reasonable at this point to be restricted into the vertex contribution of the integral involved in eq. (3.6). Note that the latter is essentially a sum of integrals of the form:

$$\int_0^\infty \bar{G}(t) t^{-p-1} \exp \{jk g(t)\} dt$$

where $\vec{G}(t)$ is a slowly varying function of t and $\Re(p) < 0$. Such types of integrals are evaluated asymptotically in Appendix A and result in expressions involving the parabolic cylinder function of order p . Thus, the vertex diffracted field associated with face 1 of the wedge and predicted by the end point contribution to the radiation integral of the Physical Optics currents can be expressed as follows:

$$\begin{aligned} \vec{E}_1^{c,po}(\vec{s}_c) \approx & -\frac{jk_0^\nu Z_0 \sin^\nu \alpha_1 C(\nu) A_\nu^e(\rho', \phi')}{4\pi s_c s_c'^{\nu+1} (1 - \cos \beta)} \left\{ [s_c' \sin \beta I_{-\nu}^0(k_0) \right. \\ & - (\sin \beta \cos \alpha_1 + \sin \alpha_1 \cos \beta \cos \phi) I_{-\nu-1}^0(k_0)] \hat{\beta} \\ & \left. + \sin \alpha_1 \sin \phi I_{-\nu-1}^0(k_0) \hat{\phi} \right\}. \end{aligned} \quad (3.7)$$

In the above equation, $I_p^0(k_0)$ expresses the end point contribution to the integral

$$I_p(k_0) = \int_0^\infty t^{-p-1} \exp \{-jk_0(R + r_0)|_{u=0}\} dt$$

which is examined in detail in Appendix A. For the specific semi-infinite wedge geometry under consideration, the integral $I_p^0(k_0)$ can be approximated by:

$$\begin{aligned} I_p^0(k_0) \approx & \Gamma(-p) k_0^p \exp(-jp\pi/2) \exp\{-jk_0(s_c + s_c')\} \\ & \cdot \frac{F_p^c[k_0 a_1^2(\vec{s}_c; s_c')]}{[\sin \alpha_1 \sin \beta \cos \phi + \cos \alpha_1 (1 - \cos \beta)]^{-p}}, \end{aligned} \quad (3.8)$$

in which

$$a_1(\vec{s}_c; s_c') \approx -\text{sign}(\pi - \alpha_1 - \beta_1) \left| \sqrt{(s_c' + s_c) - (s_1' + s_1)} \right| \quad (3.9)$$

and s_1' , s_1 denote the distance of the dipole source point and the receiver from the origin Q_1^e of the Keller cone of diffracted rays from the terminating edge (edge (1) in Fig. 10). The branch of the bracketed expression in eq. (3.8) is chosen according to

$$(-1)^{-p} = \exp(-jp\pi)$$

Recall that eq. (3.7) furnishes a non-uniform approximation of the corner diffracted field associated with face 1 of the wedge. Moreover, this becomes evident from the singularity of the field as the receiver approaches the z-axis ($\beta \rightarrow 0$). A uniform approximation incorporates the coupling between the vertex and the point source and mathematically implies the multiplicative introduction of the function

$$F(2k_0 L_c \sin^2 \frac{\beta}{2}) ; L_c = \frac{s_c s'_c}{s_c + s'_c}$$

where $F(\cdot)$ is the familiar edge transition function of UTD. The above expression can be derived from the uniform asymptotic approximation of integrals, the integrands of which involve a phase function presenting a stationary phase point (in our case the dipole source) in the vicinity of an end point (the vertex). It should also be noted that the above transition function appears in the edge wave corner diffraction coefficient obtained in [4].

3.3 The Physical Optics vertex diffracted wave.

Eq. (3.7) along with eqs. (3.8), (3.9) can be used to identify a vertex diffraction coefficient associated with the Physical Optics currents flowing over the wedge surface. Retaining only the dominant term in the expression of the vertex diffracted wave (dominant with respect to the parameter $2k_0 s'_c$) one obtains

$$\begin{aligned} \bar{E}^{c,po}(\bar{s}_c) \approx & \exp\{j(\nu - 1)\pi/2\} \Gamma(\nu) C(\nu) Z_0 A_\nu^e(\rho', \phi') \frac{\exp\{-jk_0(s_c + s'_c)\}}{4\pi s_c s'_c{}^\nu} \\ & \cdot \cot \frac{\beta}{2} F(2k_0 L_c \sin^2 \beta/2) \left\{ \frac{F_{-\nu}^c[k_0 a_1^2(\bar{s}_c; s'_c)]}{[\cot \alpha_1(1 - \cos \beta) + \sin \beta \cos \phi]^\nu} \right. \\ & \left. + \frac{F_{-\nu}^c[k_0 a_2^2(\bar{s}_c; s'_c)]}{[\cot \alpha_2(1 - \cos \beta) + \sin \beta \cos(n\pi - \phi)]^\nu} \right\} \hat{\beta} \end{aligned} \quad (3.10)$$

Eq. (3.10) can be rewritten in a more familiar notation by employing the following expressions for the incident field on the vertex Q' produced by the dipole p'

radiating in free space:

$$\begin{Bmatrix} E_{\beta'}^i(Q^c) \\ E_{\phi'}^i(Q^c) \end{Bmatrix} \approx -jk_0 Z_0 \frac{\exp(-jk_0 s'_c)}{4\pi s'_c} \begin{Bmatrix} p_{\beta'}^e \\ p_{\phi'}^e \end{Bmatrix}$$

Then,

$$\tilde{E}^{c,p_0}(\bar{s}_c) \approx E_{\beta}^{c,p_0}(\bar{s}_c) \hat{\beta} \quad (3.11a)$$

with

$$\begin{aligned} E_{\beta}^{c,p_0}(\bar{s}_c) \approx & \frac{\exp(j\nu\pi/2) \Gamma(\nu) C(\nu)}{k_0} \frac{E_{\beta'}^i(Q^c) \sin \nu\phi' + E_{\phi'}^i(Q^c) \cos \nu\phi'}{\sin^{1-\nu} \beta'} \\ & \cdot \cot \frac{\beta}{2} F(2k_0 L_c \sin^2 \frac{\beta}{2}) \left\{ \frac{F_{-\nu}^c[k_0 a_1^2(\bar{s}_c; s'_c)]}{[\cot \alpha_1 (1 - \cos \beta) + \sin \beta \cos \phi]^\nu} \right. \\ & \left. + \frac{F_{-\nu}^c[k_0 a_2^2(\bar{s}_c; s'_c)]}{[\cot \alpha_2 (1 - \cos \beta) + \sin \beta \cos(n\pi - \phi)]^\nu} \right\} \frac{\exp(-jk_0 s_c)}{s_c} \end{aligned} \quad (3.11b)$$

where α_1, α_2 are the angles formed by the terminating edges (1) and (2) and the guiding edge (0) for faces 1 and 2 respectively and the parameters $a_{1,2}$ are defined by

$$a_{1,2}(\bar{s}_c; s'_c) = -\text{sign}(\pi - \alpha_{1,2} - \beta_{1,2}) \left| \sqrt{(s_c + s'_c) - (s'_{1,2} + s_{1,2})} \right| \quad (3.12)$$

with $s'_{1,2}, s_{1,2}$, as before, denoting the distances between the dipole or the receiver and the origin of the Keller cone of diffracted rays from the edges (1) and (2) of faces 1 and 2 respectively, while β_1, β_2 are the elevation angles of the observation point in terms of the edge (1) and (2) fixed coordinate systems. The transition function $F_{-\nu}^c(\cdot)$, which is examined in detail in Appendix B, is defined by

$$F_{-\nu}^c(|x|) = \exp(j\nu\pi/4) (2|x|)^{\nu/2} \exp(j|x|/2) D_{-\nu}[\exp(j\pi/4)\sqrt{2|x|}] \quad (3.13)$$

where $D_{-\nu}(\cdot)$ is the parabolic cylinder function of order $-\nu$. For large values of its argument, $F_{-\nu}^c(|x|)$ reduces to unity, while it compensates the singularity of the field when either $Q_1^c \rightarrow Q^c$ or $Q_2^c \rightarrow Q^c$ ($\beta_{1,2} = \pi - \alpha_{1,2}$). Furthermore, after some elementary manipulation and according to a similar analysis in [8] the approximation

$$s'_{1,2} + s_{1,2} \approx (s'_c + s_c) - L_c [1 + \cos(\alpha_{1,2} + \beta_{1,2})] \quad (3.14)$$

can be justified for large values of the parameter L_c , defined by:

$$L_c = \frac{s_c s'_c}{s_c + s'_c} \quad (3.15)$$

so that:

$$\alpha_{1,2} \approx 2 L_c \cos^2 \left(\frac{\alpha_{1,2} + \beta_{1,2}}{2} \right) \quad (3.16)$$

Finally, noting that:

$$\cos \beta_1 = \sin \alpha_1 \sin \beta \cos \phi - \cos \alpha_1 \cos \beta$$

and

$$\cos \beta_2 = \sin \alpha_2 \sin \beta \cos(n\pi - \phi) - \cos \alpha_2 \cos \beta$$

eq. (3.11b) can be rewritten in terms of the edge (1) and (2) fixed coordinate systems as

$$\begin{aligned} E_{\beta}^{c,po} \approx & \frac{\exp(j\nu\pi/2) \Gamma(\nu) C(\nu)}{k_0} \frac{E_{\beta'}^i(Q^c) \sin \nu \phi' + E_{\phi'}^i(Q^c) \cos \nu \phi'}{\sin^{1-\nu} \beta'} \\ & \cdot \cot \frac{\beta}{2} F(2k_0 L_c \sin^2 \frac{\beta}{2}) \left\{ \frac{\sin^{\nu} \alpha_1 F_{-\nu}^c[2k_0 L_c \cos^2 \left(\frac{\alpha_1 + \beta_1}{2} \right)]}{(\cos \alpha_1 + \cos \beta_1)^{\nu}} \right. \\ & \left. + \frac{\sin^{\nu} \alpha_2 F_{-\nu}^c[2k_0 L_c \cos^2 \left(\frac{\alpha_2 + \beta_2}{2} \right)]}{(\cos \alpha_2 + \cos \beta_2)^{\nu}} \right\} \frac{\exp(-jk_0 s_c)}{s_c} \quad (3.17) \end{aligned}$$

For the particular case of the plane angular sector ($n = 2$, $\nu = 1/2$ and $\alpha_1 = \alpha_2 = \alpha$, $a_1 = a_2 = a$) eq. (3.11b) reduces to

$$E_{\beta}^{c,po} \approx - \frac{1}{\sqrt{2} \pi k_0} \frac{E_{\beta'}^i(Q^c) \sin(\phi'/2) + E_{\phi'}^i(Q^c) \cos(\phi'/2)}{\sqrt{\sin \beta'}} \cdot \cot \frac{\beta}{2} F(2k_0 L_c \sin^2 \frac{\beta}{2}) \cdot \frac{F_{-1/2}^c[k_0 a^2(\bar{s}_c; s_c')]}{\sqrt{\cot \alpha (1 - \cos \beta) + \sin \beta \cos \phi}} \frac{\exp(-jk_0 s_c)}{s_c} \quad (3.18)$$

and for the right angular sector ($\alpha = \pi/2$) it simplifies to the following

$$E_{\beta}^{c,po} \approx - \frac{1}{\sqrt{2} \pi k_0} \frac{E_{\beta'}^i(Q^c) \sin(\phi'/2) + E_{\phi'}^i(Q^c) \cos(\phi'/2)}{\sqrt{\sin \beta'}} \cdot \cot \frac{\beta}{2} F(2k_0 L_c \sin^2 \frac{\beta}{2}) \cdot \frac{F_{-1/2}^c[k_0 L_c (1 - \sqrt{1 - \sin^2 \beta \cos^2 \phi})]}{\sqrt{\sin \beta \cos \phi}} \frac{\exp(-jk_0 s_c)}{s_c} \quad (3.19)$$

3.4 Numerical results and discussion.

The corner diffracted field described by eqs. (3.11a)-(3.11b) does not satisfy either the boundary conditions on the surface or reciprocity with respect to the azimuthal coordinate. Both of these inadequacies are inherent with the Physical Optics approximation of the diffracted wave. Besides, the asymptotic evaluation of the radiation integral required that the observation point was not close to the surface of the semi-infinite wedge, where the direct dipole field (edge wave) is dominant. However, the Physical Optics solution based on the true currents that would flow over the surface of the wedge yields a satisfactory approximation of the scattered field, provided that no diffracted rays from edges (1) and (2) reach the observation point. The latter corresponds to the case where $\alpha_{1,2} + \beta_{1,2} > \pi$. A remarkable fact is that the vertex diffracted field is dominantly $\hat{\beta}$ -directed, which is

physically justifiable since the current is accumulated in the vicinity of the guiding edge, flowing parallel to it. Note also that as $\alpha \rightarrow \pi$ the vertex diffracted field vanishes and the total solution reduces to the edge wave term as it should.

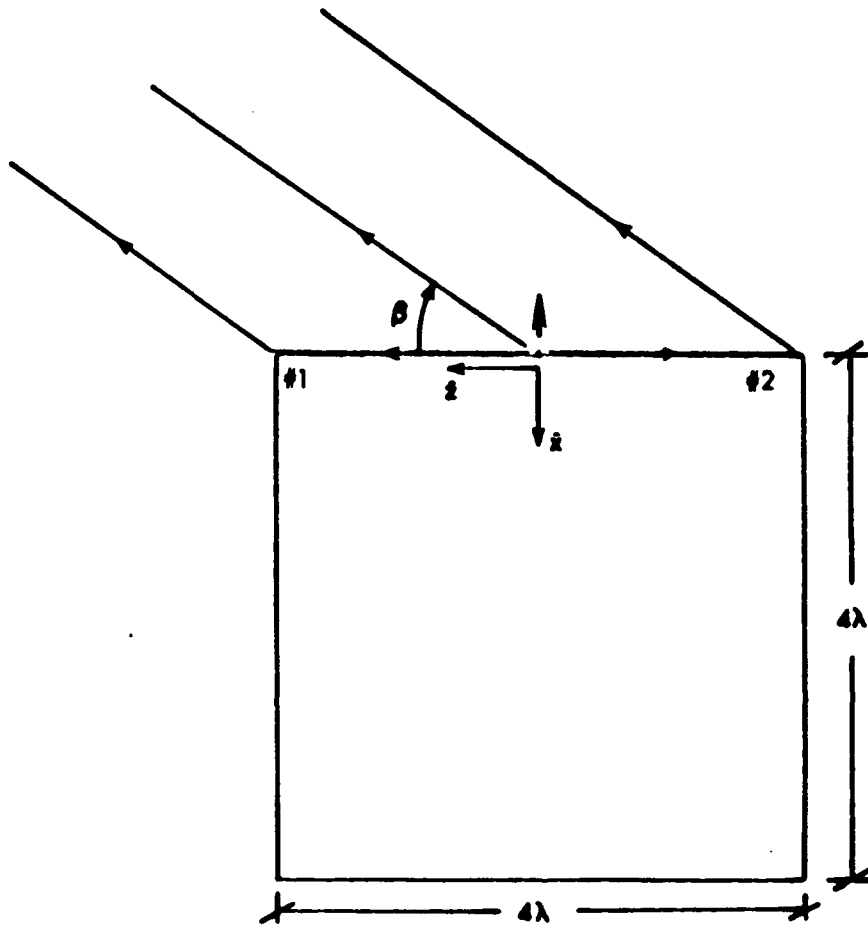


Figure 12: The square plate used in the numerical application of the Physical Optics solution.

The radiation of a dipole in the close vicinity of a flat square plate (see Fig. 12) is examined in Figs. 13-20. The dipole is located at a distance $\rho' = 0.01\lambda$ from the center of one of the edge of a rectangular plate with dimensions $4\lambda \times 4\lambda$ as depicted in Fig. 12. The pattern is evaluated in the elevation plane associated with the guiding edge fixed reference frame, centered at the point of projection of the

dipole to the edge, for several values of the azimuthal angle ϕ of the observation point. In particular, the radiated field is approximated by the direct dipole field (edge wave) multiplicatively corrected by the transition dyadic which is developed in Chapter IV, and the superposition of two corner diffracted rays from the corners of the guiding edge. Other possible diffraction mechanisms which may contribute for small azimuthal coordinates of the observation point are neglected in the present analysis.

The predicted radiation patterns are compared with moment method results [9]. It is noted that moment method under those circumstances should not be viewed as exact since its surface patch monopoles may not accurately approximate the singular current flowing along the guiding edge as well as the strong coupling between the dipole and that edge. As an independent technique, however, it yields comparable results, which for certain aspects of observation show good agreement with the Physical Optics approximation developed earlier.

The edge wave itself and the edge wave corner diffracted field clearly dominate the total $\hat{\beta}$ -directed field in the paraxial region of the guiding edge. Both mechanisms, however, decay as the observer is removed from the paraxial region. The non-oscillatory behavior of the $\hat{\phi}$ -directed field amplitudes (see, for instance, Figs. 19, 20) also reveals that the corner diffracted contribution to that component of the field appears indeed to be negligible. Besides, this component of the radiated wave may be attributed to double edge diffractions or higher order terms in the asymptotic expansion of the radiation integral of the edge wave currents.

The comparability of the moment method results and the Physical Optics solution deteriorates at small azimuthal angles. However, at these lower cuts other secondary diffraction mechanisms (corner, double edge diffraction, etc.) may contribute significantly to the radiation pattern.

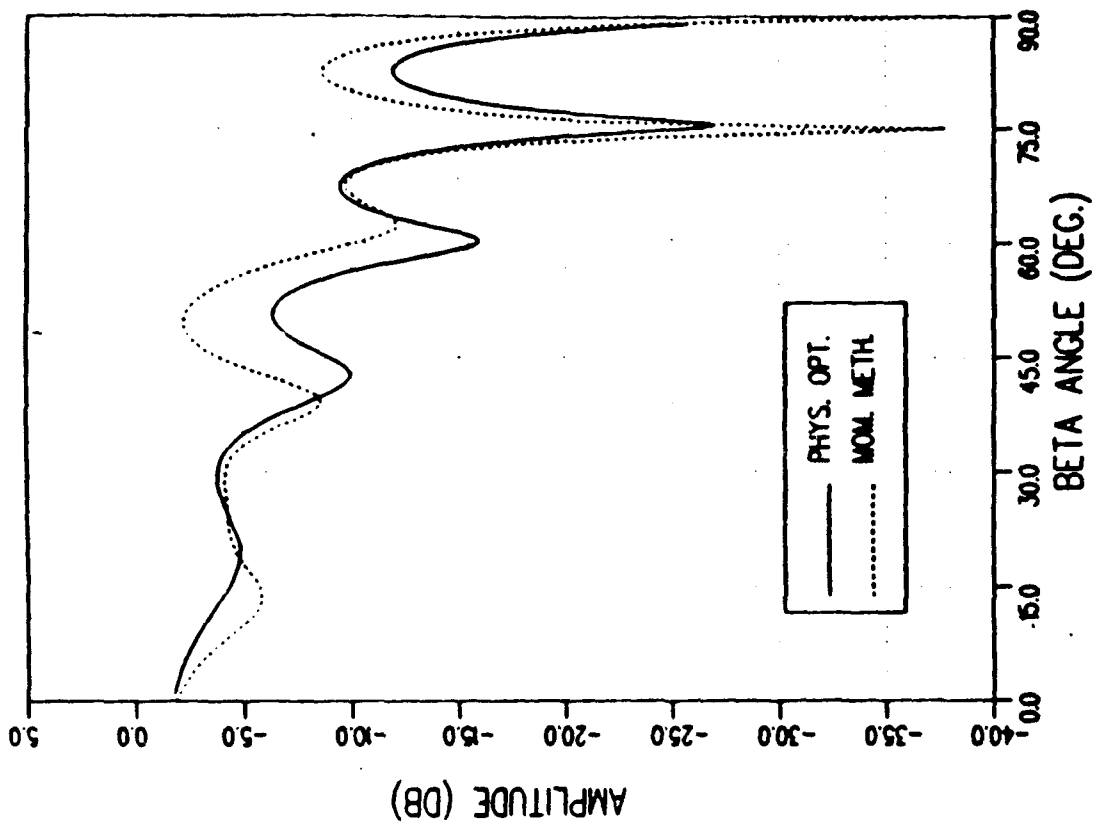


Figure 13: Far field region β -directed wave radiated by the dipole of Fig. 12 at an azimuthal angle $\phi = 30^\circ$.

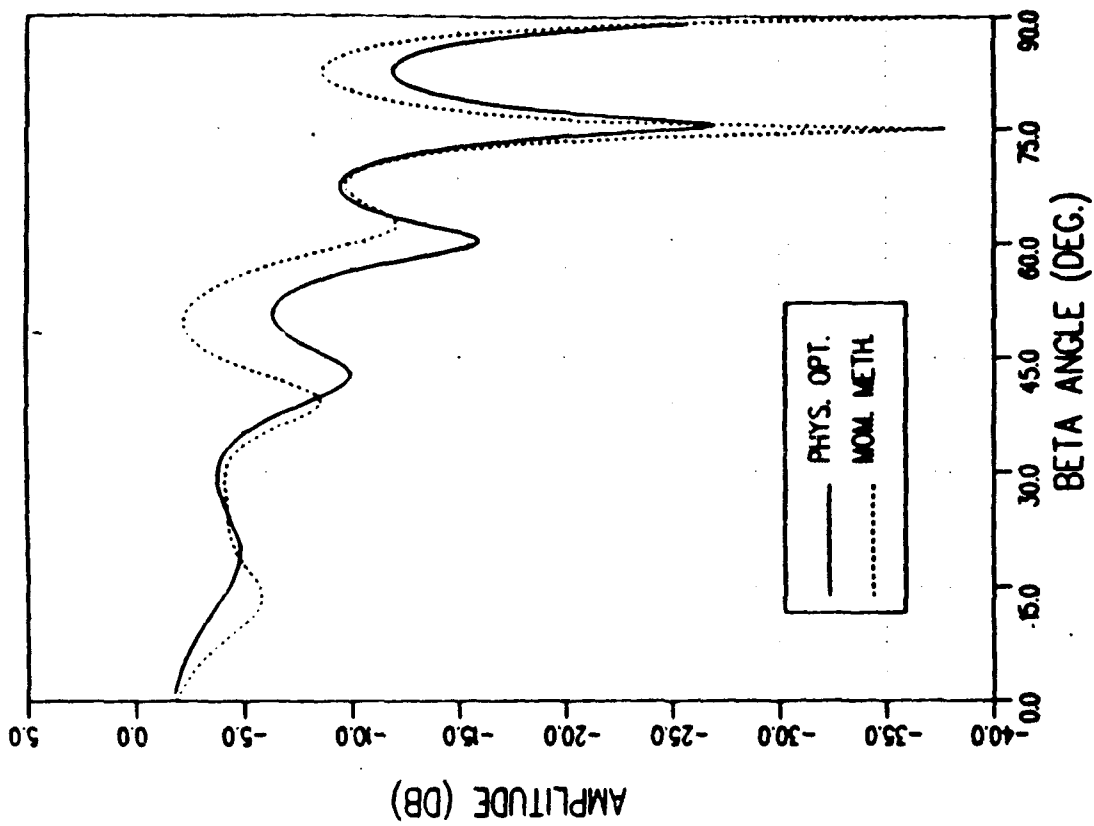


Figure 14: Far field region β -directed wave radiated by the dipole of Fig. 12 at an azimuthal angle $\phi = 45^\circ$.

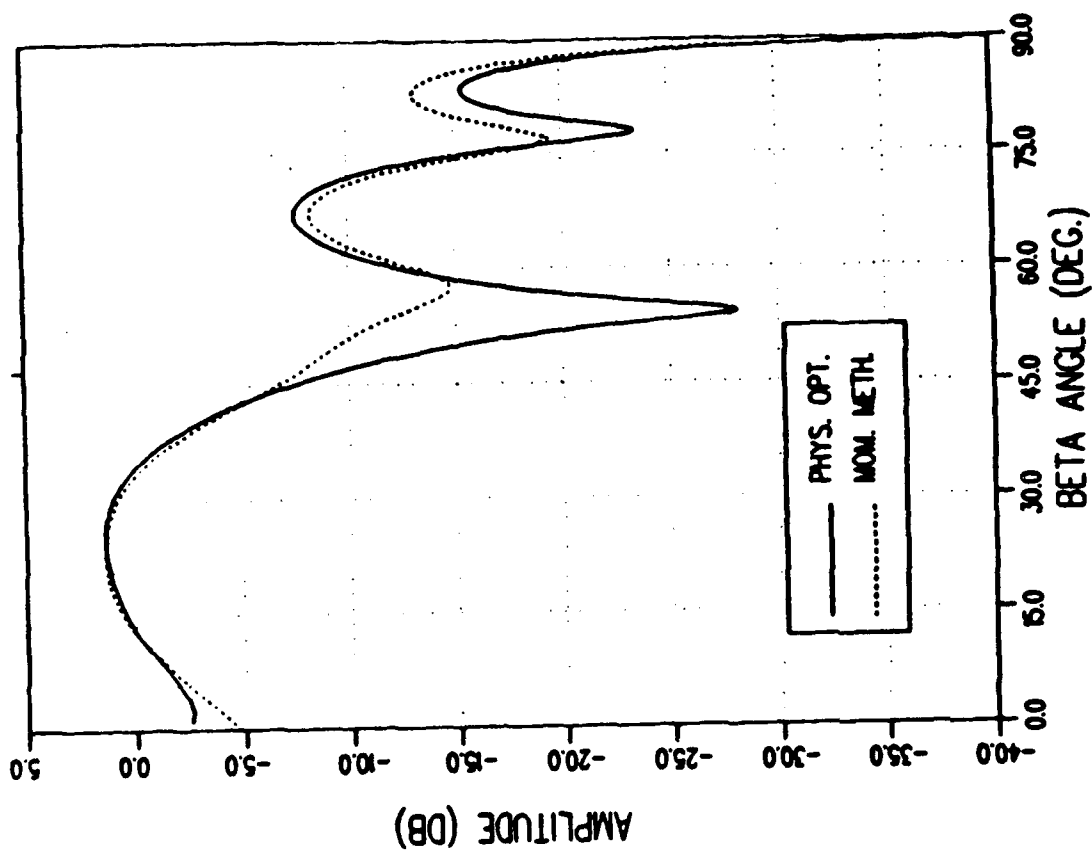


Figure 15: Far field region $\hat{\rho}$ -directed wave radiated by the dipole of Fig. 12 at an azimuthal angle $\phi = 90^\circ$.

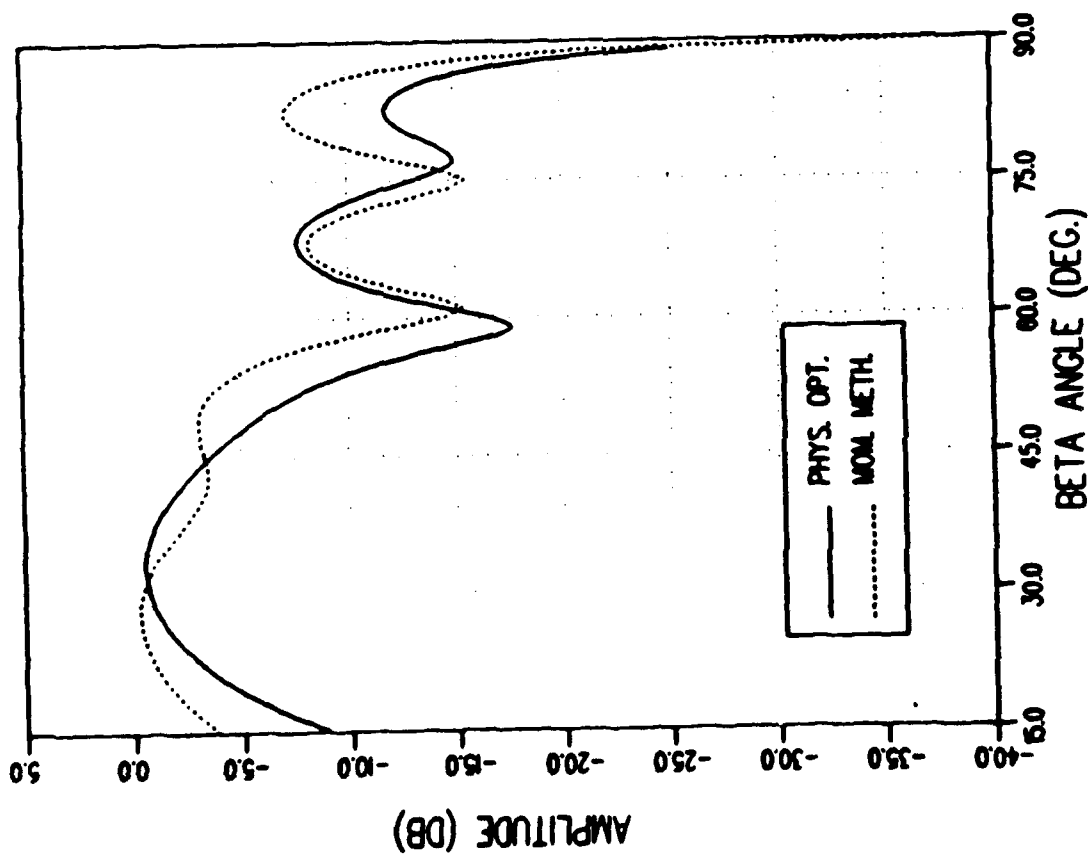


Figure 16: Far field region $\hat{\rho}$ -directed wave radiated by the dipole of Fig. 12 at an azimuthal angle $\phi = 120^\circ$.

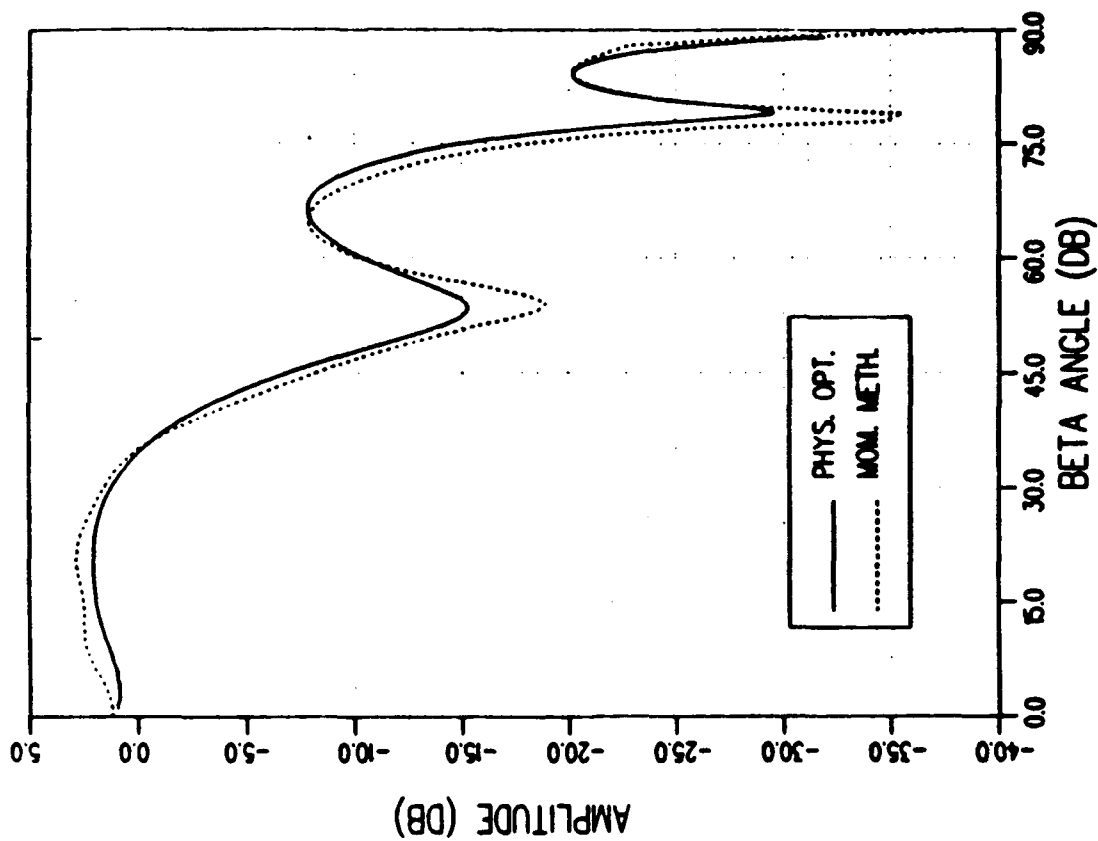


Figure 18: Far field region β -directed wave radiated by the dipole of Fig. 12 at an azimuthal angle $\phi = 180^\circ$.

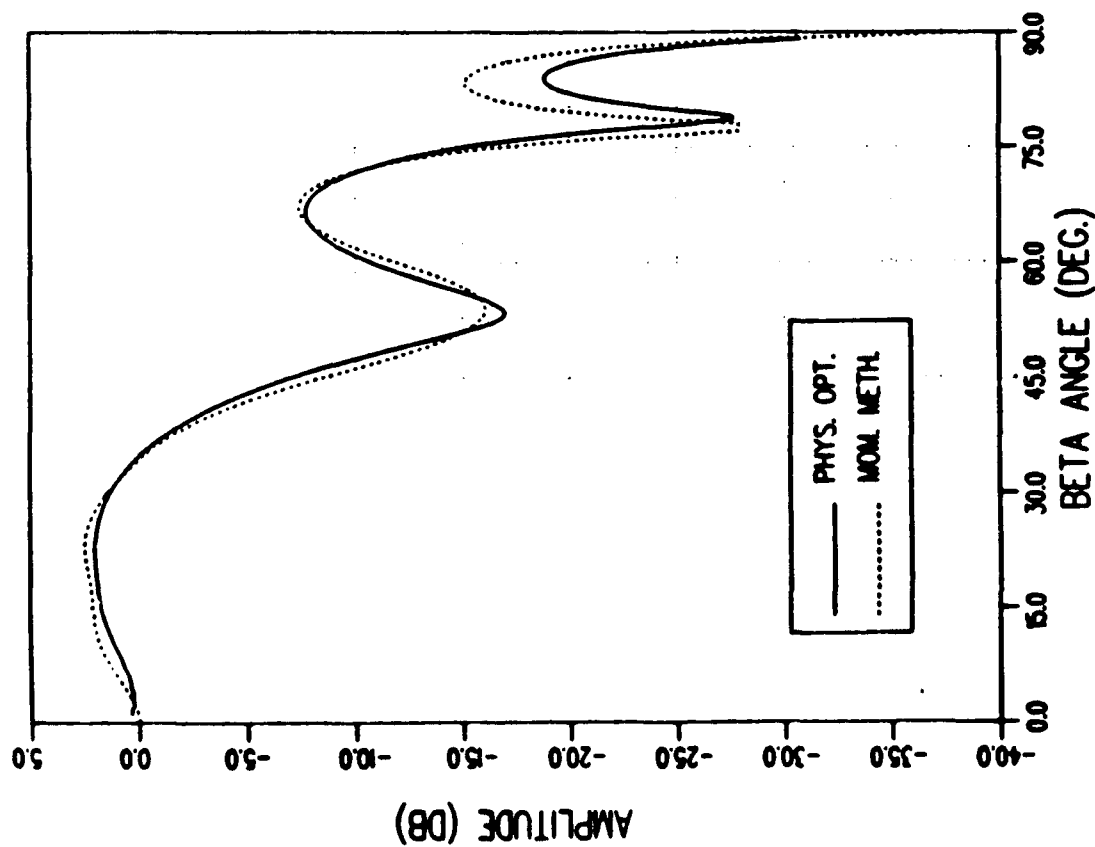


Figure 17: Far field region β -directed wave radiated by the dipole of Fig. 12 at an azimuthal angle $\phi = 150^\circ$.

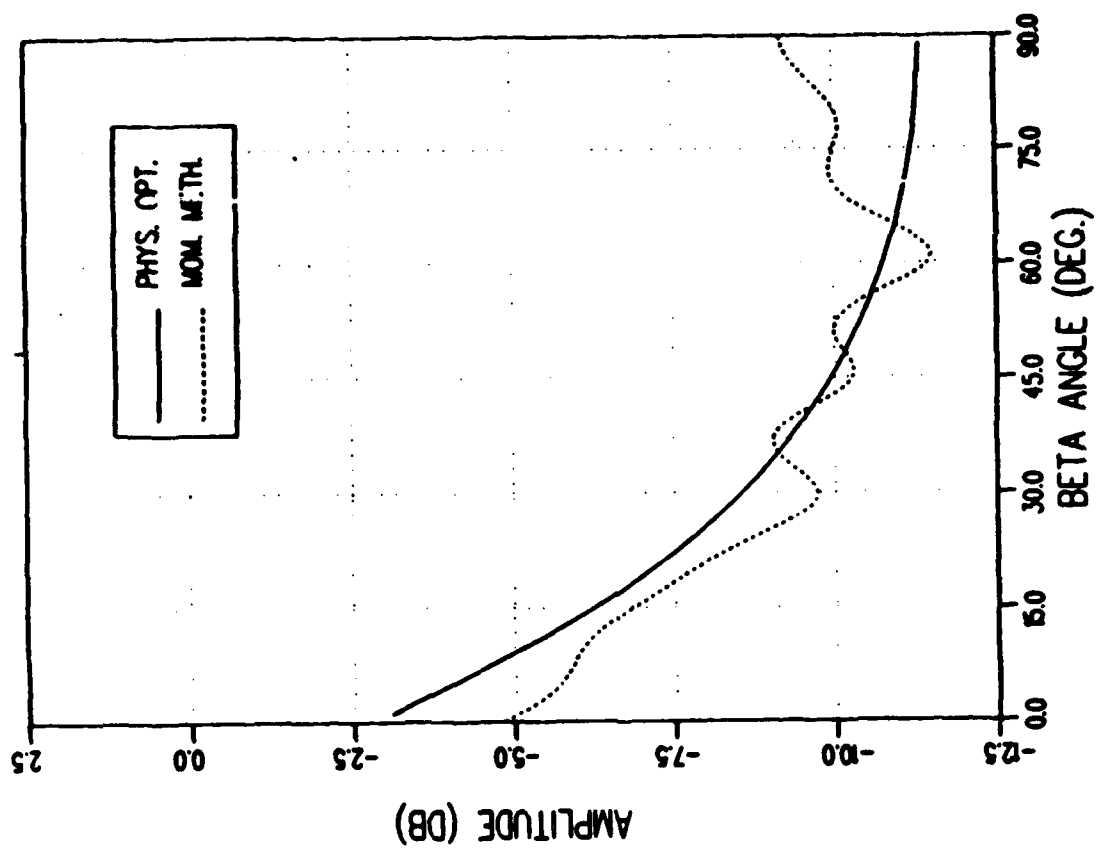


Figure 19: Far field region $\hat{\phi}$ -directed wave radiated by the dipole of Fig. 12 at an azimuthal angle $\phi = 120^\circ$.

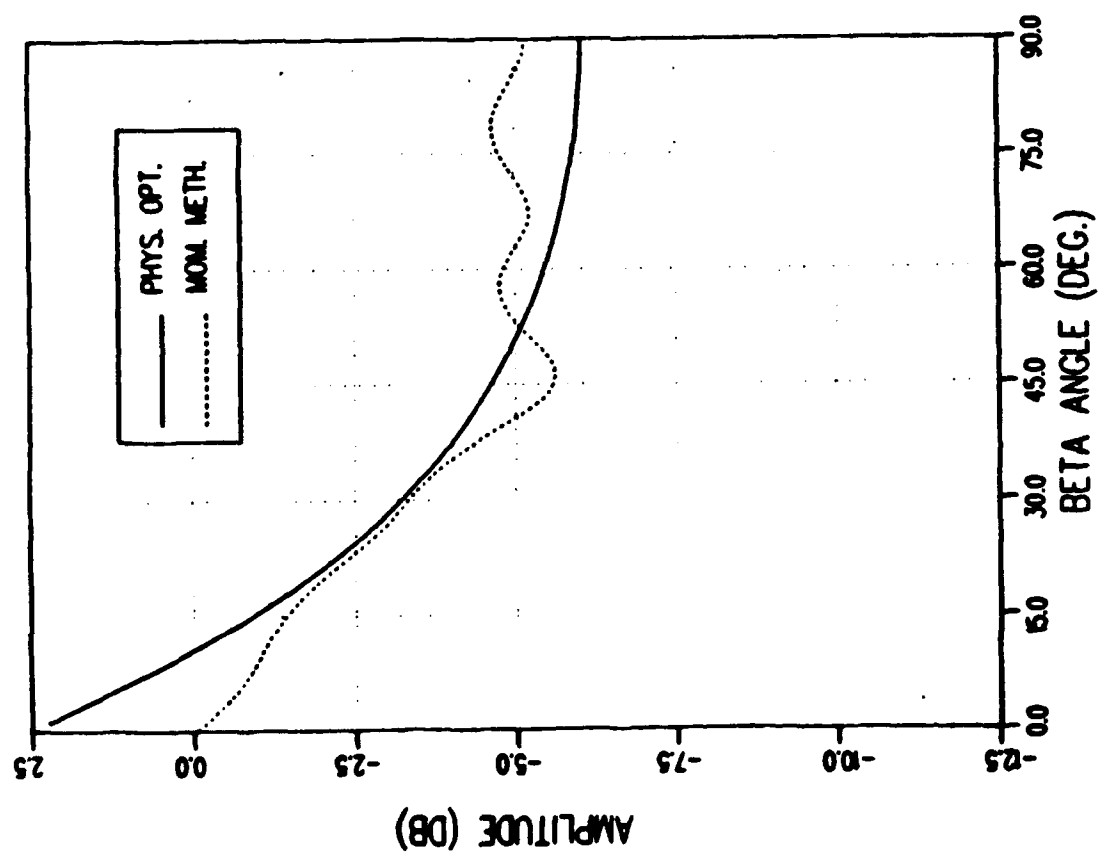


Figure 20: Far field region $\hat{\phi}$ -directed wave radiated by the dipole of Fig. 12 at an azimuthal angle $\phi = 150^\circ$.

CHAPTER IV

An Equivalent Current Approach

4.1 Introduction.

It was shown in Chapter III that the surface radiation integral can be asymptotically reduced to a line integral along the terminating edges of the semi-infinite wedge. In other words, the high frequency radiated field can be adequately approximated by the radiation integral of equivalent electric and magnetic edge currents flowing along these terminating edges. In the Physical Optics approximation developed earlier, those equivalent edge currents asymptotically incorporated the physical optics induced current effect.

Within the frame of the Physical Theory of Diffraction [10,11,12] the scattered field from a body can be considered as the superposition of the waves produced by two current components flowing along the surface of the body: a uniform component related with the geometrical optics field (physical optics currents) and a non-uniform current due to the possible curvature or discontinuities in the curvature of the surface of the scatterer (fringe currents). Hence, in the particular edge wave vertex diffraction problem, the geometry of which is illustrated in Fig. 10, the solution can be improved by superimposing to the uniform currents fringe currents due to the presence of the terminating edge discontinuity. In the context of our asymptotic analysis the field is approximated by the radiation integral of the sum of two types of edge (both electric and magnetic) equivalent currents: the first

set corresponding to the uniform (physical optics) currents and the second incorporating the fringe current effect. The asymptotic reduction of the edge current radiation integral involves a stationary phase point contribution (edge diffracted wave) together with an end point effect. The former, as the origin of Keller's cone of diffracted rays moves away from the vertex, and in the region that is illuminated by the edge diffracted field, should normally reduce to the UTD solution, whereas the latter is interpreted as a vertex diffracted wave.

The available representations of the edge equivalent currents are based on the canonical solution to the infinite wedge problem or its asymptotic reductions (Keller's Theory, UTD), which clearly fail in the vicinity of the vertex. However, the uniform asymptotic representation of the total field obtained from the truncated equivalent currents radiation integral presents a reasonable qualitative behavior and shows good agreement with moment method and measured results.

4.2 The equivalent edge currents concept.

The concept of the equivalent edge currents in the theory of diffraction, based on Sommerfeld's half plane solution, was initially developed by Millar [13,14,15] and Clemmow [16] as a simple method for deriving asymptotic approximations of the electromagnetic wave diffracted by large apertures in perfectly conducting screens. Later, the same concept was formalized by Ryan and Peters [17] and employed to correct the singular GTD fields in the caustic regions. A UTD representation of the Ryan and Peters equivalent edge currents for plane wave incidence on a perfectly conducting wedge and for observation points sufficiently far from the edge of the wedge, may be written in terms of the diffraction angle β_0 , the distance s of the observation points from the point Q of the wedge at which the currents are evaluated, and the azimuthal coordinates ϕ, ϕ' of the diffracted and

incident ray with respect to the edge fixed reference frame, as follows:

$$I^{eq}(Q) = -\frac{jY_0}{nk_0} \bar{E}^i(Q) \cdot \hat{i}(s; \phi, \phi'; \beta_0) \quad (4.1a)$$

$$M^{eq}(Q) = -\frac{jZ_0}{nk_0} \bar{H}^i(Q) \cdot \hat{i}(s; \phi, \phi'; \beta_0) \quad (4.1b)$$

with

$$\begin{aligned} \begin{Bmatrix} i(s; \phi, \phi'; \beta_0) \\ m(s; \phi, \phi'; \beta_0) \end{Bmatrix} &= \frac{1}{\sin^2 \beta_0} \left[\cot \left(\frac{\pi + (\phi - \phi')}{2n} \right) F[k_0 s a^+(\phi - \phi')] \right. \\ &\quad + \cot \left(\frac{\pi - (\phi - \phi')}{2n} \right) F[k_0 s a^-(\phi - \phi')] \\ &\quad \mp \left\{ \cot \left(\frac{\pi + (\phi + \phi')}{2n} \right) F[k_0 s a^+(\phi + \phi')] \right. \\ &\quad \left. \left. + \cot \left(\frac{\pi - (\phi + \phi')}{2n} \right) F[k_0 s a^-(\phi + \phi')] \right\} \right], \quad (4.1c) \end{aligned}$$

$$a^\pm(\gamma) = 2 \cos^2 \left(\frac{2n\pi N^\pm - \gamma}{2} \right), \quad (4.1d)$$

N^\pm being the integers that most nearly satisfy the equations

$$2\pi n N^\pm - \gamma = \pm \pi \quad (4.1e)$$

and $\bar{E}^i(Q)$, $\bar{H}^i(Q)$ denoting the incident at Q electric and magnetic field, respectively. As before, the parameter n (wedge number) is related with the wedge angle (WA) via $(WA) = (2 - n)\pi$. Note, also, that the edge transition functions $F(\cdot)$ are not normally associated with the Ryan and Peters form. It should be emphasized that Ryan and Peters equivalent currents are valid for directions of observation lying on Keller's cone of diffracted rays. Knott and Senior [18] suggested a generalization of the expressions of the equivalent currents in order to include arbitrary directions of incidence and observation by deforming the term $\sin^2 \beta_0$ appearing in

the denominator of eqs. (4.1a)-(4.1e) to the product $\sin \beta \sin \beta'$ with β, β' denoting the angle of observation and incidence respectively in a predefined edge fixed coordinate system. But their proposal is merely a postulate, since it is based on intuitive symmetry considerations rather than any mathematical derivation.

Recently, Michaeli [19,20,21,22] proposed explicit expressions for the equivalent edge currents deduced from the exact solution of the canonical wedge problem and valid for arbitrary directions of illumination and observation. His currents are related with true currents flowing along the wedge surface, since their derivation is based on the asymptotic relationship between the Physical Theory of Diffraction surface radiation integral and the equivalent current line integral.

Equivalent currents, including higher order interaction effects, were utilized by Sikta [4] for the computation of the off principal plane RCS of flat plate structures. Although Sikta used a modified version of the currents of eqs. (4.1a)-(4.1e), which is conceptually empirical his results are comparable with those presented later in [22] where the more rigorous Michaeli's edge currents were used. As pointed out in Chapter I, Burnside and Pathak [3] employed the radiation integral of the truncated equivalent currents to asymptotically identify a corner diffraction coefficient after an empirical modification of the final result. A similar approach is adopted in this chapter, using two types of equivalent currents, to develop an edge wave vertex diffraction coefficient which incorporates the singular behavior of the edge wave in the vicinity of the guiding edge and an edge diffraction coefficient valid as the origin of Keller's cone approaches the vertex point.

4.2.1 Generalized equivalent currents. The half plane case.

Non grazing incidence

A plane wave illuminates a half plane as illustrated in Fig. 2. The problem as already pointed out is essentially two dimensional. The total field can be expressed in terms of the vector potentials

$$\vec{A} = \hat{z} \psi^a ; \quad \vec{F} = \hat{z} \psi^f \quad (4.2)$$

via the following equations:

$$\vec{E} = -\nabla \times \vec{F} - j\omega_0\mu_0 (\vec{\bar{I}} + k_0^{-2}\nabla\nabla) \cdot \vec{A} \quad (4.3a)$$

$$\vec{H} = \nabla \times \vec{A} - j\omega_0\epsilon_0 (\vec{\bar{I}} + k_0^{-2}\nabla\nabla) \cdot \vec{F} \quad (4.3b)$$

where $\vec{\bar{I}}$ is the unit dyadic. Furthermore, the total field can be viewed as a field created by fictitious equivalent line sources flowing along the edge of the half plane, so that one may write

$$\psi^a(\vec{s}) = \int_{-\infty}^{\infty} I^t(\vec{s}; \beta', \phi'; z') G_0(\rho, z|z') dz' \quad (4.4)$$

$$\psi^f(\vec{s}) = \int_{-\infty}^{\infty} M^t(\vec{s}; \beta', \phi'; z') G_0(\rho, z|z') dz' \quad (4.5)$$

in which

$$G_0(\rho, z|z') = \frac{\exp\{-jk_0\sqrt{(z-z')^2 + \rho^2}\}}{4\pi\sqrt{(z-z')^2 + \rho^2}} \quad (4.6)$$

is the free space scalar Green's function, \vec{s} is the vector pointing to the observer in an arbitrarily chosen reference frame, β' is the angle between the incident ray and the wedge and the superscript t indicates the connection with the total field. It is also reminded that the $\hat{\rho}$ and $\hat{\phi}$ -directed components of the electric and magnetic field can be expressed in terms of its \hat{z} -directed components as indicated

mathematically by eqs. (2.1a), (2.1b). Thus, from eqs. (4.2)-(4.6), one obtains for the \hat{z} -directed components

$$E_z(\vec{s}) = -j\omega_0\mu_0 \int_{-\infty}^{\infty} \{I^t(\vec{s}; \beta', \phi'; z') G_0(\rho, z|z') + k_0^{-2} \frac{\partial^2}{\partial z'^2} [I^t(\vec{s}; \beta', \phi'; z') G_0(\rho, z|z')]\} dz' \quad (4.7a)$$

$$H_z(\vec{s}) = -j\omega_0\epsilon_0 \int_{-\infty}^{\infty} \{M^t(\vec{s}; \beta', \phi'; z') G_0(\rho, z|z') + k_0^{-2} \frac{\partial^2}{\partial z'^2} [M^t(\vec{s}; \beta', \phi'; z') G_0(\rho, z|z')]\} dz' \quad (4.7b)$$

which can be employed for a unique solution for I^t , M^t . Noting the convolution type of the integrals involved in the integral equations (4.7a), (4.7b) the latter can be formally solved with the aid of the Fourier transform with respect to the variable z (the z coordinate of the observation point). It is also remarked that the principal value of the integrals involved in eqs. (4.7a), (4.7b) with respect to the arbitrarily chosen origin on the \hat{z} -axis should be considered, along with the definition of the Fourier transform [23]. Without presenting the details of the derivation and restricting our attention to the diffracted term of the total field, which is physically related with currents flowing in the vicinity of the edge, one obtains the following expressions for the edge currents:

$$\begin{aligned} \begin{Bmatrix} I^f(\vec{s}; \beta', \phi'; z') \\ M^f(\vec{s}; \beta', \phi'; z') \end{Bmatrix} &= \frac{2 \exp(-j\pi/4)}{k_0 \sqrt{2\pi k_0}} \\ &\quad \cdot \frac{\exp(-jk_0 s \sin \beta \sin \beta')}{\sqrt{s \sin \beta \sin \beta'} H_0^{(2)}(k_0 s \sin \beta \sin \beta')} \\ &\quad \cdot \begin{Bmatrix} Y_0 \vec{E}^i(z') \cdot \hat{z} i^f(\vec{s}; \beta', \phi'; z') \\ Z_0 \vec{H}^i(z') \cdot \hat{z} m^f(\vec{s}; \beta', \phi'; z') \end{Bmatrix} \end{aligned} \quad (4.8a)$$

Now, the superscript f indicates relation with the diffracted field and the distance s is related with the radial coordinate ρ via $\rho = s \sin \beta$. Moreover,

$$\begin{aligned} \left\{ \begin{array}{l} i^f(\bar{s}; \beta'; \phi'; z') \\ m^f(\bar{s}; \beta'; \phi'; z') \end{array} \right\} &= \frac{1}{\sin^2 \beta'} \left\{ \frac{F[2k_0 s \sin \beta \sin \beta' \cos^2 \left(\frac{\phi - \phi'}{2} \right)]}{\cos \left(\frac{\phi - \phi'}{2} \right)} \right. \\ &\quad \left. \mp \frac{F[2k_0 s \sin \beta \sin \beta' \cos^2 \left(\frac{\phi + \phi'}{2} \right)]}{\cos \left(\frac{\phi + \phi'}{2} \right)} \right\} \end{aligned} \quad (4.8b)$$

Note that the same result can be obtained by merely dividing the diffracted field with the two dimensional free space Green's function. For large arguments of the Hankel function and if the origin of the \hat{z} -axis coincides with the diffraction point Q^e the equivalent edge currents reduce to Ryan and Peters expressions presented by eqs. (4.1a)-(4.1e). One can modify the above expressions for arbitrary directions of incidence and observation and spherical wave incidence by substituting the factor $\sin^2 \beta'$ appearing in the denominator of eq. (4.8b) with $\sin \beta \sin \beta'$ and s with the distance parameter $L = s s' / (s + s')$, where s' denoting the distance of the source from the point Q at which the equivalent edge currents are evaluated. Then, for large values of the parameter L , one obtains

$$\left\{ \begin{array}{l} I^f(Q) \\ M^f(Q) \end{array} \right\} \approx \frac{-j}{k_0} \left\{ \begin{array}{l} Y_0 \bar{E}^i(Q) \cdot \hat{i} i^f(L; \beta, \phi; \beta', \phi') \\ Z_0 \bar{H}^i(Q) \cdot \hat{i} m^f(L; \beta, \phi; \beta', \phi') \end{array} \right\} \quad (4.9a)$$

where now

$$\begin{aligned} \left\{ \begin{array}{l} i^f(L; \beta, \phi; \beta', \phi') \\ m^f(L; \beta, \phi; \beta', \phi') \end{array} \right\} &\approx \frac{1}{\sin \beta \sin \beta'} \left\{ \frac{F[2k_0 L \sin \beta \sin \beta' \cos^2 \left(\frac{\phi - \phi'}{2} \right)]}{\cos \left(\frac{\phi - \phi'}{2} \right)} \right. \\ &\quad \left. \mp \frac{F[2k_0 L \sin \beta \sin \beta' \cos^2 \left(\frac{\phi + \phi'}{2} \right)]}{\cos \left(\frac{\phi + \phi'}{2} \right)} \right\} \end{aligned} \quad (4.9b)$$

and \hat{i} is again the unit vector tangent to the edge at Q .

The perturbation of the original expressions (4.8a), (4.8b) is based on the same arguments stated by Knott and Senior and has no mathematical justification. Evidently, the above representation can be generalized for the wedge case. The final result is merely a symmetric perturbation of Ryan and Peters edge currents. It should be emphasized that asymptotic evaluation of the radiation integral of the edge currents described by eqs. (4.9a)-(4.9b) over a finite (possibly curved) edge yields always a reciprocal result and the correct field for observation directions in the Keller's cone of diffracted rays. Besides, the more general expressions (4.8a), (4.8b) can be used for corrections in caustic regions in the near field of the wedge where the GTD related Ryan and Peters equivalent currents fail.

Grazing incidence

An interesting case arises when the incident plane wave grazes the edge of the half plane ($\beta' \rightarrow 0$). The equivalent edge currents that would support the edge guided wave given by eqs. (2.13), (2.14) can be derived following a similar procedure. However, in this case, the integral equations (4.7a), (4.7b) as $\beta' \rightarrow 0$ yield an indeterminate form which implies an infinity of solutions for the unknown edge currents. This ambiguity originates from the fact that grazing plane wave incidence is essentially a theoretical idealization. Nevertheless, based on the dipole excitation problem examined in Section 2.3, one can obtain expressions for the equivalent currents which are physically reasonable. Beginning with the integral equations:

$$E_{\rho}^{ew} = - \int_{-\infty}^{\infty} \left\{ \frac{1}{\rho} \frac{\partial}{\partial \phi} [M^{ew}(\bar{s}; \beta', \phi'; z') G_0(\rho, z|z')] + j\omega_0 \mu_0 k_0^{-2} \frac{\partial^2}{\partial \rho \partial z} [I^{ew}(\bar{s}; \beta', \phi'; z') G_0(\rho, z|z')] \right\} dz' \quad (4.10a)$$

$$E_{\phi}^{ew} = - \int_{-\infty}^{\infty} \left\{ - \frac{\partial}{\partial \rho} [M^{ew}(\bar{s}; \beta', \phi'; z') G_0(\rho, z|z')] \right. \\ \left. + j\omega_0 \mu_0 k_0^{-2} \frac{1}{\rho} \frac{\partial^2}{\partial \phi \partial z} [I^{ew}(\bar{s}; \beta', \phi'; z') G_0(\rho, z|z')] \right\} dz' \quad (4.10b)$$

as $\beta' \rightarrow 0$, one may postulate

$$\begin{pmatrix} I^{ew}(\bar{s}; \beta', \phi'; z) \\ M^{ew}(\bar{s}; \beta', \phi'; z) \end{pmatrix} = - \frac{8 \exp(j\pi/4)}{\sqrt{2\pi k_0}} \frac{\sqrt{\rho} S_0(\beta', \phi')}{H_0^{(2)}(k_0 \rho \sin \beta')} \\ \exp(-jk_0 z) \begin{pmatrix} Y_0 \sin(\phi/2) \\ -\cos(\phi/2) \end{pmatrix} \quad (4.11)$$

where

$$S_0(\beta', \phi') = \frac{E_{0\beta'} \sin(\phi'/2) + E_{0\phi'} \cos(\phi'/2)}{\sqrt{\sin \beta'}} \quad (4.12)$$

is an excitation related factor.

4.3 Michaeli's edge currents in an oblique edge fixed frame.

For the general wedge case one obtains the following equations for the total edge magnetic and electric equivalent currents excited at the point Q of the edge of the wedge [19]:

$$I(Q) = -\bar{E}^i(Q) \cdot i \frac{2jY_0 \sin(\phi'/n)}{nk_0 \sin^2 \beta'} \left\{ \frac{1}{\cos[(\pi - \gamma_1)/n] - \cos(\phi'/n)} \right. \\ \left. + \frac{1}{\cos[(\pi - \gamma_2)/n] + \cos(\phi'/n)} \right\} - \bar{H}^i(Q) \cdot i \frac{2j}{nk_0 \sin \beta'} \\ \left\{ \frac{\sin[(\pi - \gamma_1)/n]}{\sin \gamma_1} \frac{\mu_1 \cot \beta' - \cot \beta \cos \phi}{\cos[(\pi - \gamma_1)/n] - \cos(\phi'/n)} \right. \\ \left. - \frac{\sin[(\pi - \gamma_2)/n]}{\sin \gamma_2} \frac{\mu_2 \cot \beta' - \cot \beta \cos(n\pi - \phi)}{\cos[(\pi - \gamma_2)/n] + \cos(\phi'/n)} \right\} \quad (4.13a)$$

$$M(Q) = \bar{H}^i(Q) \cdot i \frac{2jZ_0}{nk_0 \sin \beta \sin \beta'}$$

$$\cdot \left\{ \frac{\sin[(\pi - \gamma_1)/n] \sin \phi}{\sin \gamma_1 \{ \cos[(\pi - \gamma_1)/n] - \cos(\phi'/n) \}} + \frac{\sin[(n\pi - \gamma_2)/n] \sin(n\pi - \phi)}{\sin \gamma_2 \{ \cos[(\pi - \gamma_2)/n] + \cos(\phi'/n) \}} \right\} \quad (4.13b)$$

where the complex angles $\gamma_{1,2}$ are defined by the equation

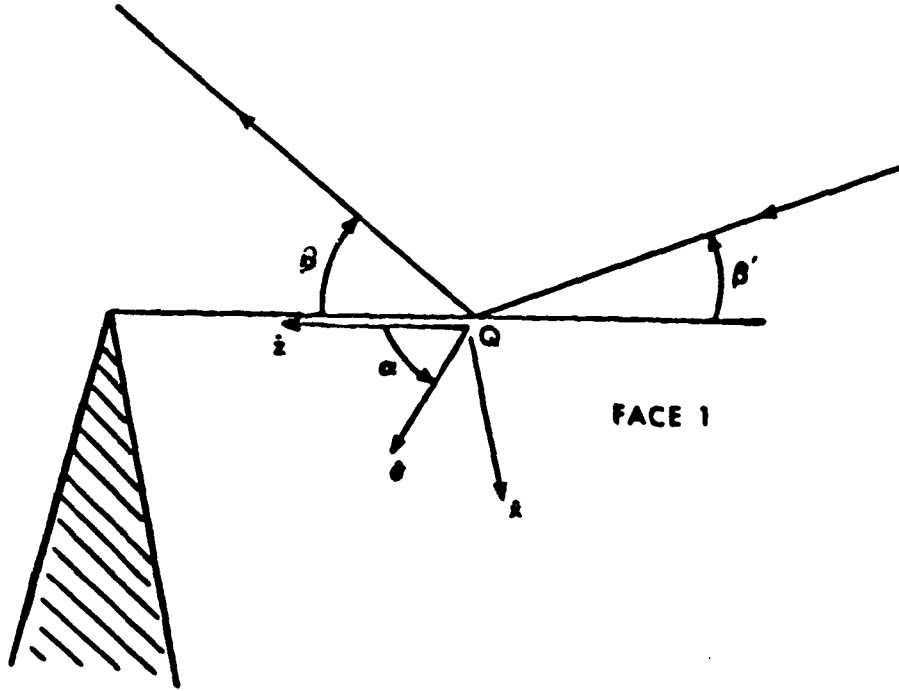


Figure 21: Oblique edge fixed coordinate system for the definition of Michaeli's equivalent currents.

$$\gamma_{1,2} = -j \ln(\mu_{1,2} + \sqrt{\mu_{1,2}^2 - 1}) \quad (4.14)$$

along with the following choice of the branch of the square root in eq. (4.14):

$$\sqrt{\mu^2 - 1} = \begin{cases} |\sqrt{\mu^2 - 1}| & ; \quad \mu > 1 \\ j|\sqrt{\mu^2 - 1}| & ; \quad -1 < \mu < 1 \\ -|\sqrt{\mu^2 - 1}| & ; \quad \mu < -1 \end{cases} \quad (4.15)$$

The parameter μ depends on the coordinates β, ϕ and β', ϕ' of the observer and the source, respectively, in terms of the edge fixed reference frame centered at Q as well as the choice of the edge fixed system of coordinates itself, i.e., the angle α between the unit vector \hat{i} tangent to the edge at Q and the unit vector $\hat{\sigma}$ tangent to face 1 of the wedge at Q , as shown in Fig. 21. The latter implies a nonuniqueness in the presentation of the Michaeli's equivalent currents. For a general α angle, μ_1 is found equal to

$$\mu_1(\alpha) = \frac{\sin \alpha \sin \beta \cos \phi + \cos \alpha (\cos \beta - \cos \beta')}{\sin \alpha \sin \beta'} \quad (4.16)$$

For the definition of μ_2 which is associated with face 2, ϕ should be substituted by $\pi - \phi$ and β, β' by $\pi - \beta, \pi - \beta'$, respectively. If the classical edge fixed system of coordinates is chosen, then $\alpha = \pi/2$ and μ_1 becomes

$$\mu_1(\pi/2) = \sin \beta \cos \phi / \sin \beta' \quad (4.17)$$

On the other hand, if the $\hat{\sigma}$ -axis is chosen parallel to the diffracted ray that grazes face 1 surface, as suggested by Michaeli in [20], i.e., when $\alpha = \beta'$ from eq. (4.15) one obtains

$$\mu_1(\beta') = \frac{\sin \beta \sin \beta' \cos \phi + \cos \beta' (\cos \beta - \cos \beta')}{\sin^2 \beta'} \quad (4.18)$$

For a more systematic approach to the approximation of the edge wave vertex diffraction mechanism, it is convenient to extract the physical optics components from the total equivalent edge currents presented by Michaeli. In accordance with [24], the total currents given by eqs. (4.13a), (4.13b) can be split into the Physical Optics current components M^{po}, I^{po} and the fringe current components M^f, I^f with

$$I(Q) = I^{po}(Q) + I^f(Q) ; \quad M(Q) = M^{po}(Q) + M^f(Q) \quad (4.19)$$

Specifically, the Physical Optics components associated with face 1 of the wedge are given by the following equations:

$$I_1^{PO}(Q) = \frac{2j U(\pi - \phi')}{k_0 \sin \beta' (\mu_1 + \cos \phi')} \left[\vec{E}^i(Q) \cdot \hat{i} \frac{\sin \phi'}{Z_0 \sin \beta'} - \vec{H}^i(Q) \cdot \hat{i} (\cot \beta' \cos \phi' + \cot \beta \cos \phi) \right] \quad (4.20a)$$

$$M_1^{PO}(Q) = -\vec{H}^i(Q) \cdot \hat{i} \frac{2j Z_0 \sin \phi U(\pi - \phi')}{k_0 \sin \beta \sin \beta' (\mu_1 + \cos \phi')} \quad (4.20b)$$

while the fringe currents can be derived from eqs. (4.13a), (4.13b), (4.19) and (4.20a), (4.20b).

4.4 Vertex diffraction of an edge wave excited by a dipole.

An excitation dipole is placed in the close vicinity of the edge of a semi-infinite wedge and at a distance s'_c (with $k_0 s'_c \gg 1$) from its vertex. The interaction between the dipole and the edge produces an edge guided wave which, sufficiently far from the dipole, can be treated as ray optical. This ray optical edge wave is diffracted in accordance with the generalized Fermat's principle. In our case, despite the direct field which is essentially the edge wave suitably modified for a semi-infinite structure, the observer is reached by a vertex and, possibly, two edge diffracted rays emanating from the vertex point Q^c and the terminating edges points Q_1^e, Q_2^e , respectively, where Q_1^e, Q_2^e are the origins of the classical Keller's cone of diffracted rays. The observer is in the illuminated or shadowed region of the edge wave edge diffracted fields from the points Q_1^e, Q_2^e , if Q_1^e, Q_2^e are points of the semi-infinite edges (1), (2) or points of their extensions, respectively.

A uniform solution is investigated herein using the equivalent currents described earlier in this chapter and excited by the edge wave impinging on the terminating edges (1) and (2). The "uniformity" of the solution requires the continuity of the total field at the shadow boundary of the direct field (edge wave)

and the boundaries of the regions illuminated by the edge diffracted rays from Q_1^c, Q_2^c . Furthermore, the solution should remain finite at the extension of the guiding edge. One may write for the total field

$$\vec{E}^t = \vec{E}^{ew} \cdot \vec{T} + \vec{E}_1^c U(t_{Q_1^c}) + \vec{E}_2^c U(t_{Q_2^c}) + \vec{E}^c \quad (4.21)$$

where \vec{E}^{ew} is the field produced by the dipole in the presence of an infinite wedge, \vec{T} is a heuristic transition dyadic which assures the continuity across its shadow boundaries and its finiteness along the extension of the guiding edge, $\vec{E}_{1,2}^c$ are the edge diffracted fields with $t_{Q_{1,2}^c}$ denoting the t coordinate of the points $Q_{1,2}^c$ in terms of the edges (1) and (2) fixed coordinate systems depicted in Fig. 10, and \vec{E}^c is the vertex diffracted wave. It is reminded that $U(\cdot)$ represents the unit step function ($U(x) = 1$ if $x > 0$, $U(x) = 0$ if $x < 0$).

As before, our attention is restricted to face 1 of the wedge. The equivalent currents presented earlier for grazing edge wave incidence at the point Q_1 of the edge (1) may be rewritten as

$$I_1(Q_1) = \frac{2j}{k_0} \frac{\vec{H}^{ew}(Q_1) \cdot \hat{t}_1}{2} i_1(\vec{s}_c; t_1) \quad (4.22a)$$

$$M_1(Q_1) = \frac{2jZ_0}{k_0} \frac{\vec{H}^{ew}(Q_1) \cdot \hat{t}_1}{2} m_1(\vec{s}_c; t_1) \quad (4.22b)$$

where $\vec{H}^{ew}(Q_1)$ is the field produced by the dipole radiating in the presence of an infinite wedge evaluated at the point Q_1 , \hat{t}_1 is the unit vector tangent to the edge at Q_1 and i_1, m_1 are known and, in general, slowly varying functions of the observer's location in the vertex fixed coordinate system and the distance of Q_1 from the tip Q^c of the trihedron. The wedge number n_1 is related now with the wedge formed by face 1 and the plane surface defined by the edges (1) and (2). Note also that a factor of 1/2 has been introduced due to grazing incidence. It can

be easily shown using eq. (2.19) and the relationship

$$\vec{H}^{ew}(\vec{r}) = Y_0 \vec{r} \times \vec{E}^{ew}(\vec{r})$$

which is valid for ray optical waves, that

$$\vec{H}^{ew}(Q_1) \cdot \hat{i}_1 = -jk_0^\nu \sin^\nu \alpha_1 C(\nu) A_\nu^e(\rho', \phi') s_c' \frac{\exp(-jk_0 r_1)}{r_1^{\nu+1}} t_1^{\nu-1} \quad (4.23)$$

with

$$r_1 = \sqrt{s_c'^2 + t_1^2 - 2 t_1 s_c' \cos \alpha_1}. \quad (4.24)$$

As before,

$$A_\nu^e(\rho', \phi') = \rho'^{\nu-1} (p_{\rho'}^e \sin \nu \phi' + p_{\phi'}^e \cos \nu \phi')$$

and the constant $C(\nu)$ is defined by eq. (2.17).

It is presumed that the edge and vertex diffracted edge wave associated with face 1 of the wedge can be approximated by the radiation integral of the equivalent currents $I_1(Q_1)$, $M_1(Q_1)$ flowing along the edge (1), which in the Fresnel or the Fraunhofer region of the edge can be explicitly written as

$$\begin{aligned} \vec{E}_1^d(\vec{s}_c) \approx & jk_0^\nu Z_0 \sin^\nu \alpha_1 C(\nu) A_\nu^e(\rho', \phi') s_c' \\ & \cdot \int_0^\infty [\hat{R} \times \hat{R} \times \hat{i}_1 i_1(\vec{s}_c; t_1) + \hat{R} \times \hat{i}_1 m_1(\vec{s}_c; t_1)] \\ & \cdot t_1^{\nu-1} \frac{\exp\{-jk_0(R + r_1)\}}{4\pi R r_1^{\nu+1}} dt_1 \end{aligned} \quad (4.25)$$

with $R = \|\vec{s}_c - t_1 \hat{i}_1\|$ and $\hat{R} = (\vec{s}_c - t_1 \hat{i}_1)/R$

For large values of the parameter k_0 the asymptotic evaluation of the radiation integral reveals a vertex contribution and, also, an edge diffracted term. if

$$\cos \alpha_1 (1 - \cos \beta) + \sin \alpha_1 \sin \beta \cos \phi > 0.$$

i.e., if Q_1^e lies on the edge (1) itself rather than on its extension. These two terms are examined separately in Sections 4.4.1 and 4.4.2 respectively.

4.4.1 Edge wave vertex diffracted field.

Interpreting the end point contribution to the radiation integral as a vertex diffraction term, one obtains the approximate relationship

$$\begin{aligned} \bar{E}_1^c(\bar{s}_c) \approx & j k_0^\nu Z_0 \sin^\nu \alpha_1 A_\nu^c(\rho', \phi') \frac{\exp\{-j k_0(s_c + s'_c)\}}{4\pi s_c s'_c{}^\nu} \\ & \cdot \bar{G}_1^c(\bar{s}_c) I_{-\nu}^0(k_0) \end{aligned} \quad (4.26)$$

where we have substituted

$$\bar{G}_1^c(\bar{s}_c) = \hat{s}_c \times \hat{s}_c \times \hat{i}_1 i_1(\bar{s}_c; 0) + \hat{s}_c \times \hat{i}_1 m_1(\bar{s}_c; 0) \quad (4.27)$$

and $I_{-\nu}^0(k_0)$ denotes the end point contribution to the integral

$$\int_0^\infty t_1^{\nu-1} \exp\{-j k_0(R + r_0)\} dt_1.$$

Referring to eq. (3.8) one writes

$$\begin{aligned} I_{-\nu}^0(k_0) \approx & \Gamma(\nu) k_0^{-\nu} \exp(j\nu\pi/2) \exp\{-j k_0(s_c + s'_c)\} \\ & \frac{F_{-\nu}^c[k_0 a_1^2(\bar{s}_c; s'_c)]}{[\sin \alpha_1 \sin \beta \cos \phi + \cos \alpha_1 (1 - \cos \beta)]^\nu} \end{aligned} \quad (4.28)$$

in which the edge wave transition function has been defined by eq. (3.13). The vertex diffracted field associated with face 1 of the wedge becomes

$$\begin{aligned} \bar{E}_1^c(\bar{s}_c) \approx & \exp\{j(\nu + 1)\pi/2\} \Gamma(\nu) C(\nu) Z_0 A_\nu^c(\rho', \phi') \frac{\exp\{-j k_0(s_c + s'_c)\}}{4\pi s_c s'_c{}^\nu} \\ & \cdot \bar{G}_1^c(\bar{s}_c) \frac{F_{-\nu}^c[k_0 a_1^2(\bar{s}_c; s'_c)]}{[\cot \alpha_1 (1 - \cos \beta) + \sin \beta \cos \phi]^\nu} \end{aligned} \quad (4.29)$$

Michaeli's equivalent currents

It has been pointed out that Michaeli's equivalent line sources can be derived from the asymptotic reduction of the surface radiation integral of the true surface currents evaluated from the canonical solution and flowing over the faces of the

wedge and can be split into geometrical optics and fringe current components. Moreover, when these currents are truncated to reveal an end point effect, one should be cautious about the choice of the parameter μ involved in the expressions of these currents, i.e., the choice of the edge fixed coordinate system, so that the terminated equivalent edge currents represent correctly the end point effect of the truncation by the edges of the trihedron true surface induced currents. In this context, a correct choice of the parameter μ_1 for the Physical Optics component of the equivalent currents, using eq. (4.16), is the following:

$$\mu_1^{po} = \mu_1(\alpha_1) = \frac{\sin \alpha_1 \sin \beta_1 \cos \phi_1 + \cos \alpha_1 (\cos \beta_1 + \cos \alpha_1)}{\sin^2 \alpha_1} \quad (4.30)$$

so that the unit vector \hat{o} in Fig. 21 is parallel to the guiding edge, whereas for the fringe currents the proper choice is

$$\mu_1^f = \mu_1(\pi - \alpha_1) = \frac{\sin \alpha_1 \sin \beta_1 \cos \phi_1 - \cos \alpha_1 (\cos \beta_1 + \cos \alpha_1)}{\sin^2 \alpha_1} \quad (4.31)$$

and, now, \hat{o} is parallel to the edge diffracted ray from Q^c that grazes the plane of face 1. In the above equations β_1, ϕ_1 are the elevation and azimuthal angle of the observation point in terms of the edge (1) fixed coordinate system centered at Q^c .

The previous discussion also suggests the decomposition

$$\vec{G}_1^c(\vec{s}_c) = \vec{G}_1^{c,po}(\vec{s}_c) + \vec{G}_1^{c,f}(\vec{s}_c) \quad (4.32)$$

where the superscripts po and f imply connection with the physical optics and fringe current components, respectively. Not surprisingly, using eq. (4.30) for the definition of the parameter μ in the eqs. (4.20a)-(4.20b) of the physical optics equivalent edge currents and after some tedious manipulation, which, however, involves only elementary operations, it can be shown that:

$$\vec{G}_1^{c,po}(\vec{s}_c) = -\hat{\beta} \cot \frac{\beta}{2} \quad (4.33)$$

so that the vertex diffracted field assumes the approximation

$$\vec{E}^c(\vec{s}_c) \approx \vec{E}^{c,po}(\vec{s}_c) + \vec{E}^{c,f}(\vec{s}_c) \quad (4.34)$$

in which $\vec{E}^{c,po}(\vec{s}_c)$ is the field given by eq. (3.10) or eqs. (3.11a), (3.11b), while the fringe currents related wave is equal to

$$\begin{aligned} \vec{E}^{c,f}(\vec{s}_c) \approx & \exp\{j(\nu+1)\pi/2\} \Gamma(\nu) C(\nu) Z_0 A_\nu^c(\rho', \phi') \\ & \cdot \frac{\exp\{-jk_0(s_c + s'_c)\}}{4\pi s_c s'_c{}^\nu} F(2k_0 L_c \sin^2 \frac{\beta}{2}) \\ & \cdot \left[\frac{\vec{G}_1^{c,f}(\vec{s}_c) F_{-\nu}^c[k_0 a_1^2(\vec{s}_c; s'_c)]}{[\cot \alpha_1(1 - \cos \beta) + \sin \beta \cos \phi]^\nu} \right. \\ & \left. + \frac{\vec{G}_2^{c,f}(\vec{s}_c) F_{-\nu}^c[k_0 a_2^2(\vec{s}_c; s'_c)]}{[\cot \alpha_2(1 - \cos \beta) + \sin \beta \cos(n\pi - \phi)]^\nu} \right] \end{aligned} \quad (4.35)$$

The vector functions $\vec{G}_l^{c,f}(\vec{s}_c)$ ($l = 1, 2$) are related with the Michaeli's equivalent currents at Q^c via the equations:

$$\vec{G}_l^{c,f}(\vec{s}_c) = i_l^f(Q^c) \hat{s}_c \times \hat{s}_c \times \hat{i}_l + m_l^f(Q^c) \hat{s}_c \times \hat{i}_l \quad (4.36)$$

where

$$\begin{Bmatrix} i_l^f(Q^c) \\ m_l^f(Q^c) \end{Bmatrix} = \begin{Bmatrix} i_l(Q^c) \\ m_l(Q^c) \end{Bmatrix} - \begin{Bmatrix} i_l^{po}(Q^c) \\ m_l^{po}(Q^c) \end{Bmatrix} \quad (4.37)$$

and $i_l(Q^c)$, $m_l(Q^c)$, $i_l^{po}(Q^c)$, $m_l^{po}(Q^c)$ are described explicitly by the expressions

$$\begin{aligned} i_l(Q^c) = & -\frac{1}{n_l \sin \alpha_l} \left\{ \frac{\mu_{l1}^f \cot \alpha_l + \cot \beta_l \cos \phi_l}{\sin \gamma_{l1}} \frac{\sin[(\pi - \gamma_{l1})/n_l]}{1 - \cos[(\pi - \gamma_{l1})/n_l]} \right. \\ & \left. + \frac{\mu_{l2}^f \cot \alpha_l + \cot \beta_l \cos(n_l \pi - \phi_l)}{\sin \gamma_{l2}} \frac{\sin[(\pi - \gamma_{l2})/n_l]}{1 + \cos[(\pi - \gamma_{l2})/n_l]} \right\} \end{aligned} \quad (4.38)$$

$$m_l(Q^c) = -\frac{1}{n_l \sin \alpha_l \sin \beta_l} \left\{ \frac{\sin \phi_l}{\sin \gamma_{l1}} \frac{\sin[(\pi - \gamma_{l1})/n_l]}{1 - \cos[(\pi - \gamma_{l1})/n_l]} - \frac{\sin(n_l \pi - \phi_l)}{\sin \gamma_{l2}} \frac{\sin[(\pi - \gamma_{l2})/n_l]}{1 + \cos[(\pi - \gamma_{l2})/n_l]} \right\} \quad (4.39)$$

and

$$i_l^{po}(Q^c) = \frac{\cot \alpha_l - \cot \beta_l \cos \phi_l}{\sin \alpha_l (1 + \mu_l^f)} \quad (4.40)$$

$$m_l^{po}(Q^c) = -\frac{\sin \phi_l}{\sin \alpha_l \sin \beta_l (1 + \mu_l^f)} \quad (4.41)$$

The index l assumes the values 1 and 2 for the edges (1) and (2) of the trihedron, respectively. The elevation and azimuthal angles $\beta_{1,2}$, $\phi_{1,2}$ of the observer in terms of the coordinate systems associated with the edges (1) and (2) and centered at the tip Q^c are related with the principal spherical coordinates β , ϕ via the easily verified equations

$$\begin{aligned} \cos \beta_1 &= \sin \alpha_1 \sin \beta \cos \phi - \cos \alpha_1 \cos \beta ; \\ \sin \beta_1 &= |\sqrt{1 - \cos^2 \beta_1}| \end{aligned} \quad (4.42)$$

$$\begin{aligned} \cos \beta_2 &= \sin \alpha_2 \sin \beta \cos(n\pi - \phi) - \cos \alpha_2 \cos \beta ; \\ \sin \beta_2 &= |\sqrt{1 - \cos^2 \beta_2}| \end{aligned} \quad (4.43)$$

$$\begin{aligned} \cos \phi_1 &= -\frac{\cos \alpha_1 \sin \beta \cos \phi + \sin \alpha_1 \cos \beta}{\sin \beta_1} ; \\ \sin \phi_1 &= \frac{\sin \beta \sin \phi}{\sin \beta_1} \end{aligned} \quad (4.44)$$

$$\begin{aligned} \cos \phi_2 &= -\frac{\cos \alpha_2 \sin \beta \cos(n\pi - \phi) + \sin \alpha_2 \cos \beta}{\sin \beta_2} ; \\ \sin \phi_2 &= \frac{\sin \beta \sin(n\pi - \phi)}{\sin \beta_2} \end{aligned} \quad (4.45)$$

In accordance with eq. (4.31) the parameters μ_{l1}^f , μ_{l2}^f should be chosen equal to

$$\mu_{l1}^f = \frac{\sin \alpha_l \sin \beta_l \cos \phi_l - \cos \alpha_l (\cos \beta_l + \cos \alpha_l)}{\sin^2 \alpha_l} \quad (4.46)$$

$$\mu_{l2}^f = \frac{\sin \alpha_l \sin \beta_l \cos(n_l \pi - \phi_l) - \cos \alpha_l (\cos \beta_l + \cos \alpha_l)}{\sin^2 \alpha_l} \quad (4.47)$$

The above expressions simplify considerably for the case of the plane angular sector, with $\alpha_1 = \alpha_2 = \alpha$, $a_1 = a_2 = a$. Without presenting the details of the derivation which again involves only elementary manipulations, for the field related with the fringe currents one derives

$$\begin{aligned} \bar{E}^{c,f}(\bar{s}_c) \approx & \frac{-jZ_0}{\sqrt{2}\pi} A^c(\rho', \phi') \frac{\exp\{-jk_0(s_c + s'_c)\}}{4\pi s_c \sqrt{s'_c}} \\ & F(2k_0 L_c \sin^2 \frac{\beta}{2}) \frac{\bar{G}^{c,f}(\bar{s}_c; \alpha) F_{-1/2}^c[k_0 a^2(\bar{s}_c; s'_c)]}{\sqrt{\cot \alpha (1 - \cos \beta) + \sin \beta \cos \phi}} \end{aligned} \quad (4.48a)$$

where the function $\bar{G}^{c,f}(\bar{s}_c)$ is given by

$$\bar{G}^{c,f}(\bar{s}_c) = \frac{1}{\cos(2\alpha) + \cos \delta} \left[-\hat{\beta} \sin \beta + \frac{\hat{\beta} e_\beta(\beta, \phi) + \hat{\phi} e_\phi(\beta, \phi)}{\sin^2 \alpha \sin \beta_1 \cos(\delta/2)} \right] \quad (4.48b)$$

with

$$\cos \delta = \sin(2\alpha) \sin \beta \cos \phi - \cos(2\alpha) \cos \beta \quad (4.48c)$$

$$\begin{aligned} e_\beta(\beta, \phi) = & -(\cos \alpha + \cos \beta_1) (\sin \alpha \cos \beta \cos \phi + \cos \alpha \sin \beta) \\ & \cdot [\sin \alpha \cos \phi_1 (1 - \cos \alpha \cos \beta_1) - \cos^2 \alpha \sin \beta_1] \\ & + \sin^5 \alpha \sin \phi \sin \phi_1 \end{aligned} \quad (4.48d)$$

$$\begin{aligned} e_\phi(\beta, \phi) = & \sin \alpha \sin \phi (\cos \alpha + \cos \beta_1) \\ & \cdot [\sin \alpha \cos \phi_1 (1 - \cos \alpha \cos \beta_1) - \cos^2 \alpha \sin \beta_1] \\ & + \sin^4 \alpha \sin \phi_1 (\sin \alpha \cos \beta \cos \phi + \cos \alpha \sin \beta) \end{aligned} \quad (4.48e)$$

and the angles β_1, ϕ_1 are defined by eqs. (4.42), (4.44) for $\alpha_1 = \alpha$.

For the particular case of the right angle angular sector ($\alpha = \pi/2$) it readily follows that

$$\vec{G}^{c,f}(\vec{s}_c; \pi/2) = \hat{\beta} \left(\cot \frac{\beta}{2} - \csc \frac{\beta}{2} \right) \quad (4.49)$$

and the total corner diffracted field assumes the simple representation

$$\begin{aligned} \vec{E}^c(\vec{s}_c) \approx & \frac{-jZ_0}{\sqrt{2}\pi} A^e(\rho', \phi') \frac{\exp\{-jk_0(s_c + s'_c)\}}{4\pi s_c \sqrt{s'_c}} \\ & \cdot \frac{F(2k_0 L_c \sin^2 \frac{\beta}{2})}{\sin \frac{\beta}{2}} \frac{F_{-1/2}^c[k_0 L_c (1 - \sqrt{1 - \sin^2 \beta \cos^2 \phi})]}{\sqrt{\sin \beta \cos \phi}} \hat{\beta} \end{aligned} \quad (4.50)$$

where $A^e(\rho', \phi')$ is defined by eq. (2.21). In a more familiar notation

$$\begin{aligned} \vec{E}^c(\vec{s}_c) \approx & \frac{1}{\sqrt{2}\pi k_0} \frac{E_{\beta'}^i(Q^c) \sin \frac{\phi'}{2} + E_{\phi'}^i(Q^c) \cos \frac{\phi'}{2}}{\sqrt{\sin \beta'}} \\ & \cdot \frac{F(2k_0 L_c \sin^2 \frac{\beta}{2})}{\sin \frac{\beta}{2}} \frac{F_{-1/2}^c[2k_0 L_c (1 - \sqrt{1 - \sin^2 \beta \cos^2 \phi})]}{\sqrt{\sin \beta \cos \phi}} \\ & \frac{\exp(-jk_0 s_c)}{s_c} \hat{\beta} \end{aligned} \quad (4.51)$$

Generalized equivalent currents

The vertex diffracted field derived with Michaeli's equivalent currents has a clear physical interpretation in that it is essentially the field produced by the superposition of the truncated physical optics currents that would flow over an infinite wedge and the fringe currents excited by the terminated edges for edge wave grazing incidence. However, it does not satisfy the boundary conditions on the trihedron surface. Although the latter may be a minor concern for Fraunhofer region observations, as far as the earlier derived equations serve as a good approximation of the

region observations, as far as the earlier derived equations serve as a good approximation of the vertex diffracted edge wave, it would be interesting to obtain a vertex diffraction coefficient which would satisfy the appropriate boundary conditions on the surface of the trihedron. For this purpose one may introduce the generalized equivalent currents described for the half plane case by eqs. (4.9a)-(4.9b). The approach is essentially empirical since the generalized equivalent currents are not necessarily related with true surface currents, but merely is a symmetric perturbation of the edge currents that would produce the correct edge diffracted field from an infinite edge.

For simplicity the plane right angular sector rather than the complex trihedron problem is examined. The total vertex diffracted field is related with the end point contribution to the radiation integral of two equivalent line sources: the first associated with the guiding edge (edge (0)) which is grazed by the dipole excited field and can be derived by a heuristic modification of the currents of eq. (4.11), and the second associated with the terminated edge (edge (1)) and evaluated from eqs. (4.9a)-(4.9b) for edge wave incidence. The edge wave equivalent currents given by eq. (4.11) are clearly valid only for plane wave incidence which is also evident in their $k_0^{-1/2}$ dependence rather than the k_0^{-1} dependence of Ryan and Peters as well as Michaeli equivalent currents. The empirical modification concerned with the edge wave dipole excitation problem involves a multiplicative introduction of a "reflection coefficient" similar to that suggested by Sikta in [4], namely

$$R^{ew} = -\frac{\exp(-j\pi/4)}{4\sqrt{\pi k_0 s'_c}} \quad (4.52)$$

as well as the multiplication by the edge wave transition function

$$F_{-1/2}^e(2k_0 L_c \sin^2 \frac{\beta}{2})$$

which assures the finiteness of the total solution as $\beta \rightarrow 0$. The corner diffracted field associated with the guiding edge is then equal to

$$\begin{aligned}\bar{E}_0^c(\bar{s}_c) \approx & \frac{j}{\sqrt{2}\pi k_0} \frac{E_{\beta'}^i(Q^c) \sin \frac{\phi'}{2} + E_{\phi'}^i(Q^c) \sin \frac{\phi'}{2}}{\sqrt{\sin \beta \sin \beta'}} \\ & \cdot (\hat{\beta} \sin \frac{\phi}{2} + \hat{\phi} \cos \frac{\phi}{2}) \frac{F(2k_0 L_c \sin^2 \frac{\beta}{2})}{\sin \frac{\beta}{2}} \\ & \cdot F_{-1/2}^c(2k_0 L_c \sin^2 \frac{\beta}{2})\end{aligned}\quad (4.53)$$

Note that the field exhibits a similar qualitative behavior with the edge wave corner diffracted field derived in [4] from a limiting manipulation of the corner diffraction coefficient. The term associated with the terminated edge is written

$$\begin{aligned}\bar{E}_1^c(\bar{s}_c) \approx & -\frac{1}{\sqrt{2}\pi k_0} \frac{E_{\beta'}^i(Q^c) \sin \frac{\phi'}{2} + E_{\phi'}^i(Q^c) \cos \frac{\phi'}{2}}{\sqrt{\sin \beta'}} \\ & \cdot (\hat{\beta} \sin \phi + \hat{\phi} \cos \beta \cos \phi) \frac{F(2k_0 L_c \sin^2 \beta_1 \cos^2 \frac{\phi_1}{2})}{\sin \beta_1 \cos \frac{\phi_1}{2}} \\ & \frac{F_{-1/2}^c[k_0 L_c (1 - \sqrt{1 - \sin^2 \beta \cos^2 \phi})]}{\sqrt{\sin \beta \cos \phi}}\end{aligned}\quad (4.54)$$

The total vertex diffracted field, however, cannot be simply obtained from the superposition of \bar{E}_0^c and \bar{E}_1^c , because the effect of the truncated currents may be double counted. Therefore, a modification of the final expressions is necessary in order to obtain results compatible with those presented earlier.

Although the new expressions for the field satisfy the appropriate boundary conditions on the half plane, they exhibit a discontinuity on the plane of the sector as the boundary $\beta = 0$ is crossed, i.e., the field has a definite finite value as $\beta \rightarrow 0$ on the $\phi = \pi$ half plane, while it vanishes on the $\phi = 0$ semi-plane. This inadequacy is also present in Sikta's expressions of the edge wave corner diffracted field. Note also that the field expressions exhibit a $\hat{\phi}$ -directed component which

does not vanish, as it should, on the plane of the plate. The same problem occurs in the expression of the corner diffraction coefficient and is coherent with the nature of the truncated equivalent currents which are derived from the half plane solution. It can be possibly overcome by incorporating higher order interaction effects between the currents flowing along edge (1) and the adjacent edge (edge (0)), which, however, appears cumbersome.

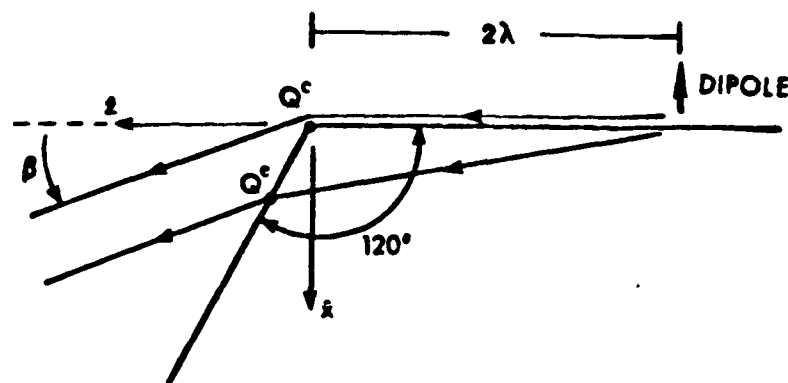


Figure 22: Angular sector geometry for the comparison of the generalized and Michaeli's equivalent edge currents.

The generalized equivalent current field associated with the edge (1) (GEC (1)) is compared with the Michaeli's current (MEC) and Physical Optics (PO) solution in Figs. 23 through 28 for an angular sector with $\alpha = 120^\circ$, the geometry of which is shown in Fig. 22. The direct dipole field is not incorporated in any of the above calculations. The singularity of the field predicted by the Physical Optics solution is evident in Figs. 23 and 25. The three approaches show good agreement for small values of the elevation angle θ and sufficiently far from the

plane of the angular sector. At $\phi = 180^0$ the generalized equivalent current field presents a non-vanishing $\hat{\phi}$ -directed component, which is not physically acceptable. However, it satisfies the boundary conditions on the sector surface. The solutions diverge at the vicinity of the guiding edge (i.e., when $\beta \rightarrow 180^0$). But in that region the total field is dominated by the singular direct dipole field (edge wave).

— MEC
 - - - GEC(1)
 - - - P0

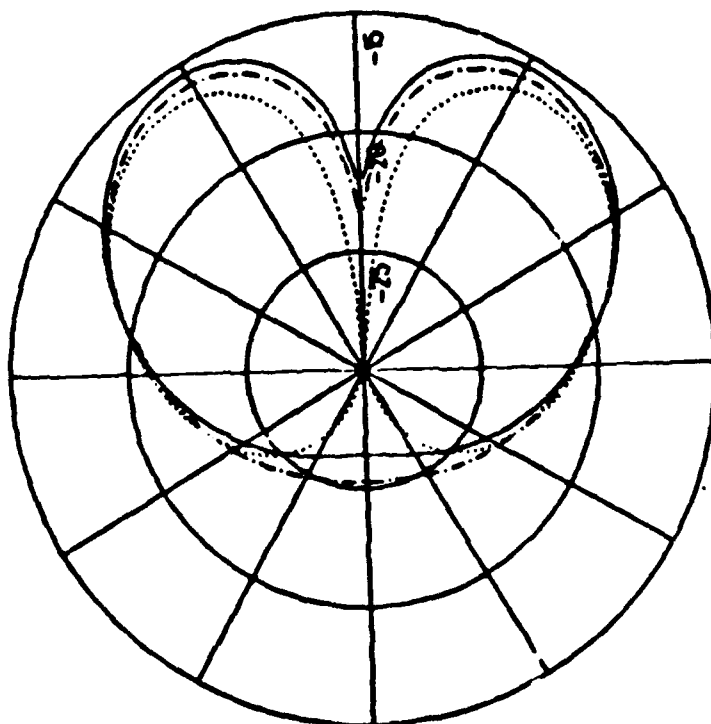


Figure 23: Far field β -directed component at an elevation angle $\beta = 30^\circ$ for the angular sector geometry of Fig. 22.

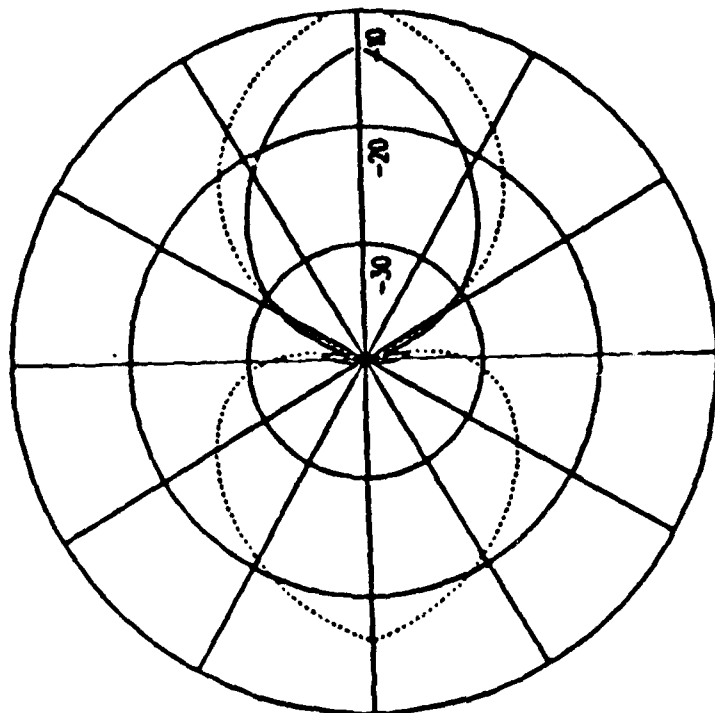


Figure 24: Far field ϕ -directed component at an elevation angle $\beta = 30^\circ$ for the angular sector geometry of Fig. 22.

— MEC
 GEC(1)
 - - - - - P0

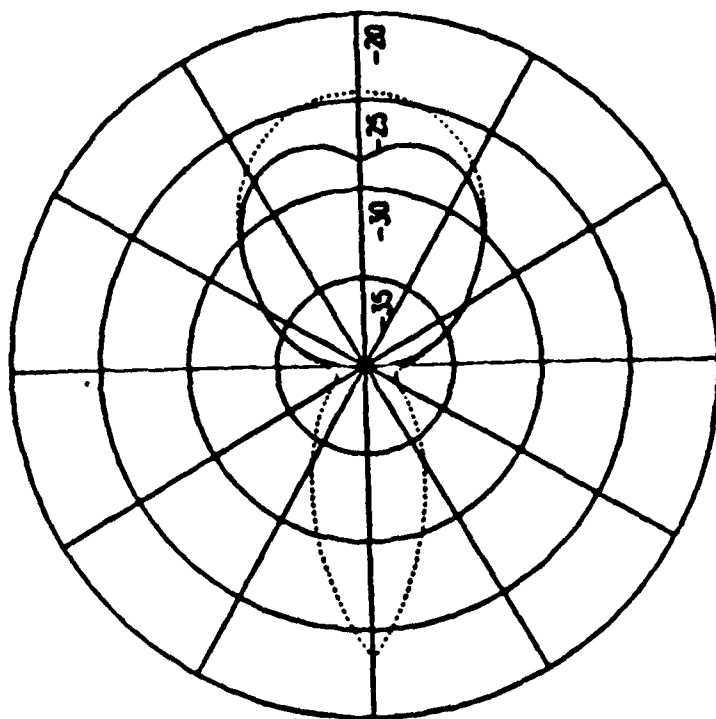


Figure 26: Far field ϕ -directed component at an elevation angle $\beta = 90^\circ$ for the angular sector geometry of Fig. 22.

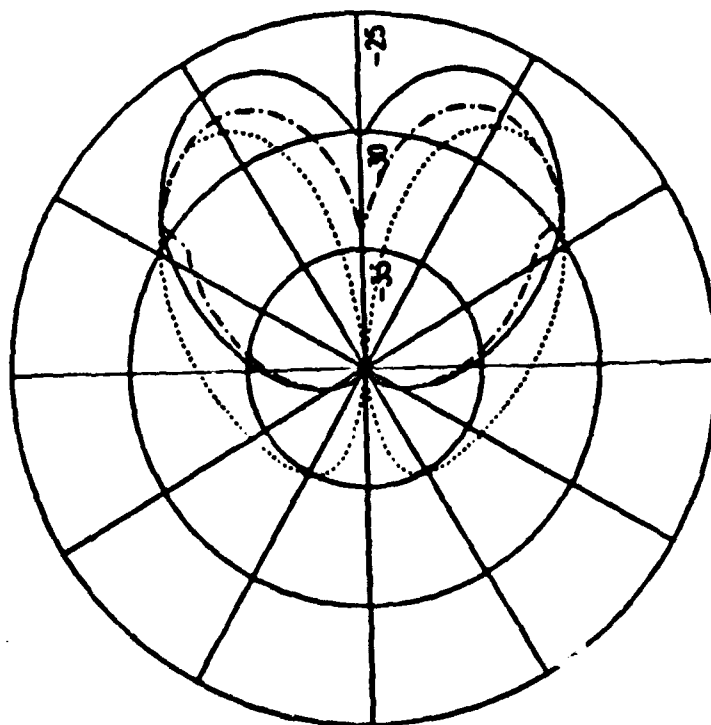


Figure 25: Far field β -directed component at an elevation angle $\beta = 90^\circ$ for the angular sector geometry of Fig. 22.

— MEC
 — GEC(1)
 PO

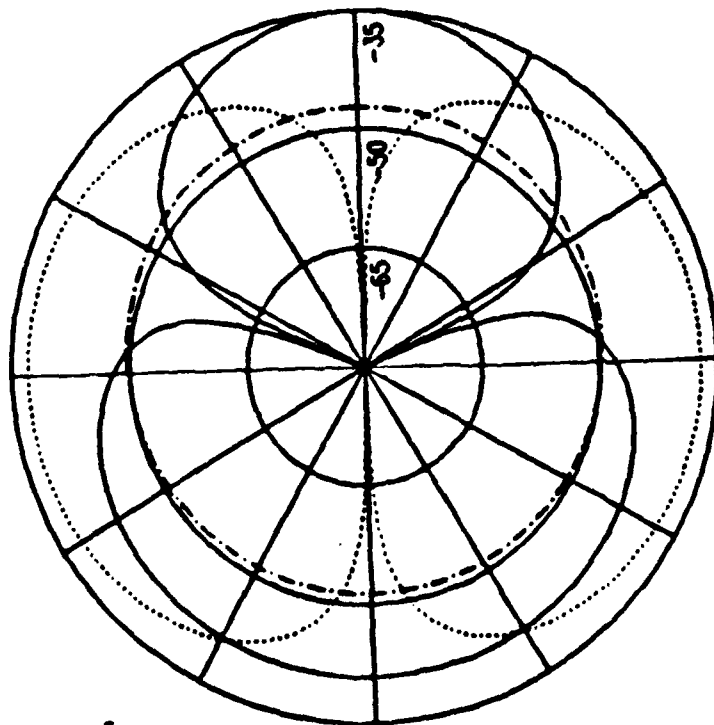


Figure 27: Far field β -directed component at an elevation angle $\beta = 150^\circ$ for the angular sector geometry of Fig. 22.

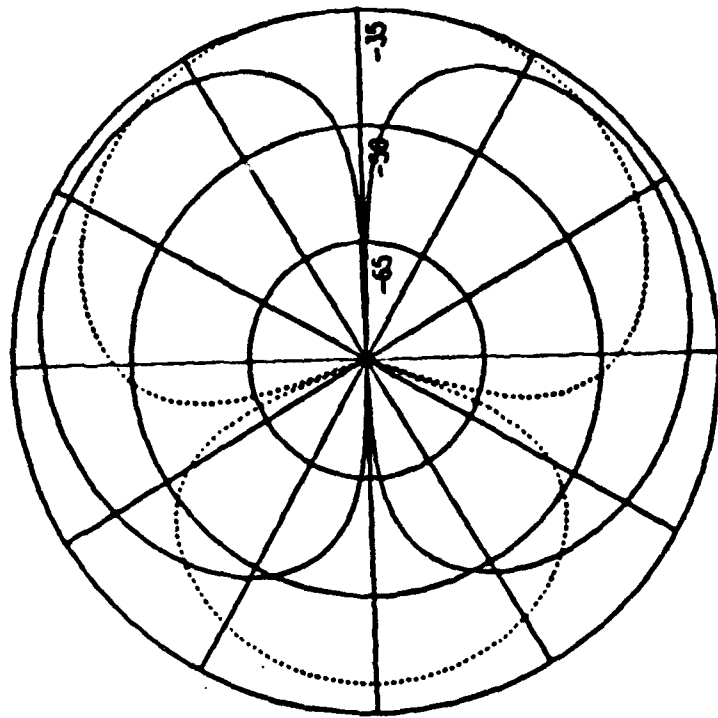


Figure 28: Far field ϕ -directed component at an elevation angle $\beta = 150^\circ$ for the angular sector geometry of Fig. 22.

4.4.2 Edge wave edge diffracted field.

In the general wedge problem the point Q_1^e lies on the semi-infinite edge (1) if

$$\cot \alpha_1 (1 - \cos \beta) + \sin \beta \cos \phi > 0.$$

The angle of diffraction β_1^e in this circumstance is defined by the equation

$$\sin \beta_1^e = \frac{s'_c \sin \alpha_1}{s'_1} \quad (4.55)$$

where

$$s'_1 = \sqrt{t_{Q_1^e}^2 + s_c'^2 - 2 t_{Q_1^e} s'_c \cos \alpha_1} \quad (4.56)$$

and the distance $t_{Q_1^e}$ of the point Q_1^e from the tip Q^c is given by

$$t_{Q_1^e} = \frac{s_c s'_c \sin(\alpha_1 + \beta_1)}{s'_c \sin \alpha_1 + s_c \sin \beta_1} \quad (4.57)$$

The non-uniform representation of the edge diffracted edge wave from Q_1^e (non-uniform with respect to the singular behavior of the impinging edge wave as well as the discontinuity at the boundary of the illuminated by the diffracted field region) can be obtained either using UTD or, equivalently, evaluating the isolated stationary phase point contribution to the radiation integral of the edge currents. (Note that both types of equivalent currents utilized earlier for the approximation of the vertex diffracted field result in the Ryan and Peters equivalent currents when evaluated at the point Q_1^e). For instance, employing UTD the edge diffracted edge wave reads

$$\begin{aligned} \vec{E}_1^e(\vec{s}_c) = & \hat{\phi}_1 E_{\phi_1}^{ev}(Q_1^e) \frac{\exp(-j\pi/4)}{2n_1 \sqrt{2\pi k_0} \sin \beta_1^e} \\ & \left[\cot \left(\frac{\pi + \phi_1}{2n_1} \right) F[k_0 L_1 a^+(\phi_1)] \right. \\ & \left. + \cot \left(\frac{\pi - \phi_1}{2n_1} \right) F[k_0 L_1 a^-(\phi_1)] \right] \end{aligned}$$

$$\sqrt{\frac{s'_1}{s_1(s'_1 + s_1)}} \exp(-jk_0 s_1) \quad (4.58a)$$

where

$$L_1 = \frac{s_1 s'_1}{s_1 + s'_1} \sin^2 \beta_1^e \quad (4.58b)$$

and

$$s_1 = \sqrt{t_{Q_1^e}^2 + s_c^2 - 2t_{Q_1^e} s_c \cos \beta_1} \quad (4.58c)$$

The incident edge wave $E_{\phi_1}^{ew}$ can be derived from eq. (2.19) and is given by

$$E_{\phi_1}^{ew}(Q_1^e) = jk_0^\nu Z_0 C(\nu) A_\nu^e(\rho', \phi') \sin^{\nu-1} \alpha_1 t_{Q_1^e}^{\nu-1} \frac{\exp(-jk_0 s'_1)}{s_1'^\nu} \quad (4.59)$$

Note, also, that a factor of 1/2 has been introduced into eq. (4.58a) due to grazing incidence [25]. Clearly, as $Q_1^e \rightarrow Q^c$, $\bar{E}_1^e(\bar{s}_c)$ becomes infinite. The singularity of the field in accordance with the development in Appendix A can be compensated with the multiplicative introduction of the transition function

$$F_{\nu-1}^e [2k_0 L_{e_1} \cos^2 \left(\frac{\alpha_1 + \beta_1}{2} \right)]$$

where

$$F_{\nu-1}^e(\cdot) = [F_{\nu-1}^e(\cdot)]^* \quad (4.60)$$

with the star denoting complex conjugate. The large parameter L_{e_1} equals

$$L_{e_1} = \frac{s_1 s'_1}{s_1 + s'_1} \quad (4.61)$$

Besides, the same modification factor insures the continuity of the total diffracted field (edge and vertex diffracted waves) at the boundary plane

$$\cos \alpha_1 (1 - \cos \beta) + \sin \alpha_1 \sin \beta \cos \phi = 0 \quad (4.62)$$

To illustrate the resulting continuity of the diffracted field at this boundary the particular case of the plane angular sector ($\nu = 1/2$; $\alpha_1 = \alpha$) is examined. In this circumstance the proposed uniform approximation of the edge diffracted field may be written in the following manner:

$$\begin{aligned} \bar{E}^e(\tilde{s}_c) \approx & -\frac{Z_0 A^e(\rho', \phi')}{4\pi^2 \sqrt{\sin \alpha}} \sqrt{\frac{s'_c \sin \alpha + s_c \sin \beta_1}{s_c s'_c s_1 (s_1 + s'_1)}} \exp\{-jk_0(s_1 + s'_1)\} \\ & \cdot \frac{F(2k_0 L_e \sin^2 \beta_1^e \cos^2 \frac{\phi_1}{2})}{\sin \beta_1^e \cos \frac{\phi_1}{2}} \frac{F_{-1/2}^e[2k_0 L_e \cos^2(\frac{\alpha + \beta_1}{2})]}{\sqrt{\sin(\alpha + \beta_1)}} \hat{\phi}_1 \end{aligned} \quad (4.63)$$

On the other hand, using the fact that Michaeli's equivalent currents reduce to those of Ryan and Peters at the origin of Keller's cone of diffracted rays, or alternatively employing eqs. (3.18), (4.34), (4.48a)-(4.48e) (for $\alpha = \alpha_1$), it can be easily shown that the corner diffracted field, as $Q_1^e \rightarrow Q^c$, equals

$$\begin{aligned} \bar{E}^c(\tilde{s}_c) = & -\frac{j Z_0 A^e(\rho', \phi')}{4\sqrt{2}\pi^2 \sqrt{\sin \alpha}} \frac{\exp\{-jk_0(s_c + s'_c)\}}{s_c \sqrt{s'_c}} \frac{F(2k_0 L_c \sin^2 \frac{\beta}{2})}{\cos \frac{\phi_1}{2}} \\ & \cdot \lim_{\beta_1 \rightarrow \pi - \alpha} \left[\frac{F_{-1/2}^c[2k_0 L_c \cos^2(\frac{\alpha + \beta_1}{2})]}{\sqrt{\cos \alpha + \cos \beta_1}} \right] \hat{\phi}_1 \end{aligned} \quad (4.64)$$

Then based on the definition (3.13) of the edge wave transition function and the relationship (4.63) it is trivial to show that the total diffracted field remains continuous as the boundary of the region illuminated by the edge diffracted field is crossed. The transition function $F_{\nu-1}^e(\cdot)$ for the general wedge case appears as a type of caustic correction factor in the sense that it compensates the singularity of the edge diffracted field at the extension of the guiding edge. However, in our case the singularity arises from the behavior of the incident field on the edge rather than the focusing of the diffracted rays into a caustic.

4.4.3 A transition function for the guiding edge diffracted field.

As pointed out in Section 2.5 the rigorous solution of the radiation of a dipole in the presence of an infinite wedge predicts a singular field at the edge of the wedge, in consistency with Meixner's edge condition. However, this singularity of the edge wave is not physically acceptable in the extension of a semi-infinite edge. For overcoming this discrepancy the multiplicative correction of the edge wave associated with a semi-infinite or finite edge with the use of a suitable transition function (in general transition dyadic) has been suggested. Such a transition function can be empirically derived by requiring the continuity of the total field at the shadow boundaries of the direct wave (edge wave), namely at the planes $\phi_{1,2} = \pi$. This continuity was guaranteed by the UTD evaluation of edge diffracted field as expressed by eqs. (4.58a)-(4.58c), but it is violated in the paraxial region after the introduction of the function $F_{\nu-1}^e$, which assures the uniformity of the total diffracted field. Obviously, the edge wave can be multiplied by a similar transition function so that the total field retains its continuity in the paraxial region as well as outside of it, where the transition function reverts to unity. In addition, such a multiplicative correction would yield a finite total field along the extension of the edge.

The edge wave contribution to the total radiated field by the dipole-trihedron configuration is given explicitly by eq. (2.19) which, for the half plane case, reduces to eq. (2.20). For the plane angular sector, a convenient modification of the edge wave reads:

$$\begin{aligned} \bar{E}^{ew}(\bar{s}_c) \approx & -\frac{\sqrt{k_0} Z_0 \exp(j\pi/4)}{2\pi\sqrt{2\pi}} A^e(\rho', \phi') \\ & \cdot [\hat{\beta}_0 \cos \beta_0 \sin(\phi/2) + \hat{\phi} \cos(\phi/2)] \end{aligned}$$

$$\frac{F_{-1/2}^e [2k_0 L_e \sin^2 \frac{\beta_0}{2}] \exp(-jk_0 s_0)}{\sqrt{\sin \beta_0} s_0} \quad (4.65)$$

with s_0 denoting the distance of the observation point from the dipole and β_0 is the elevation angle of the observer in the guiding edge fixed coordinate system centered at the point of the projection of the dipole onto the edge. The continuity of the field at the boundary $\phi = 0$, $\phi_1 = \pi$ is shown trivially by noting that, for $\phi = 0$, $\beta_0 = \pi - \alpha - \beta^e$.

4.5 Discussion and numerical results.

The edge wave vertex diffracted field is a higher order term with respect to the large parameter k_0 in the asymptotic solution of the radiation of a dipole in the vicinity of the edge of a trihedron. Nonetheless, it contributes significantly to the field especially in the paraxial region of the guiding edge and along its extension. And its major contribution concerns the $\hat{\beta}$ -directed component of the field. The latter, as pointed out in the discussion of the Physical Optics solution, is due to the accumulation of electric current flow lines in the vicinity of the guiding edge excited by the ray optical edge wave, which is consistent with the theoretically predicted singularity of the field as the edge is approached.

The solution based on Michaeli's equivalent currents is essentially an asymptotic PTD approach, in that a fringe current effect due to the terminating edges is added to the uniform edge wave currents. The rigorness of the approach may be questioned at this point, since the derivation of the fringe edge currents assume an infinite edge and uniform plane wave illumination. However, the field is expected to retain its singular behavior in the vicinity of the vertex, which, moreover, does not contradict the "tip condition" (i.e., the behavior of the field in the neighborhood of a vertex) as investigated rigorously by several authors. Besides, the addition of

the fringe current to the physical optics current effect improves the total solution as shown in Figs. 29-34, where these results are compared with moment method ones. It should be emphasized that the solution attempted in this chapter by no means presents a complete rigorous representation of the tip diffracted field, but it merely includes the information of the truncation of known components of the currents flowing over the edge surface and can serve as a good engineering approximation to the problem. Again in a PTD context the completeness of a solution requires the addition of a vertex current component, i.e., a current excited by the vertex of the trihedron, which however remains unknown and it does not appear possible that it can be extracted from the rigorous solutions [1,2].

Comparisons of the calculated field (denoted as MEC on the graphs) with moment method results (MM) are made in Figs. 29-34, for the square plate shown in Fig. 12. The direct edge wave (EW) properly modified in accordance with the discussion in Section 4.4.3 is also plotted so that the effect of the corner diffracted fields is better illustrated. Note that in Fig. 29 the edge wave edge diffracted wave has been added to the direct dipole field (EW+EWED).

The field evaluated with the equivalent current method shows good agreement for those flat plate geometries where the dipole is placed in the close vicinity of one of the edges of the plate and sufficiently far from its corners, especially in regions where contributions from other diffraction mechanisms other than the corner adjacent to the guiding edge are known to be negligible. This becomes evident in Figs. 29-34, where the agreement between the moment method data and the calculated field progressively improves for larger values of the ϕ angle. In fact, for $\phi = 60^\circ$, other mechanisms such as diffraction from the remote corners of the square plate as well as double and triple edge diffraction may contribute significantly, while their effect diminishes as $\phi \rightarrow 180^\circ$. Our approximate analysis

also improves when the paraxial region is approached ($\beta \rightarrow 0$), where, as a matter of fact, the total field is stronger. The latter justifies the validity of the asymptotic analysis which resulted into the multiplicative introduction of two transition functions as well as the choice of the correction factor for the direct dipole field. Unfortunately, the $\hat{\phi}$ -directed field does not exhibit an analogous agreement basically because the analysis does not include secondary mechanisms which clearly contribute significantly to the pattern of that polarization.

The results also reveal a small variation of the total field with respect to the azimuthal coordinate (angle ϕ), in contrast with the relative large changes of the calculated pattern in the elevation plane. The ϕ dependence becomes significant only at lower cuts where the contribution from the opposite edge and its two adjacent corners is appreciable.

The second example examined involves also the radiation of a small monopole in the close vicinity of one of the edges of a rectangular plate, but now in different distances from its corners. The geometry of this monopole-rectangular plate configuration is depicted in Fig. 35. The calculated field is compared again with moment method results as well as measured data, as shown in Figs. 36, 37 on the azimuthal planes $\phi = 180^\circ$, $\phi = 150^\circ$, respectively. The accuracy of the measured data deteriorated for measurements in smaller azimuthal angles, where the support of the structure influenced significantly the measured radiation pattern. In Fig. 36, a ram has been placed around the remote corners and the opposite edge of the rectangular plate, so that their effect in the total pattern is reduced. Clearly, the agreement is better in this case (Fig. 36), in contrast with the results of Fig. 37 where the ram was removed.

It should be noted that neither the Physical Optics solution nor the equivalent current formulation are expected to yield accurate results for small angular sector

angles ($\alpha \ll \pi/2$). In this case a strong coupling between the two edges forming the sector occurs, which is not encountered in the evaluation of the radiation integral of the currents flowing along the edge (1). Moreover, when $\alpha \rightarrow \pi$, the Physical Optics corner diffracted field vanishes and the total solution reduces to the edge wave over an infinite wedge, whereas the same property is not true for the equivalent current formulation of the vertex diffracted field. The latter, therefore, fails in cases of very wide angles, which require a more careful treatment.

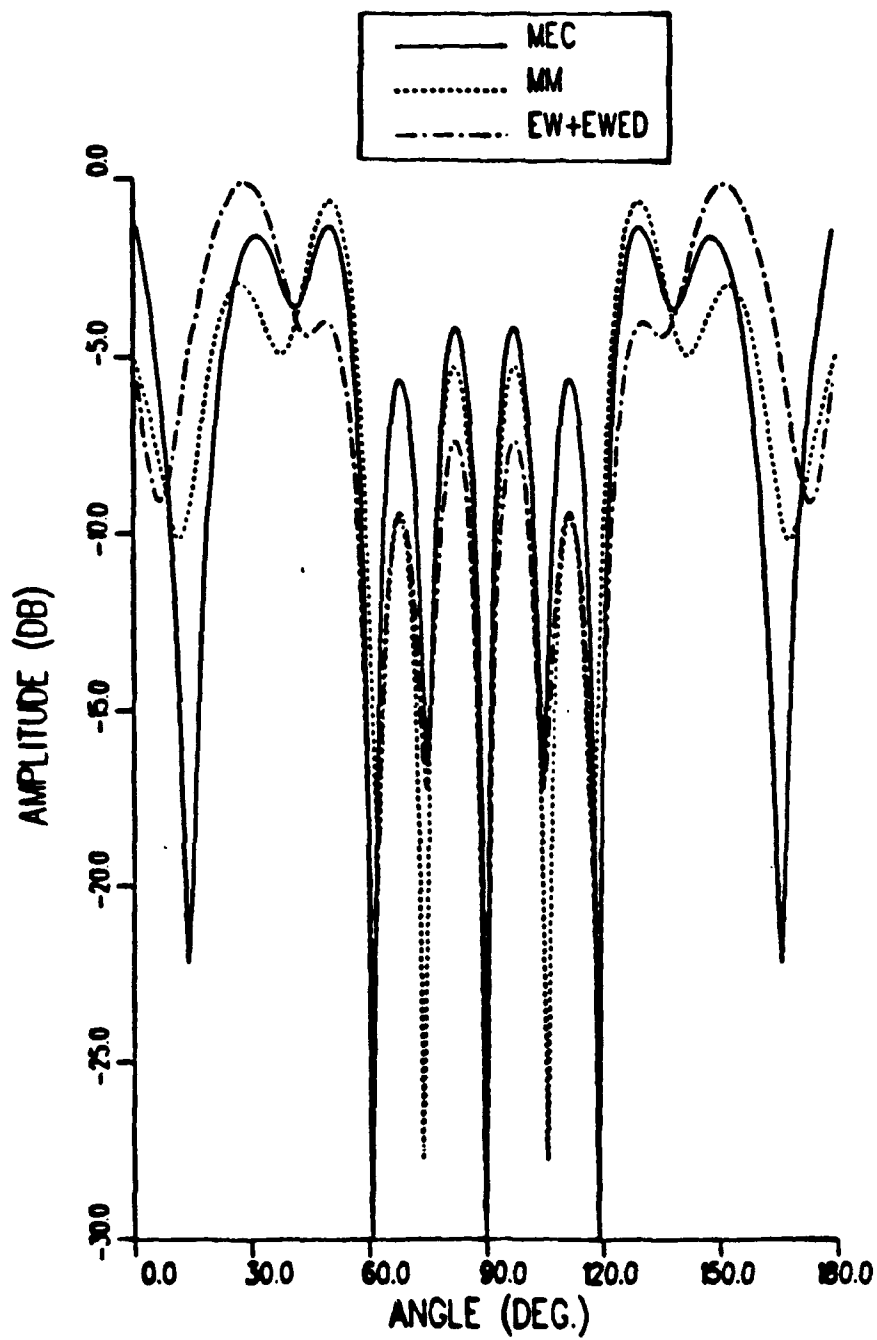


Figure 29: Far field $\hat{\beta}$ -directed field at an azimuthal angle $\phi = 60^\circ$ for the square plate of Fig. 12.

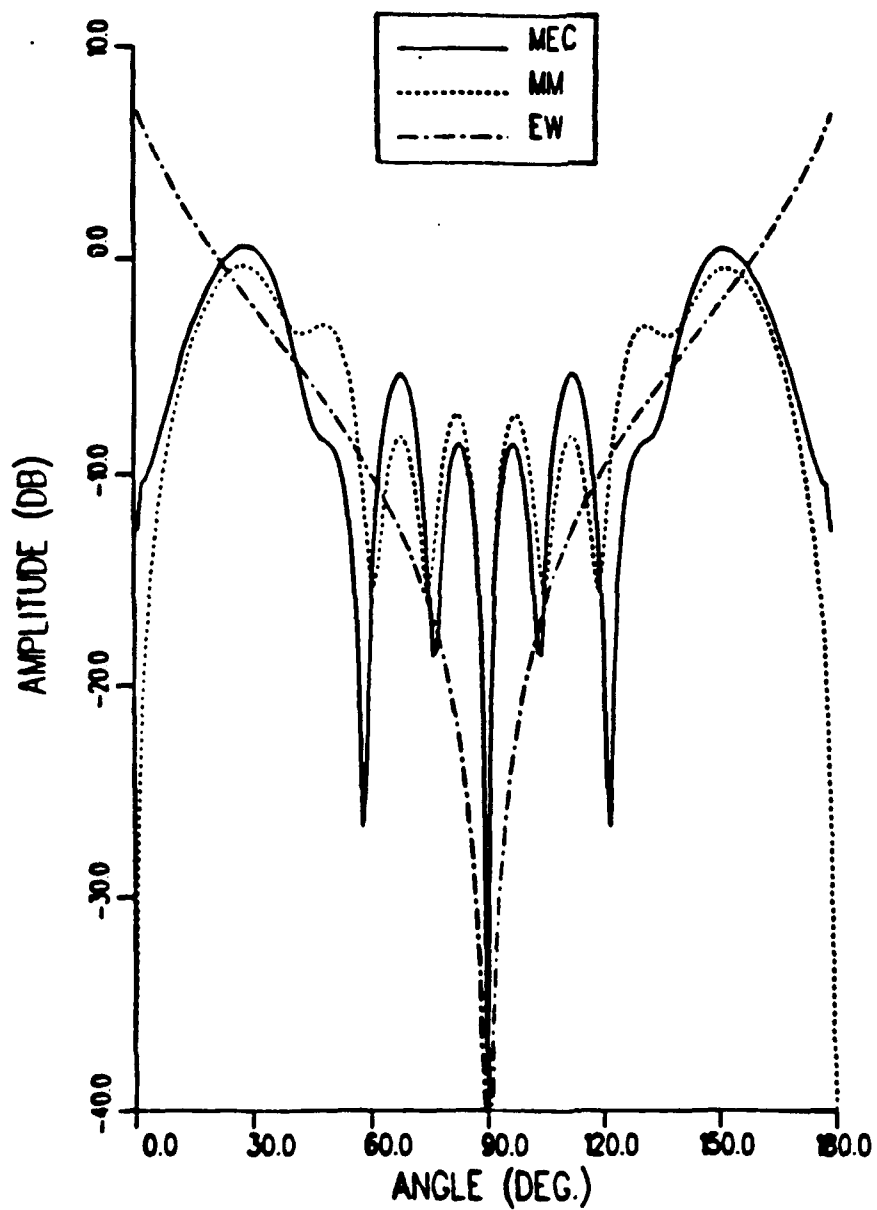


Figure 30: Far field $\hat{\beta}$ -directed field at an azimuthal angle $\phi = 90^\circ$ for the square plate of Fig. 12.

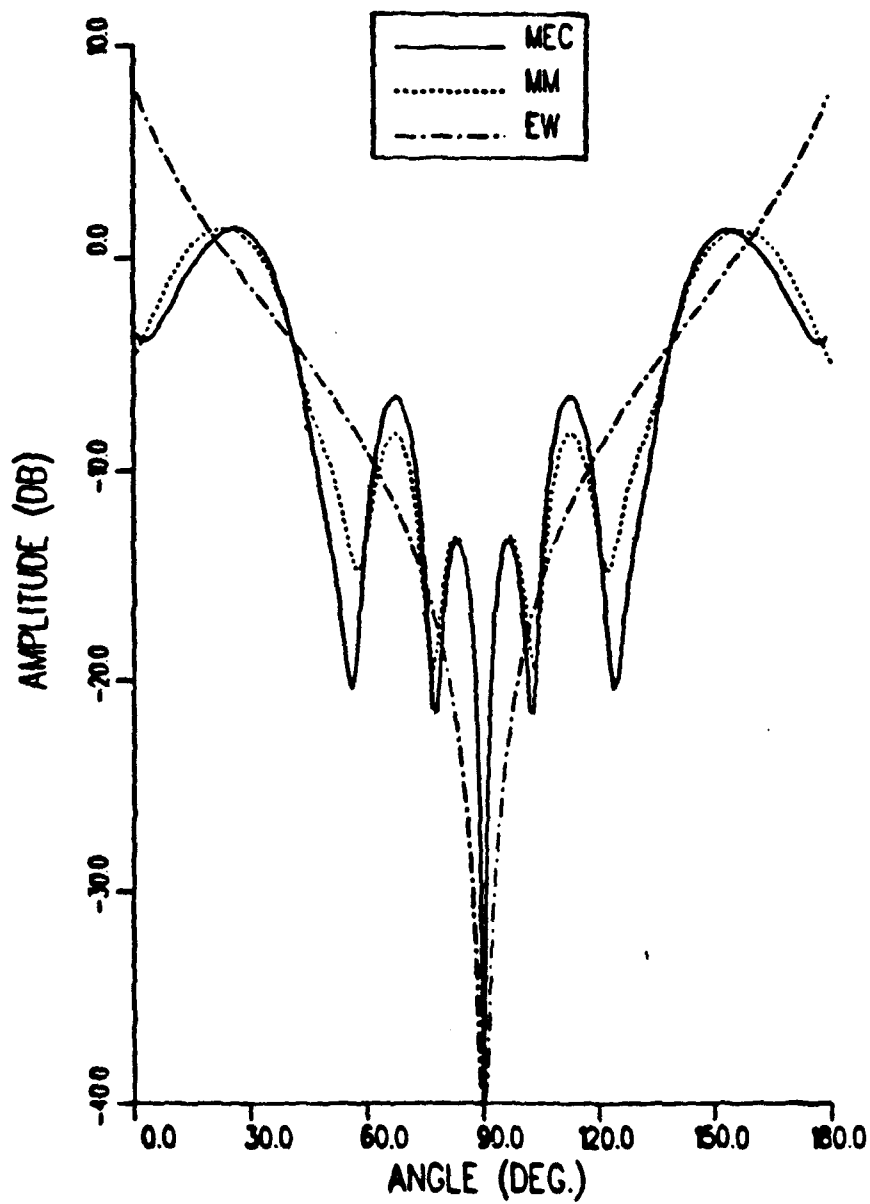


Figure 31: Far field $\hat{\beta}$ -directed field at an azimuthal angle $\phi = 120^\circ$ for the square plate of Fig. 12.

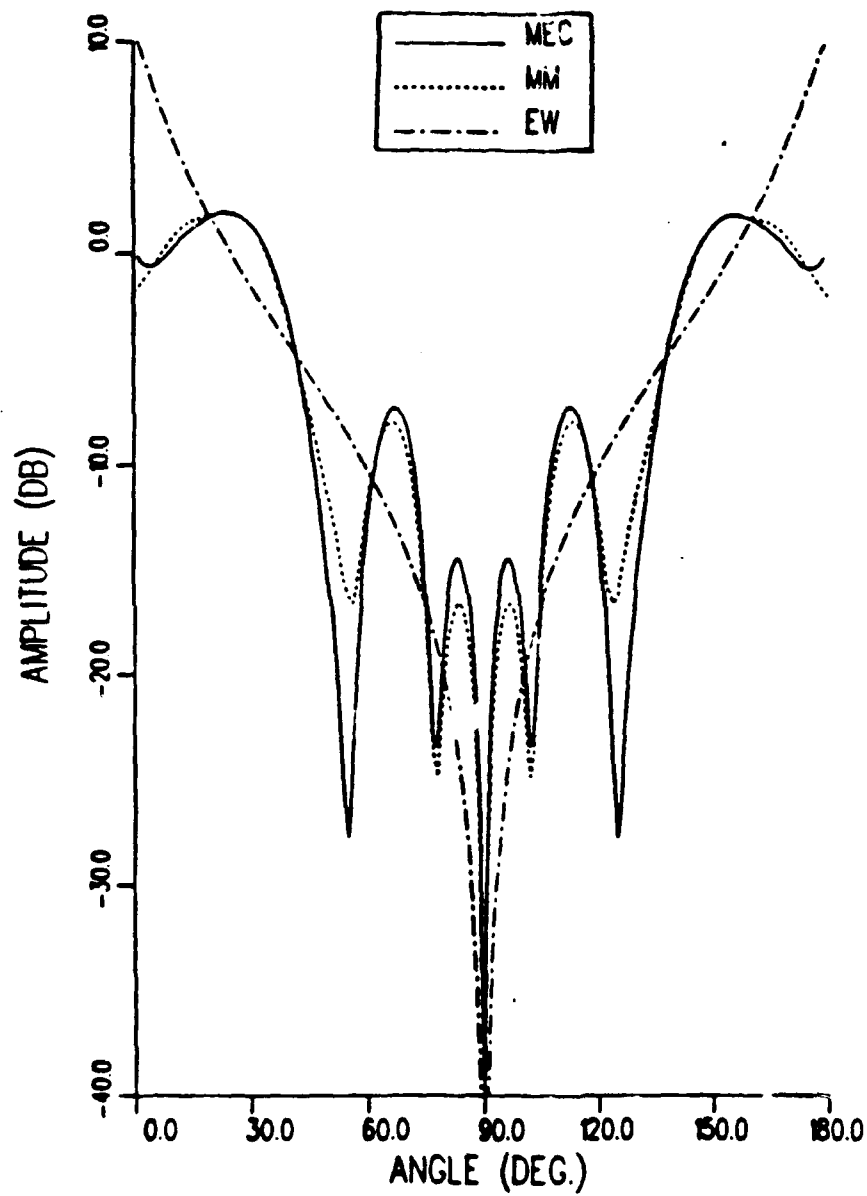


Figure 32: Far field β -directed field at an azimuthal angle $\phi = 135^\circ$ for the square plate of Fig. 12.

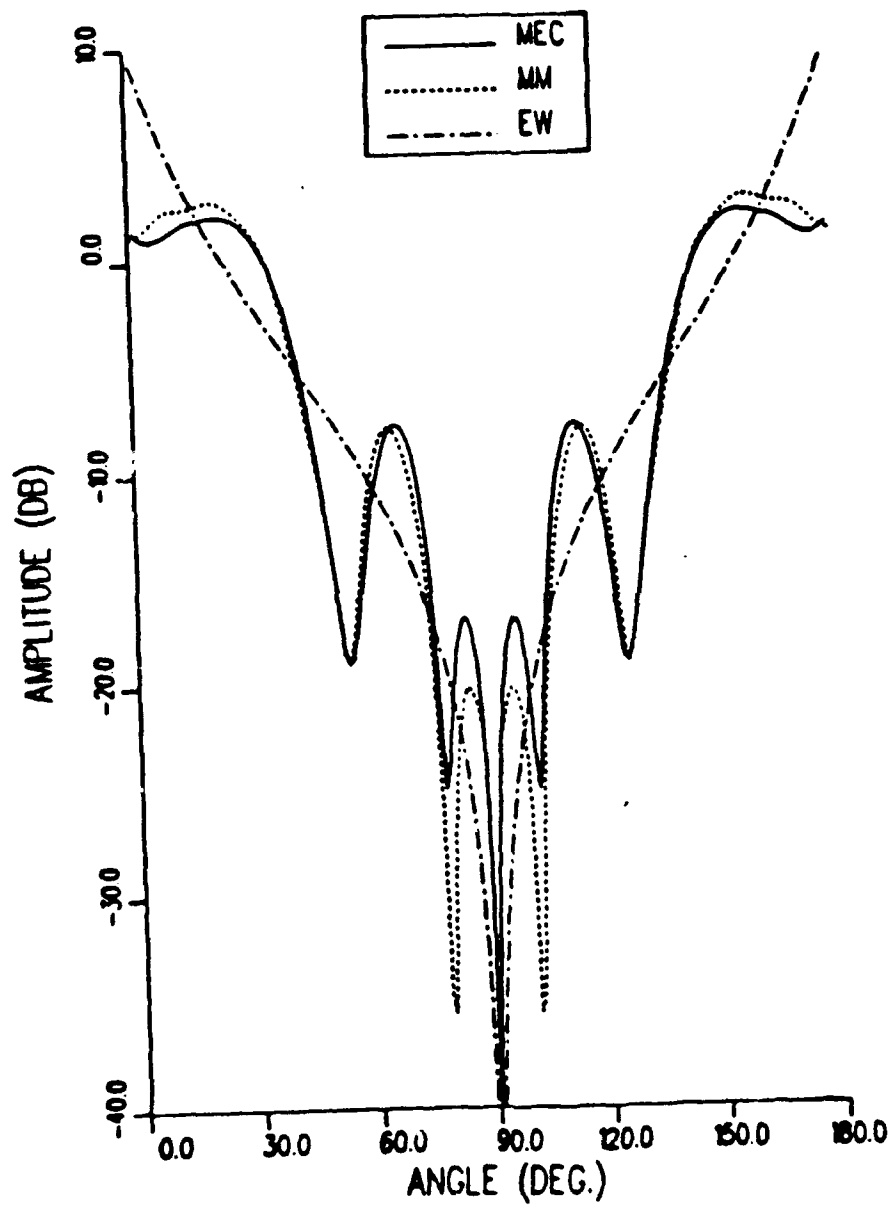


Figure 33: Far field $\hat{\beta}$ -directed field at an azimuthal angle $\phi = 150^\circ$ for the square plate of Fig. 12.

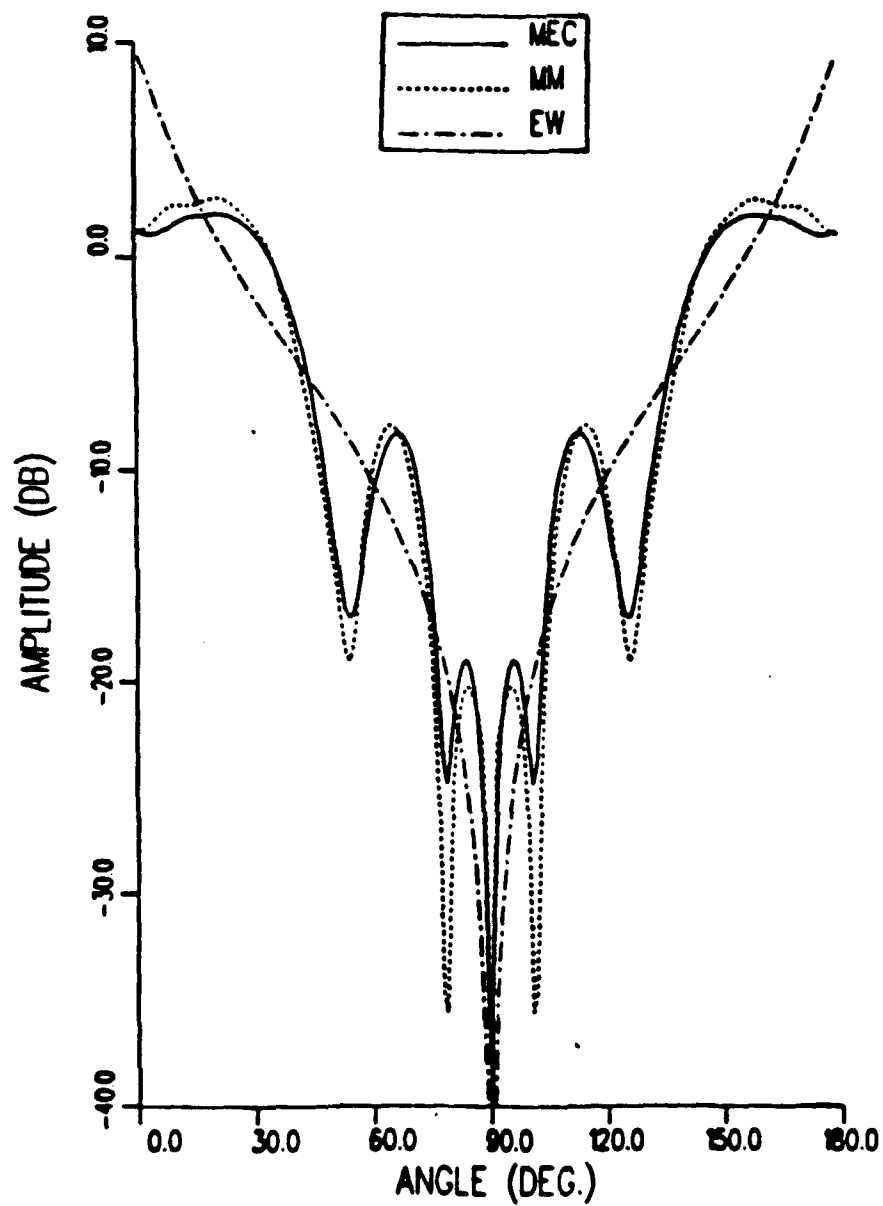


Figure 34: Far field $\hat{\beta}$ -directed field at an azimuthal angle $\phi = 180^\circ$ for the square plate of Fig. 12.

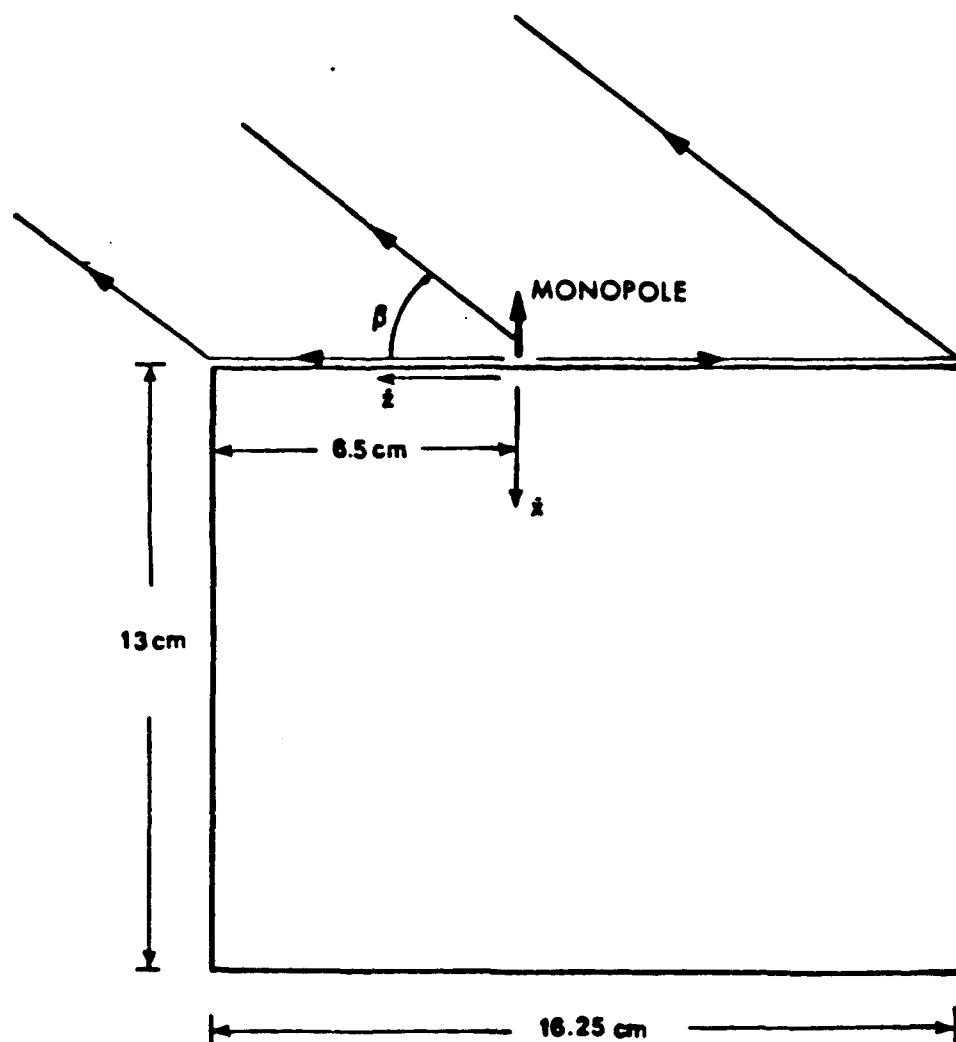


Figure 35: Geometry of the monopole-rectangular plate configuration used for comparison with measured data.

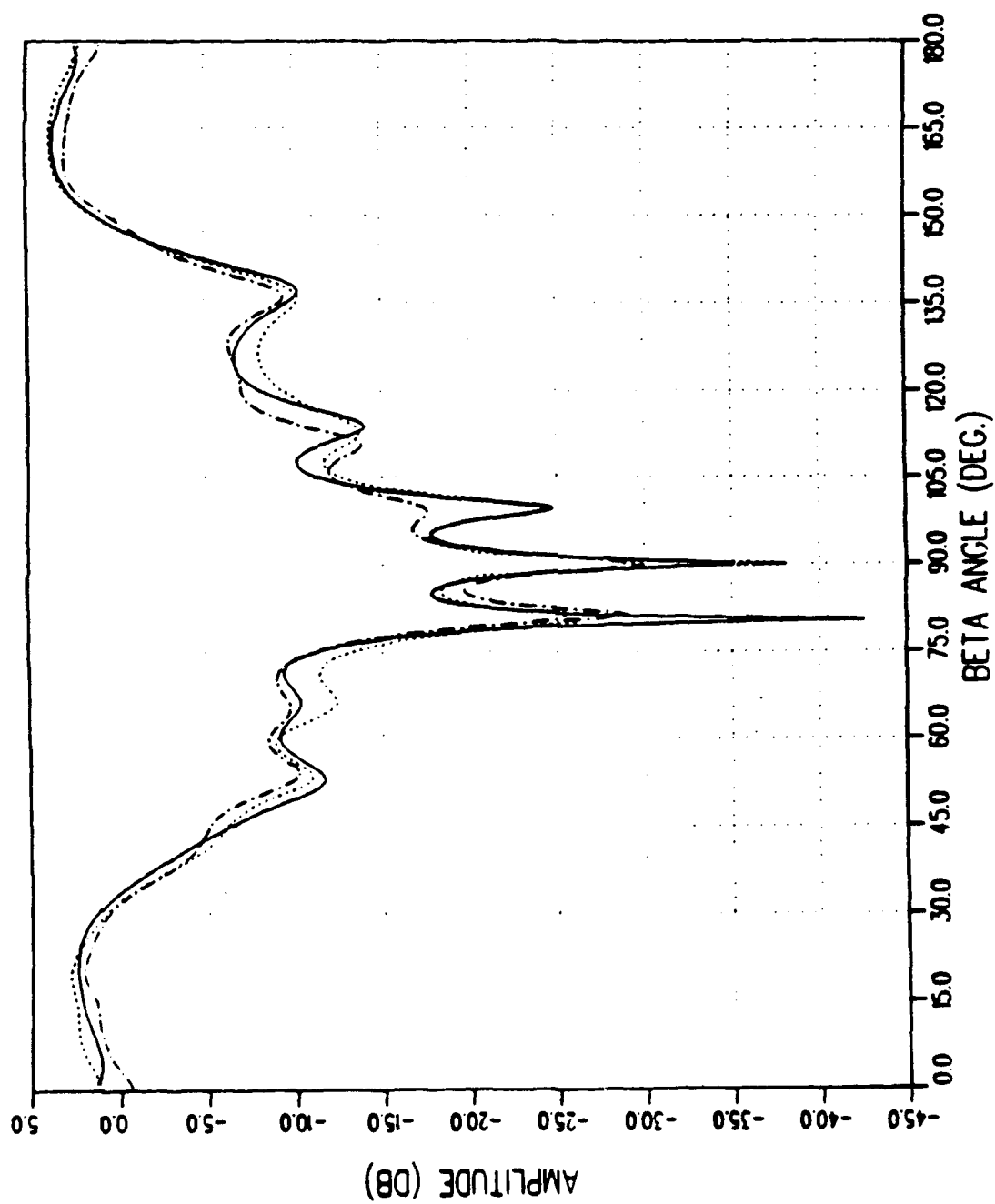


Figure 36: Far field β -directed field at an azimuthal angle $\phi = 180^\circ$ for the rectangular plate of Fig. 35. Solid line: Calculated field, Dashed line: Measured field, Dotted line: Moment method solution.

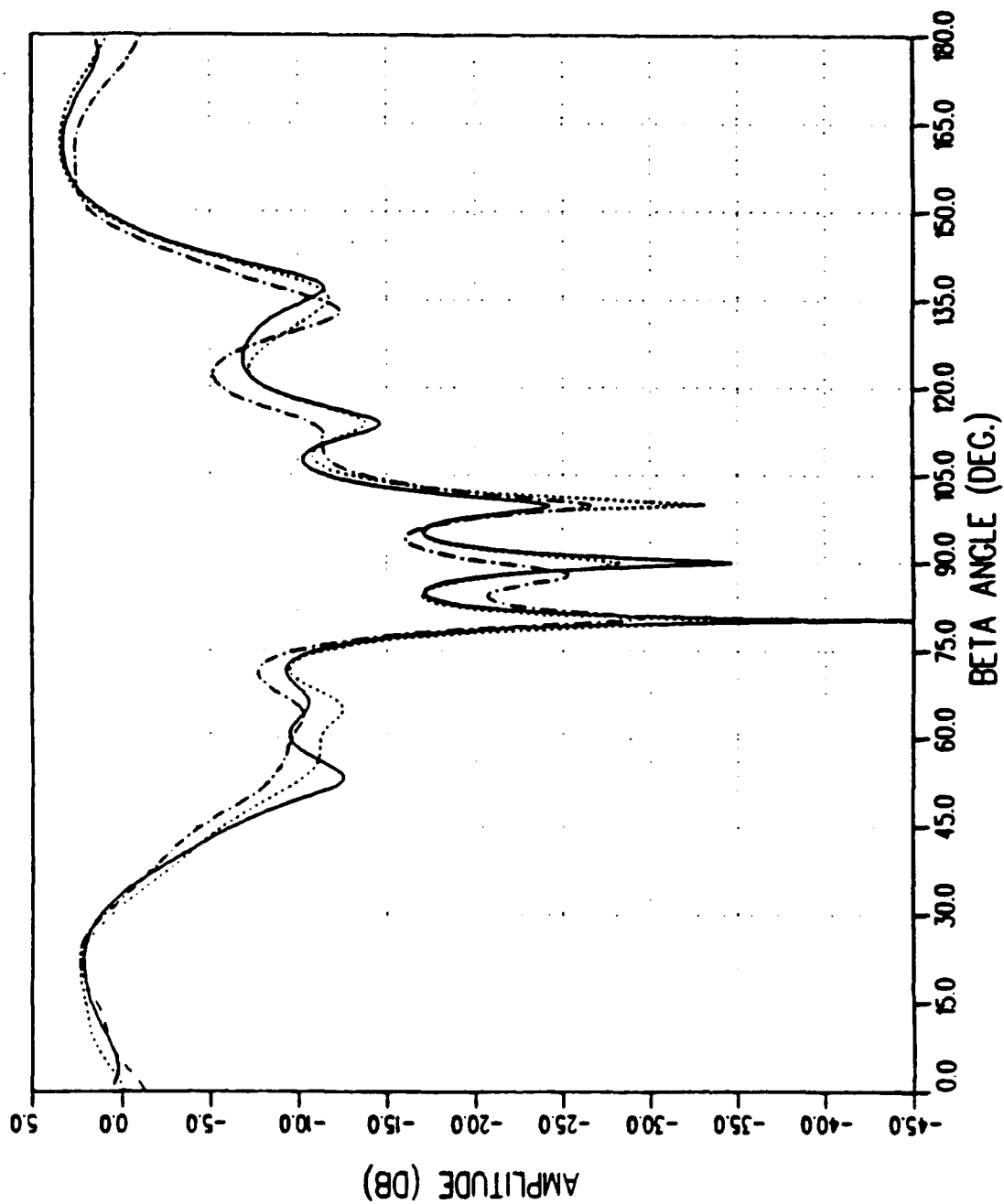


Figure 37: Far field β -directed field at an azimuthal angle $\phi = 150^\circ$ for the rectangular plate of Fig. 35. Solid line: Calculated field, Dashed line: Measured field, Dotted line: Moment method solution.

CHAPTER V

Conclusions

The major objective and motivation of this study was to describe approximately the edge wave diffraction mechanisms associated with the interaction of an edge wave and the vertex of an ideal trihedron as well as two adjacent vertices in a realistic three dimensional structure containing finite edges. These mechanisms may contribute significantly in the radiation patterns of several antennas (such as rectangular horns) and the RCS of edge structures investigated with UTD techniques, and therefore their incorporation improves the total UTD solution and extend UTD as a powerful high frequency theory.

Explicit expressions of the edge wave were presented in Chapter II, derived from the canonical half plane and infinite wedge problems. The investigation of such idealized configurations was dictated by the need of a complete definition of the edge waves and a better understanding of its behavior. It was found that the edge wave, which, independently of its excitation, is essentially an edge guided ray optical field, highly dominates the paraxial region of the edge due to its singular behavior there. These characteristics imply that there must be a strong coupling between antennas placed close to the edge of a wedge (which has been already proven by Buyukdura [7]) and between two adjacent vertices in a polyhedral body, as found by Sikta [4].

The next simple configuration examined was the trihedron (a truncated

wedge), as a first step to the approximation of more complex geometries. A dipole radiating in the close vicinity of one of its edges produces an edge wave which behaves essentially as a ray optical field in the vicinity of the vertex, provided that the distance of the excitation dipole from the tip is sufficiently large. To approximate the vertex diffracted wave a Physical Optics approach was adopted. The latter was improved in Chapter IV, by adding to the uniform current a fringe current component flowing in the vicinity of the terminating edges. Although, the approach is neither rigorous nor complete from a PTD point of view, it yields comparable results with moment method as well measured data and can be used as a first engineering approximation to the edge wave edge and vertex diffraction problems.

Within the limits of our ray optical approximations the results established in Chapter IV can be possibly utilized for the examination of the double corner and edge edge wave diffraction mechanisms, with several practical applications. The latter, being also a possible extension of the present UTD so that it may incorporate higher order diffraction mechanisms, awaits future work.

APPENDIX A

A Uniform Asymptotic Approximation of the Integral

$$I_p(k) = \int_0^\infty G(t) t^{-p-1} dt \text{ for } \Re(p) < 0$$

In the above integral $G(t)$ is a slowly varying continuous function of t . Moreover, let the large parameter k have a small negative imaginary part, i.e., it is presumed that the medium of propagation is slightly lossy. The phase function $g(t)$ is stationary at the point t_s ($g'(t_s) = 0$). Since in our applications $g(t)$ expresses the negative sum of the distance from a point Q on a straight line in space to two discrete points not on this line, with t denoting the signed arc length from the origin ($t = 0$) to the point Q , then $g(t)$ is negative definite and attains a maximum at t_s . In this case it can be shown that

$$g'(0) = \text{sign}(t_s) |g'(0)| \tag{A.1}$$

and

$$g''(t) < 0 \text{ ; for every real } t. \tag{A.2}$$

For convenience, it is assumed that eqs. (A.1), (A.2) are true in the following analysis. Besides, the final result can be easily generalized for a phase function not satisfying the above imposed properties.

For $t_s > 0$ the major contribution to the integral $I_p(k)$ arises from the vicinities of the stationary phase ($t = t_s$) and the end point ($t = 0$), which coincides with the branch point singularity of the integrand. We examine the asymptotic

behavior of the integral $I_p(k)$ for the particular case where $p = -1/2$. An evident transformation of variables is then $\xi = \sqrt{t}$, which yields the equivalent form

$$I_{-1/2}(k) = 2 \int_0^\infty H(\xi) \exp \{jk h(\xi)\} d\xi \quad (\text{A.3})$$

where we have set

$$H(\xi) = G(\xi^2), \quad h(\xi) = g(\xi^2) \quad (\text{A.4})$$

Since $g(t)$ is stationary at t_s , where t_s is real, then $h(\xi)$ exhibits three collinear, equidistant saddle points at $\xi_0 = 0, \xi_{1,2} = \pm\sqrt{t_s}$. (Note that $\xi_{1,2}$ may be imaginary if $t_s < 0$). A convenient transformation in this circumstance is [28]

$$h(\xi) = a_0 - (a + s^2)^2 \quad (\text{A.5})$$

It readily follows that

$$a_0 = h(\xi_{1,2}) = g(t_s) \quad (\text{A.6})$$

$$a = -\text{sign}(t_s) |\sqrt{h(\xi_{1,2}) - h(0)}| = -\text{sign}(t_s) |\sqrt{g(t_s) - g(0)}|$$

Provided that a is not very large the integral $I_{-1/2}(k)$ can be approximated by

$$I_{-1/2} \approx 2G(0) \frac{d\xi}{ds} \Big|_{s=0} \int_0^\infty \exp \{jk[a_0 - (a + s^2)^2]\} ds \quad (\text{A.7})$$

Using

$$h''(0) = 2g'(0) ; \quad h''(\xi_1) = 4t_s g''(t_s) ; \quad h^{(4)}(0) = 12g''(0) \quad (\text{A.8})$$

it is not difficult to verify that the mapping derivative at $s = 0$ for a sufficiently small equals to

$$\frac{d\xi}{ds}|_{s=0} = \sqrt{\frac{2|a|}{|g'(0)|}} \approx \sqrt{\frac{2|a|}{|t_s g''(t_s)|}} \approx \left[\frac{2}{|g''(0)|} \right]^{1/4} \quad (\text{A.9})$$

For the details of the derivation of eqs. (A.8), (A.9), which are useful in the examination of the limiting behavior of the asymptotic solution as $a \rightarrow 0$ (or $t_s \rightarrow 0$), the reader is referred to [28]. The integral involved in eq. (A.7) can be expressed in terms of the parabolic cylinder function of order $-1/2$. In particular, one obtains

$$I_{-1/2}(k) = G(0) \frac{\sqrt{\pi} \exp(-j\pi/8)}{(2k)^{1/4}} \exp\{jk(a_0 - a^2/2)\} \times \sqrt{\frac{2|a|}{|g'(0)|}} \mathcal{D}_{-1/2}[\exp(j\pi/4) a \sqrt{2k}] \quad (\text{A.10})$$

We can employ the formula [29]

$$\mathcal{D}_p(z) = \exp(-jp\pi) \mathcal{D}_p(-z) + \frac{\sqrt{2\pi}}{\Gamma(-p)} \exp\{-j(p+1)\pi/2\} \mathcal{D}_{-p-1}(jz) \quad (\text{A.11})$$

for $p = -1/2$ and rewrite eq. (A.10) as follows:

$$I_{-1/2}(k) = G(0) \frac{\sqrt{\pi} \exp(-j\pi/8)}{(2k)^{1/4}} \exp\{jk(a_0 - a^2/2)\} \sqrt{\frac{2|a|}{|g'(0)|}} \cdot \begin{cases} j \mathcal{D}_{-1/2}[\exp(j\pi/4)|a|\sqrt{2k}] \\ + \sqrt{2} \exp(-j\pi/4) \mathcal{D}_{-1/2}[\exp(-j\pi/4)|a|\sqrt{2k}] & ; t_s > 0 \\ \mathcal{D}_{-1/2}[\exp(j\pi/4)|a|\sqrt{2k}] & ; t_s < 0 \end{cases} \quad (\text{A.12})$$

It is reminded that the above representation is valid for small values of the parameter a . An approach valid for larger values of a appears in general cumbersome. However, one can simply perturbate the original solution given by eq. (A.12), to obtain an asymptotic approximation in which the stationary phase contribution would reduce to the well known result for an isolated stationary phase point as a

becomes large. In particular, for $t_s > 0$ using eq. (A.9) one writes

$$I_{-1/2}(k) = \frac{\sqrt{\pi} \exp(-j\pi/8)}{(2k)^{1/4}} \exp\{jk(a_0 - a^2/2)\} \sqrt{2|a|} \times \\ \{ j \frac{G(0)}{\sqrt{|g'(0)|}} \mathcal{D}_{-1/2}[\exp(j\pi/4)|a|\sqrt{2k}] + \\ \sqrt{2} \exp(-j\pi/4) \frac{G(t_s)}{\sqrt{t_s |g''(t_s)|}} \mathcal{D}_{-1/2}[\exp(-j\pi/4)|a|\sqrt{2k}] \} \quad (\text{A.13})$$

From the asymptotic form of the parabolic cylinder function of order $-1/2$ [29], for $|a|\sqrt{2k} \gg 1$, one obtains

$$\mathcal{D}_{-1/2}[\exp(-j\pi/4)|a|\sqrt{2k}] \approx \frac{\exp(j\pi/8) \exp(jka^2/2)}{\sqrt{|a|\sqrt{2k}}}$$

Substituting the above expression into the second term of eq. (A.13) it yields the isolated stationary phase contribution

$$I_{-1/2}^s(k) \approx \frac{G(t_s)}{\sqrt{t_s}} \frac{\sqrt{2\pi}}{\sqrt{k |g''(t_s)|}} \exp\{jk[g(t_s) - \pi/4]\}$$

A transformation similar to that of eq. (A.5) cannot be applied in the case of an arbitrarily negative p , because the resulting integral cannot be reduced into a closed form expression. To obtain a uniform asymptotic approximation we adopt a more empirical approach. Namely, it appears convenient to consider a quadrature approximation of the phase function $g(t)$ in the neighborhood of the end point $t = 0$, at which, as mentioned before, the integral presents a branch point singularity

$$g(t) \approx g(0) + g'(0)t + \frac{g''(0)}{2} t^2 \quad (\text{A.14})$$

Then, based on this approximation the behavior of the end point effect and the coincident branch point singularity is examined. After some elementary manipulation, which follows the same steps with the particular case examined earlier one finally obtains the asymptotic result:

$$I_p^0(k) \approx G(0) \Gamma(-p) (2k)^{p/2} \exp(jp\pi/4) \exp\{jk[g(0) + a^2/2]\} \times$$

$$\left[\frac{g'(0)}{2|a|} \right]^p \begin{cases} \exp(-jp\pi) \mathcal{D}_p[\exp(j\pi/4)|a|\sqrt{2k}] & ; t_s > 0 \\ \mathcal{D}_p[\exp(j\pi/4)|a|\sqrt{2k}] & ; t_s < 0 \end{cases} \quad (\text{A.15})$$

where now

$$a = - \frac{g'(0)}{\sqrt{2|g''(0)|}} \quad (\text{A.16})$$

It should be noted that the above equation represents the end point effect only. Evidently, it exhibits an abrupt phase change of $\exp(jp\pi)$ as the stationary phase point passes through the origin. This discontinuity should normally compensate the discontinuity of the stationary phase contribution to the integral $I_p(k)$ in order for the total asymptotic solution to remain uniform across the boundary $t_s = 0$. Such a stationary phase point effect which guarantees the uniformity of the total solution is derived by a heuristic multiplicative correction of the isolated stationary phase contribution with the proper transition function.

The substitution

$$F_p^c(ka^2) = \exp(-jp\pi/4)(\sqrt{2k}|a|)^{-p} \exp(jka^2/2) \mathcal{D}_p[\exp(j\pi/4)|a|\sqrt{2k}] \quad (\text{A.17})$$

furnishes an alternative expression for the end point contribution, namely

$$I_p^0(k) \approx G(0) \Gamma(-p) k^p \exp(-jp\pi/2) \exp\{jkg(0)\} [g'(0)]^p F_p^c(ka^2) \quad (\text{A.18})$$

where the branch

$$(-1)^p = \exp(jp\pi)$$

should be chosen. In the above equation $F_p^c(\cdot)$ behaves essentially as a complex transition function: it reduces to unity for large values of its argument and compensates the singularity of $g'(0)$ as the stationary point approaches the end point

at $t = 0$. For a detailed description of the behavior of the transition function $F_p^c(\cdot)$ the reader is referred to Appendix B.

APPENDIX B

Edge Wave Transition Functions

Two types of transition functions are extensively used in the examination of the edge and vertex edge wave diffraction mechanisms arising from the integration over the singularity of the edge wave which coincides with the end point of the integration path:

- The edge wave vertex transition function $F_{-\nu}^c(x)$
- The edge wave edge transition function $F_{-\nu}^e(x)$.

where $x > 0$. The latter for every x is the complex conjugate of the former, which is related with the parabolic cylinder function of order $-\nu$ via

$$F_{-\nu}^c(x) = \exp(j\nu\pi/4)(2|x|)^{\nu/2} \exp(j|x|/2) \mathcal{D}_{-\nu}[\exp(j\pi/4)\sqrt{2|x|}] \quad (\text{B.1})$$

For a complete discussion of the properties of the parabolic cylinder function the reader is referred to [29,30,31]. For small values of its argument it assumes the power series expansion

$$\mathcal{D}_{-\nu}(z) = \frac{\sqrt{\pi}}{2^{\frac{1}{2}}} \left[1 + \frac{1}{\Gamma(\frac{\nu+1}{2})} + \frac{\sqrt{2}}{\Gamma(\frac{\nu}{2})} z + \frac{\nu-1/2}{2\Gamma(\frac{\nu+1}{2})} z^2 \right] + O(z^3) \quad (\text{B.2})$$

while for large arguments it can be approximated by the first terms of the asymptotic expansion

$$\mathcal{D}_{-\nu}(z) = \exp(-z^2/4) z^{-\nu} \left[1 - \frac{\nu(\nu+1)}{2z^2} \right]$$

$$+ \frac{\nu(\nu+1)(\nu+2)(\nu+3)}{8z^4} + O(z^{-8}) \Big] \quad (\text{B.3})$$

Incorporating expressions (B.2), (B.3) in the definition (B.1) of the transition function outside the transition regions one may assume the approximations

$$F_{-\nu}^c(x) \approx \sqrt{\pi} \exp(j\nu\pi/4) |x|^{\nu/2} \exp(j|x|/2) \cdot \left[\frac{1}{\Gamma(\frac{\nu+1}{2})} - \frac{2 \exp(j\pi/4)}{\Gamma(\frac{\nu}{2})} \sqrt{x} + \frac{j(\nu-1/2)}{\Gamma(\frac{\nu+1}{2})} x + \dots \right] \quad (\text{B.4})$$

for $|x| \ll 1$, and

$$F_{-\nu}^c(x) \approx 1 - \frac{\nu(\nu+1)}{4jx} - \frac{\nu(\nu+1)(\nu+2)(\nu+3)}{32x^2} + \dots \quad (\text{B.5})$$

Of particular importance in our numerical applications is the transition function of order $-1/2$ ($\nu = 1/2$). The parabolic cylinder function of order $-1/2$ can be expressed in terms of the modified Bessel function K of order $1/4$ [30,31] as follows:

$$D_{-1/2}(z) = \sqrt{\frac{z}{2\pi}} K_{1/4}(z^2/4) \quad (\text{B.6})$$

Incorporating (B.6) and the relationship [30]

$$K_{1/4}(jx/2) = -\frac{\pi \exp(j3\pi/8)}{2} H_{1/4}^{(2)}(x/2)$$

into eq. (B.1) for $\nu = 1/2$ it yields the expression

$$F_{-1/2}^c(x) = \frac{1}{2} \exp(-j3\pi/8) \exp(j|x|/2) \sqrt{\pi|x|} H_{1/4}^{(2)}(|x|/2) \quad (\text{B.7})$$

Eq. (B.7) can be rewritten in terms of the Bessel functions $J_{1/4}$ and $J_{-1/4}$, namely

$$F_{-1/2}^c(x) = \frac{1}{2} \exp(j\pi/4) \exp(j|x|/2) \cdot \left[\exp(-j\pi/8) J_{-1/4}(|x|/2) - \exp(j\pi/8) J_{1/4}(|x|/2) \right] \quad (\text{B.8})$$

The Bessel functions of order $1/4$ and $-1/4$ are tabulated in [32]. Therefore, eq. (B.7) can be readily employed for the numerical computation of the function $F_{-1/2}^c$. The relatively simple computer program that follows uses a quadrature approximation of the Bessel functions for $|x| < 0.75$, an approximation up to order $|x|^{-2}$ for $|x| > 2.5$ and a third order Lagrangian interpolation in the transition region, to achieve an up to third decimal point accuracy of the edge wave transition function. The amplitude and the argument of the edge wave transition function is plotted in Figs. 38 and 39 respectively.

```

C Subroutine for the evaluation of the edge wave
C transition function D(x).
I
      COMPLEX FUNCTION PCFT(XD)
I
C Number of points in the interpolation region.
  PARAMETER INP=49
I
      COMPLEX CJ,CP18,CPJ4,CPJ8
      INTEGER I
      REAL JH(INP),JP(INP),X(INP),SH,SMLR,BG
      REAL PI,G14,G34,JM14,JP14,N,XD,AM,BH,AP,BP
      REAL DX1,DX2,P
I
C Define limits of the small argument-linear interpolation-large argument
C regions for the approximation of the Bessel Functions so that a three
C digit accuracy is achieved.
      XD=0.5*XD
I
      SMLR=1.E-5
      SH=.8
      BG=6.
      G14=3.6256099082
      G34=1.2254167024
      PI=3.141592653
      CJ=(0.,1.)
      CPJ4=(.707106781,.707106781)
      CPJ8=(.9233879532,.382683432)
      CP18=CONJG(CPJ8)
      DATA X/.6,.8,1.,1.2,1.4,1.6,1.8,2.,2.2,2.4,2.6,2.8,3.,3.2,3.4,3.6,3.8
      1.4,.4,2.4,4.4,6.4,8.4,5.,5.2,5.4,5.6,5.8,6.,6.2,6.4,6.6,6.8,7.,7.2
      2.7,4.7,6.7,8.7,8.,8.2,8.4,8.6,8.8,9.,9.2,9.4,9.6,9.8,10.,10.2/
      DATA JH/.97369,.81704,.66938,.52598,.38619,.25118,.12290,.00359,-.10447
      1,-.19919,-.27877,-.34185,-.38751,-.41537,-.42557,-.41880,-.39622
      2,-.35947,-.31059,-.25192,-.18608,-.11580,-.04387,.02694,.09403
      3,.155,.20778,.25064,.28228,.30186,.309,.30381,.28685,.25911,.22195
      4,.17706,.12638,.07201,.01615,-.039,-.091132,-.13883,-.17981,-.21281
      5,-.23671,-.25077,-.25466,-.24842,-.23251/
      DATA JP/.75888,.76901,.75223,.71291,.65453,.58035,.49366,.39781,.29623
      1,.19233,.08947,-.00916,-.10064,-.18235,-.2521,-.30815,-.34926
      2,-.37476,-.38449,-.37885,-.35873,-.32551,-.28097,-.22722,-.16663
      3,-.10174,-.03514,.03057,.09293,.14967,.19879,.23866,.268,.286
      4,.29227,.28688,.27037,.24363,.20798,.165,.11653,.06459,.01128
      5,-.04131,-.09114,-.13633,-.17521,-.20639,-.22882/
C Step size.
      N=.2
C Approximation of the Bessel functions.
      IF(XD.LT.SH) THEN
C Small argument form.
        IF(XD.LE.0.) THEN
          PCFT=(0.,0.)
          RETURN
        ELSE IF(XD.LT.SMLR) THEN
          PCFT=SQRT(PI*SQRT(2.*XD))*CPJ8*CEXP(CJ*XD)/G34
          RETURN
        ELSE
          JM14=SQRT(SQRT(2./XD))*(1.-XD*XD/3.+XD**4/42.)/G34
          JP14=4.*SQRT(SQRT(.5*XD))*(1.-XD*XD/5.+XD**4/90.)/G14
          ENDIF
        ELSE IF(XD.GE.SH.AND.XD.LT.BG) THEN
C Interpolation region.Lagrange three point interpolation formula is
C utilised.
          DO 13 I=2,INP-1
            IF(XD.GE.X(I).AND.XD.LT.X(I+1)) THEN
              DX1=XD-X(I)

```

```

        DX2=XD-X(I+1)
        IF(ABS(DX2).GT.ABS(DX1)) GOTO 14
        IF(ABS(DX2).LE.ABS(DX1)) GOTO 15
    ENDIF
13      CONTINUE
14      P=DX1/H
        JM14=.5*P*(P-1.)*JM(I-1)+(1.-P*P)*JM(I)+.5*P*(P+1.)*JM(I+1)
        JP14=.5*P*(P-1.)*JP(I-1)+(1.-P*P)*JP(I)+.5*P*(P+1.)*JP(I+1)
        GOTO 18
15      P=DX2/H
        JM14=.5*P*(P-1.)*JM(I)+(1.-P*P)*JM(I+1)+.5*P*(P+1.)*JM(I+2)
        JP14=.5*P*(P-1.)*JP(I)+(1.-P*P)*JP(I+1)+.5*P*(P+1.)*JP(I+2)
        GOTO 18
- C    Large argument form.
        ELSE IF(XD.GE.BG) THEN
            AM=COS(XD-0.125*PI)
            BM=SIN(XD-0.125*PI)
            AP=COS(XD-0.375*PI)
            BP=SIN(XD-0.375*PI)
            JM14=SQRT(2./(PI*XD))*(AM+3.*BM/(32.*XD)-105.*AM/(2048.*XD*XD))
            JP14=SQRT(2./(PI*XD))*(AP+3.*BP/(32.*XD)-105.*AP/(2048.*XD*XD))
        ENDIF
18      PCFT=SQRT(PI*XD)*CPJ4*(CP18*JM14-CPJ8*JP14)*CEXP(CJ*XD)
        RETURN
    END

```

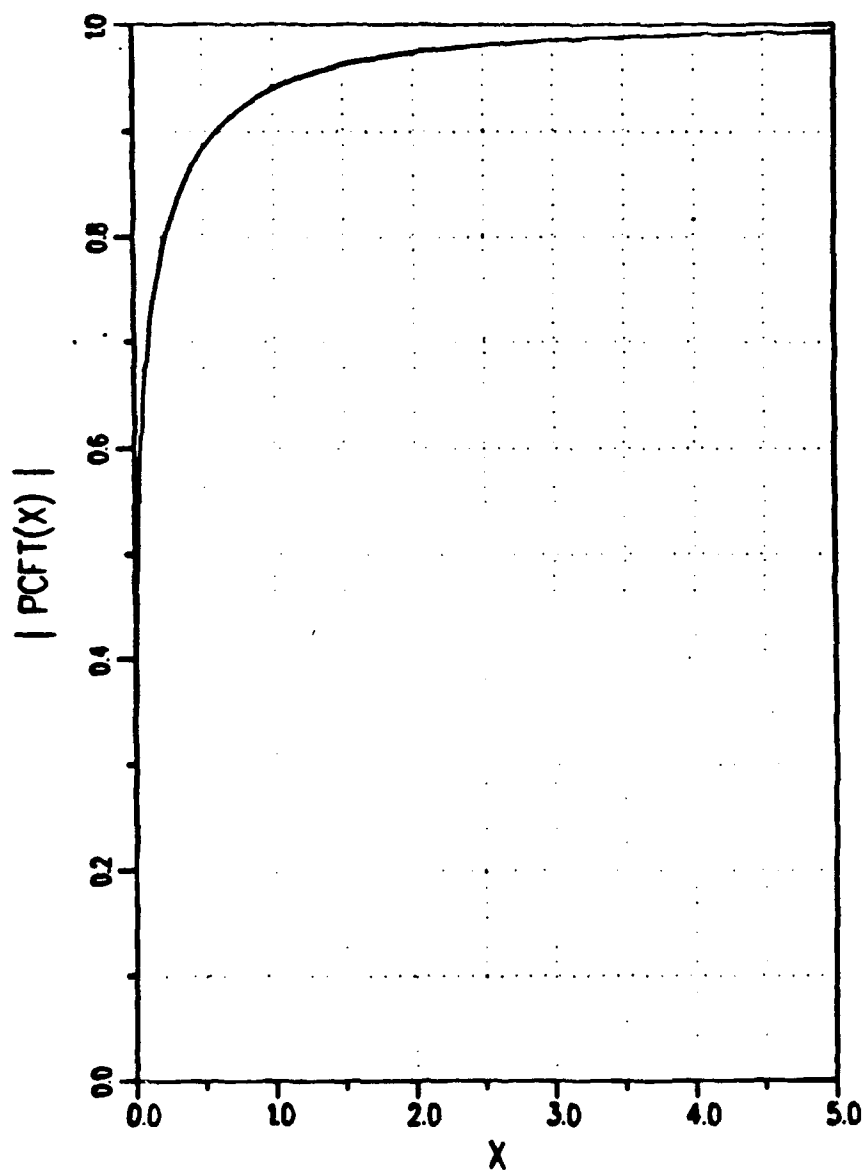


Figure 38: Amplitude of the edge wave transition function.

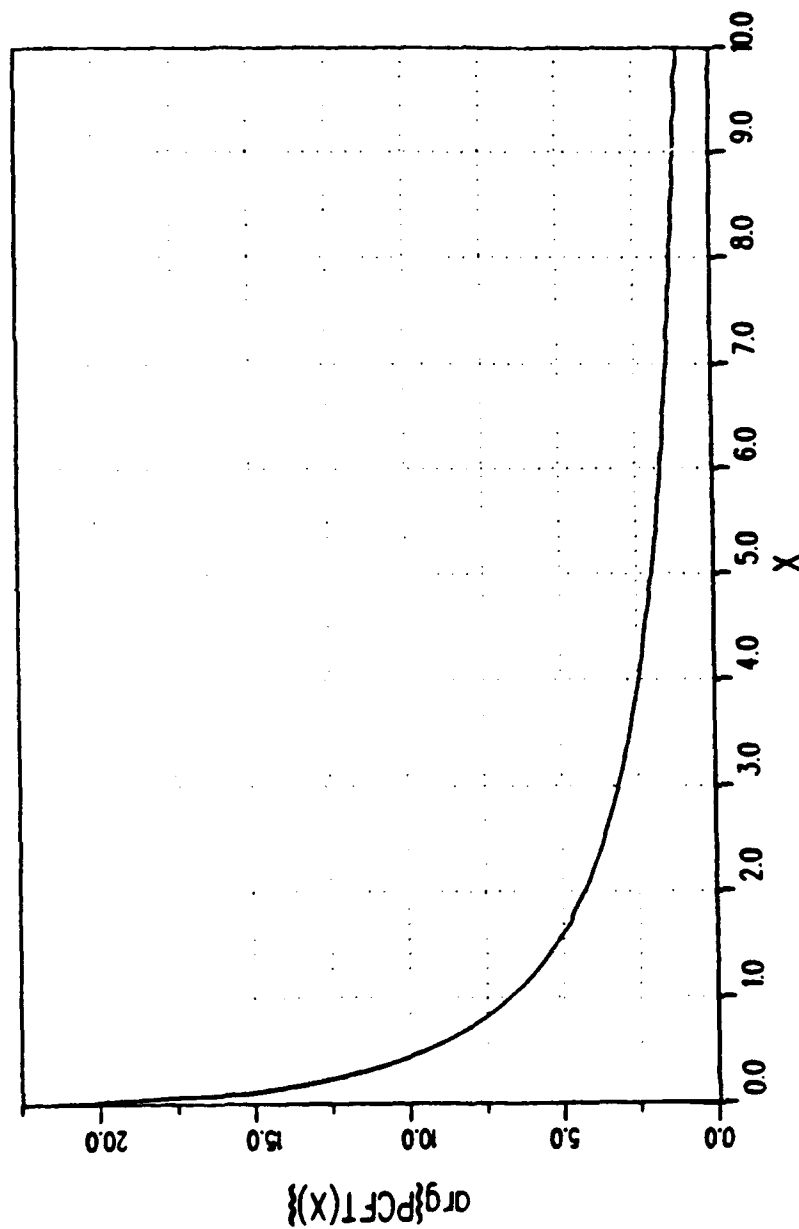


Figure 39: Phase of the edge wave transition function.

REFERENCES

- [1] L. Krauss and L. M. Levine. Diffraction by an elliptic cone. *Commun. Pure Appl. Math.*, XIV:49-68, 1961.
- [2] R. S. Satterwhite and R. G. Kouyoumjian. *Electromagnetic diffraction by a perfectly conducting plane angular section*. Technical Report 2183-2, ElectroScience Lab., Dept. Elec. Eng., Ohio State Univ., Columbus, 1970.
- [3] P. H. Pathak, R. G. Kouyoumjian and W. D. Burnside. A uniform GTD for the diffraction by edges, vertices and convex surfaces. In J. K. Skwirzynski, editor, *Theoretical Methods for Determining the Interaction of Electromagnetic Waves with Structures*, pages 497-561, Sijthoff and Noordhoff, 1981.
- [4] F. A. Sikta and L. Peters, Jr. *UTD Analysis of electromagnetic scattering by flat plate structures*. Technical Report 711930-2, ElectroScience Lab., Dept. Elec. Eng., Ohio State Univ., Columbus, 1981.
- [5] J. Meixner. The behavior of electromagnetic waves at edges. *IEEE Trans. Antennas Propagat.*, AP-20:442-446, 1972.
- [6] G. L. James. *Geometrical Theory of Diffraction for Electromagnetic Waves*. chapter 2, pages 20-21. Peter Peregrinus LTD., 1976.
- [7] O. M. Buyukdura. *Radiation from sources and scatterers near the edge of a perfectly conducting wedge*. PhD thesis, Ohio State Univ., Columbus, 1984.

- [8] P. H. Pathak and R. G. Kouyoumjian. *A dyadic diffraction coefficient for a perfectly conducting wedge*. Technical Report 2183-4, ElectroScience Lab., Dept. Elec. Eng., Ohio State Univ., Columbus, 1970.
- [9] E. H. Newman and R. L. Dilsavor. *A user's manual for the electromagnetic surface patch code: ESP Version III*. Technical Report 716148-19, ElectroScience Lab., Dept. Elec. Eng., Ohio State Univ., Columbus, 1987.
- [10] P. Ia. Ufimtsev. Approximate computation of the diffraction of plane electromagnetic waves at certain metal bodies: i. diffraction patterns at a wedge and a ribbon. *Soviet Phys.-Tech. Phys.*, 27(8):1708-1718, 1957.
- [11] P. Ia. Ufimtsev. Approximate calculation of the diffraction of plane electromagnetic waves by certain metal objects: ii. the diffraction by a disk and by a finite cylinder. *Soviet Phys.-Tech. Phys.*, 3(8):2386-2396, 1958.
- [12] P. Ia. Ufimtsev. Secondary diffraction of electromagnetic waves by a strip. *Soviet Phys.-Tech. Phys.*, 28(3):535-548, 1958.
- [13] R. F. Millar. An approximate theory of the diffraction of an electromagnetic wave by an aperture in a plane screen. *Proc. Inst. Elec. Eng.*, 103:177-185, 1955. pt. C.
- [14] R. F. Millar. The diffraction of an electromagnetic wave by a circular aperture. *Proc. Inst. Elec. Eng.*, 104:87-95, 1956. pt. C.
- [15] R. F. Millar. The diffraction of an electromagnetic wave by a large aperture. *Proc. Inst. Elec. Eng.*, 104:240-250, 1956. pt. C.
- [16] P. C. Clemmow. Edge currents in diffraction theory. *IEEE Trans. Antennas Propagat.*, AP-4:282-287, 1956.

- [17] C. E. Ryan, Jr. and L. Peters, Jr. Evaluation of edge-diffracted fields including equivalent currents for the caustic regions. *IEEE Trans. Antennas Propagat.*, AP-7:292-299, 1969.
- [18] E. F. Knott and T. B. Senior. Comparison of three high-frequency diffraction techniques. *Proc. IEEE*, 62:1468-1474, 1975.
- [19] A. Michaeli. Equivalent edge currents for arbitrary aspects of observation. *IEEE Trans. Antennas Propagat.*, AP-32:252-258, 1984.
- [20] A. Michaeli. Elimination of infinities in equivalent edge currents, Part I: fringe current components. *IEEE Trans. Antennas Propagat.*, AP-34:912-918, 1986.
- [21] A. Michaeli. Elimination of infinities in equivalent edge currents, Part II: physical optics components. *IEEE Trans. Antennas Propagat.*, AP-34:1034-1037, 1986.
- [22] A. Michaeli. Equivalent currents for second-order diffraction by the edges of perfectly conducting polygonal surfaces. *IEEE Trans. Antennas Propagat.*, AP-35:183-190, 1987.
- [23] A. Papoulis. *The Fourier Transform and its Applications*. New York: McGraw Hill, 1961.
- [24] E. F. Knott. The relationship between Mitzner's ILDC and Michaeli's equivalent currents. *IEEE Trans. Antennas Propagat.*, AP-33:112-114, 1985.
- [25] R. G. Kouyoumjian and P. H. Pathak. A uniform geometrical theory of diffraction for an edge in a perfectly conducting surface. *Proc. IEEE*, 62:1448-1461, 1974.

- [26] R. J. Marhefka and W. D. Burnside. *Numerical electromagnetic code - Basic scattering code (version 2), Part I: User's manual*. Technical Report 712242-14, ElectroScience Lab., Dept. Elec. Eng., Ohio State Univ., Columbus, 1982.
- [27] R. J. Marhefka. *Numerical electromagnetic code - Basic scattering code (version 2), Part II: Code manual*. Technical Report 712242-15, ElectroScience Lab., Dept. Elec. Eng., Ohio State Univ., Columbus, 1982.
- [28] L. B. Felsen and N. Marcuvitz. *Radiation and Scattering of Waves*. Prentice-Hall, Inc., Englewood Cliffs, NJ, 1973.
- [29] I. S. Gradshteyn and I. M. Ryzhik. *Table of Integral, Series, and Products*. Academic Press, Inc., 1980.
- [30] M. Abramowitz and I. A. Stegun, editors. *Handbook of Mathematical Functions*. Dover Publications, 1970.
- [31] A. Erdelyi et al. *Higher Transcendental Functions*. Volume II, New York: McGraw Hill, 1954.
- [32] National Bureau of Standards The Computation Laboratory of the National Applied Mathematics Laboratories. *Tables of Bessel Functions of Fractional Order*. New York: Columbia University Press, 1948.